

University of Southern Queensland
Faculty of Engineering and Surveying

How might an underground working environment effect
laser scan data when assessing Joint Roughness
Coefficient, and is it feasible to use a mobile platform?

A dissertation submitted by

Ms. Megan Braddon



In fulfilment of the requirements for

ENG4111 and ENG4112 Research Project

Towards the degree of

Bachelor of Spatial Science (Honors)(Surveying)

Submitted October, 2019

Abstract

This dissertation investigated the capabilities of a phase shift scanner when used to assess the joint roughness coefficient (JRC) of rock surfaces to gain an understanding of:

- the effects close distance-to-object range and scanner speed combinations would have on point cloud density,
- what point cloud density was needed to conduct a JRC assessment from point cloud data,
- the effects of changes in the tunnel environment on the point cloud data including light and dark environments,
- the effects of an amber flashing light and the effects of airborne dust, and
- was it feasible to use these findings with a mobile platform in future studies?

This process helped to answer the question of how a underground working environment might affect laser scan data when assessing JRC, and was it feasible to use a mobile platform? Targets were selected that represented four different JRC grades and variables were selected that could be used in future studies into using mobile laser scanning (MLS) techniques for assessing geotechnical features such as the JRC. A close distance-to-object range was used to simulate the distance a vehicle may travel off of a tunnel wall for conducting an MLS in future studies. A basic guide to a terrestrial laser scan (TLS) station setup was established. From this the effects of the distance-to-object range and scanner speeds were analysed to see at what point a suitable point cloud density could be achieved. A standard deviation range for the point cloud data was established, the environmental conditions were then assessed for their impact on the point cloud data relative to the standard deviation.

It was found that a point cloud density of 2mm was required to accurately obtain JRC. Within the environmental conditions, only airborne dust had a significant effect on the scans; however, there was scope for future studies into the effects of different flashing lights on different scanners and to review if there was a correlation between the distance-to-object range in dark conditions on the standard deviation results. When considering using a mobile platform for the same task at this stage, it is not feasible as further studies into variables affecting MLS techniques need to be assessed.

This dissertation provides a foundation for moving forward into future studies for conducting geotechnical assessments from laser scan data within a working tunnel environment with a long-term view of using MLS techniques.

Disclaimer

University of Southern Queensland

Faculty of Engineering and Surveying

ENG4111 & ENG4112 Research Project

Limits of Use

The Council of the University of Southern Queensland, its Faculty of Health, Engineering and Surveying, and the staff of the University of Southern Queensland, do not accept any responsibility for the truth, accuracy or completeness of material contained within or associated with this dissertation.

Persons using all or any part of this material do so at their own risk, and not at the risk of the Council of the University of Southern Queensland, its Faculty of Health, Engineering and Surveying, or the staff of the University of Southern Queensland.

This dissertation reports an educational exercise and has no purpose or validity beyond this exercise. The sole purpose of the course pair entitled “Research Project” is to contribute to the overall education within the student’s chosen degree program. This document, the associated hardware, software, drawings and any other material set out in the associated appendices should not be used for any other purpose: if they are so used, it is entirely at the risk of the user.

Candidates Certification

I certify that the ideas, experiments, assessments, results, analysis and conclusion set out in this dissertation are entirely my own work, except where otherwise indicated and acknowledged.

I further certify that the work is original and has not been previously submitted for assessment in any other course or institution, except where indicated and acknowledged.

Megan Braddon

Student number: [REDACTED]

[REDACTED]

9/10/2019

Students signature

Date

Endorsement

Primary: Dr. Zahra Gharineiat Secondary: Dr. Ali Mizaghorbanali.

Supervisors

[Signature]

9/10/2019

Supervisors signature

Date

Acknowledgments

I would like to give my thanks and show my appreciation to the following people for their support and assistance during this dissertation.

Dr Zahra Gharineiat who was my primary supervisor. Our weekly meetings and her valuable feedback helped to maintain my focus and direction within this project.

Kassandra Braddon MAusIMM, BScMining(WASM/Curtin), DipFIMnInfoLibStds(Curtin), GradDipmgnt(MtEliza), GradCertProjMgnt(Curtin), GradCertMinEcon(WASM/Curtin), who not only provided current industry knowledge from a working underground mine, but also her valued and continual support during the writing process of this dissertation.

Dr. Ali Mizaghorbanali for providing a larger project scope from which the seed of this dissertation came.

CloudCompare (2019) for their free to access, well-constructed point cloud processing software and all its accompanying 'how to' guides. Their software and guides made the many hours of point cloud editing and analysis an easier task then it could have been.

Table of Contents

Abstract.....	i
Disclaimer.....	ii
Candidates Certification.....	iii
Acknowledgments.....	iv
Table of Contents.....	v
Table of Figures.....	vii
List of Tables.....	x
Abbreviations and Definitions.....	xi
Chapter 1. Research question, Aim and Objective.....	1
1.1. Research question.....	1
1.2. Aim.....	1
1.3. Objective.....	2
Chapter 2. Introduction.....	3
2.1. Introduction to laser scanning.....	3
2.2. Data processing as it applies to this dissertation.....	7
2.3. Surface roughness analysis as it applies to this dissertation.....	8
Chapter 3. Literature review.....	9
3.1. Terrestrial Laser Scanning (TLS).....	9
3.2. Mobile Laser Scanning (MLS).....	11
3.3. Underground laser scanning.....	14
3.5. TLS in tunnel development and monitoring.....	18
3.6. Summary.....	20
Chapter 4. Methodology.....	23
4.1. TLS lab-based test.....	23

4.1.1.	Test area setup.....	23
4.1.2.	Data collection	28
4.2.	Data processing.....	30
4.2.1.	Raw data processing.....	30
4.2.2.	Processed data comparison	32
4.3.	Feasibility assessment of using a mobile platform	46
4.4.	Summary	46
Chapter 5.	Analysis and Results	48
5.1.	Unpainted target versus painted targets	48
5.2.	Density of point clouds	52
5.3.	Cross section for JRC comparison to BC scale.....	54
5.4.	Environmental conditions variation analysis	59
5.4.1.	Dark conditions	60
5.4.2.	Flashing Light condition results.....	62
5.4.3.	Airborne Dust condition results	66
5.6.	Summary	73
Chapter 6.	Discussion	76
6.1.	Review	77
Chapter 7.	Conclusion	81
7.1.	Key findings.....	81
7.2.	Further studies.....	82
Reference List	83
Appendix A - Project specification.....		86
Appendix B - Faro Focus3D Performance Specifications		88
Appendix C – Scanning task risk assessment		89
Appendix D - C2M statistical analysis table.....		91

Table of Figures

Figure 1: TLS laser beam deflection units (Reshetyuk 2009).....	4
Figure 2: Scanner categories based on FOV (Reshetyuk 2009).	5
Figure 3: FOV, left Faro Focus (Faro 2013), right Leica ScanStation2 (Leica 2019).	5
Figure 4: Principal of TOF (Shan & Toth 2009).	6
Figure 5: a) Phase comparison between sent and received wave form. b) Comparison of wave forms at the range finder to acquire $\Delta\lambda$ (Shan & Toth 2009).....	6
Figure 6: Range accuracy of day and night scans (Voegtle, Schwab & Landes 2008, p.1063).....	11
Figure 7: Boat mounted scanner and Cart mounted scanner (Vaaja et al. 2011).	12
Figure 8: Toprak Kalinligi shelter model (Yakar, Ulvi & Toprak 2015, p.42).....	14
Figure 9: 3D model of Cova del Parallo (Lerma et al. 2010, p503-4).	15
Figure 10: Point cloud of Cova del Parallo (Lerma et al. 2010, p503-4).....	15
Figure 11: Scanner mount (Zlot & Bosse 2014, p.764).	16
Figure 12: Processed ramp decline view (Zlot & Bosse 2014, p.777).....	16
Figure 13: MLS system utilised by Gallant and Marshall (2016).....	17
Figure 14: Identified joint sets, colours represent orientation. (Fekete, Diederichs & Lato 2010).....	19
Figure 15: Summary of statistics and 3D virtual structure of target area (Monsalve et al. 2019).	20
Figure 16: Target objects a) painted and b) unpainted.....	25
Figure 17: Test area a) natural daylight, b) closed to light.	26
Figure 18: a) Barton and Choubey scale, b) Sample rock (Barton 2013).	26
Figure 19: Target objects with Barton and Choubey scale.	27
Figure 20: Sketch of target objects within the test area.	28
Figure 21: Pre-processing window options in Scene (Faro 2019).	31
Figure 22: Point cloud created during processing.....	31
Figure 23: Surface mesh created a) with triangular frame visible, b) solid mesh view.	32
Figure 24: Point cloud a) pre-clean, b) post clean.	33

Figure 25: a) Rough alignment, b) Fine registration of a target object.	35
Figure 26: Two methods of measurement computation. a) Nearest Neighbour, b) 2D1/2 Triangulation. (CloudCompare 2019)	36
Figure 27: Point cloud alignment a) Scanner speed 1, b) Scanner speed 2.....	37
Figure 28: Matest Barton comb and Barton and Choubey scale.....	38
Figure 29: CloudCompare 'slice' function.....	39
Figure 30: a) Target object 2 with slice box (yellow), b) Slice side profile in horizontal for comparison, c) BC scale sample 10-12.	40
Figure 31: Scanner speed 1 at 1m in light a) uncleaned, b) cleaned.	42
Figure 32: Visual inspection between scan a) Lt, b) Lt_D.	42
Figure 33: Recursive subdivision of octree cubes (CloudCompare 2019).....	43
Figure 34: Octree numeric code principle (CloudCompare 2019).....	44
Figure 35: Sp1 3m flashing light a) C2M distance comparison, b) Gauss standard deviation.	45
Figure 36: Target 1 (red circle) showing the effects of airborne dust.....	45
Figure 37: Difference between unpainted and painted targets at scanner speed 2.....	49
Figure 38: Faro Focus3D perimeter settings a) SP2, b) SP1.....	52
Figure 39: Standard Deviation of Environmental Changes.	59
Figure 40: Dark conditions Std.Dev.	62
Figure 41: SP1_1m surface comparison histogram.	64
Figure 42: SP1_5m surface comparison histogram.	65
Figure 43: Flashing light conditions Std.Dev.	65
Figure 44: SP2_Dr_D_5m distance histogram.	66
Figure 45: SP2_Dr_D_3m Point cloud overlay,	67
Figure 46: SP2_Dr_D_3m Targets 3 and 4.....	67
Figure 47: Dust conditions Std.Dev, all results.	68
Figure 48: SP1_Dr_D_3m histogram.	68
Figure 49: Dust conditions Std.Dev, largest outlier removed.....	69
Figure 50: Dust conditions Std.Dev, second outlier removed.	69

Figure 51: a) SP2_Dr_D_1m, b) SP2_Lt_D_1m.	70
Figure 52: a) SP1_Dr_D_1m b) SP1_Lt_D_1m.	72

List of Tables

Table 1: Scanner technical specifications (Mechelke, Kersten & Lindstaedt 2007).....	9
Table 2: Boat and cart DEM accuracies (Vaaja et al. 2011, p.593).	13
Table 3: MLS specifications (Puente et al. 2011).	13
Table 4: Test results comparing manual measurements and MLS with 3DAM.	17
Table 5: Key points considerations.	24
Table 6: Data collection check list.	29
Table 7: Data file naming convention.	41
Table 8: Target 1 Unpainted and painted comparison.	50
Table 9: Unpainted and painted comparison of Sp2 at 5m.	51
Table 10: Point cloud density.....	53
Table 11: Sp1 T1 JRC 14-16 visual comparison.	54
Table 12: Sp1 T2 JRC 10-12 visual comparison.	55
Table 13: Sp1 T3 JRC 6-8 visual comparison.	55
Table 14: Sp1 T4 JRC 2-4 visual comparison.	56
Table 15: Sp2 T1 JRC 14-16 visual comparison.	57
Table 16: Sp2 T2 JRC 10-12 visual comparison.	57
Table 17: Sp2 T3 JRC 6-8 visual comparison.	58
Table 18: Sp2 T4 JRC 2-4 visual comparison.	58
Table 19: Dark conditions Standard Deviation results.	61
Table 20: Flashing Light Standard Deviation results.....	63
Table 21: Dusty conditions Standard Deviation results.	71

Abbreviations and Definitions

FOV – Field of view

GNSS – Global Navigation Satellite System

JRC – Joint Roughness Coefficient, 20 grades of surface roughness to assess geotechnical discontinuity features.

IMU – Inertial Measurement Unit

MSE – Mean Square Error

MLS – Mobile Laser Scanning

PS – Phase shift

Reflectance value – The measure of usable light that is reflected from a surface.

RMSE – Root Mean Square Error

SLAM – Simultaneous localisation and mapping

SNR – Signal to Noise Ratio, the ratio of returning laser signal to interference/noise.

TOF – Time of Flight

TLS – Terrestrial Laser Scanning

VRS-GPS – Virtual Reference Station-Global Positioning System, allows for real time kinematic corrections by using an established network of reference stations.

Chapter 1. Research question, Aim and Objective

1.1. Research question

The main research question for this dissertation is:

How might an underground working environment affect laser scan data when assessing JRC?

The following sub questions are formed when considering the main question:

What is already known about the use and function of TLS and MLS?

What is the best scan setup geometry for TLS?

What affects will changes in the environment have on the scan data?

Is it feasible to use a mobile platform for this task?

1.2. Aim

The study aimed to assess a PS scanner for its ability to acquire point cloud data that can be used to assess the JRC of rock when in an underground working environment. The aim of this project was to investigate through lab-based testing the ability of TLS in accurately capturing and identifying different JRC when exposed to different conditions found in an underground environment. The point clouds produced were assessed for their achievable accuracy when attempting to identify four different JRC grades.

The lab-based testing assessed the following variables:

- Three scan station distance-to-object ranges
- Two Scan speeds to assess potential accuracies
- If there was a significant difference between unpainted and painted targets
- The effects of natural light and simulated darkness
- The effects of an amber flashing light on scan data
- The effects of airborne dust on scan data
- Considerations required for using a mobile platform.

The analysis of test data obtained from a simulated underground environment allowed for a series of optimal scanning setup variables to be established. Effects on scanner speed and distance-to-object variations were assessed for their impact on the point cloud density. And the impact of changes in the environment on point cloud accuracy were assessed. It is anticipated

that the study will provide valuable information that could be used in further studies for the identification and analysis of geotechnical discontinuity features in underground environments using MLS.

1.3. Objective

The objective of this study was to assess the effects of various conditions found in an underground working environment, primarily the effects of lighting conditions, flashing amber safety lights and airborne dust particles in the atmosphere. Helping to determine the most effective combination of scanner variables and geometry to produce point cloud data of an accuracy that could be used for surface roughness assessment with an understanding of the potential effects the environmental conditions may have on the data collected.

The acquired findings could then be used to assess the feasibility of MLS in future studies.

Chapter 2. Introduction

Within the mining industry laser scanning has become a widely used tool for assessing volumes, confirmation of mined areas to plans, deformation monitoring as well as in assessing cavity and tunnel geometry and geotechnical features. When constructing or extending tunnels in underground mines, it is necessary to assess the newly mined areas for geotechnical discontinuity features such as the Joint Roughness Coefficient (JRC). The information gathered enables the development and modelling of rock mass analysis which provides information for calculating the tunnel's strength and predicting potential stability issues. The geotechnical information captured dictates the different levels and types of ground support to be installed to ensure the tunnel is safe from collapse.

The current system of using Terrestrial Laser Scanning (TLS) for assessing the geotechnical features of tunnels is effective but can result in interruptions to the production of the mine. TLS tasks may require multiple scans to capture the geometry of an area accurately. This would require the operators to be in the area for an extended period that would vary depending on the quality and accuracy of the data they wish to collect.

With the improvement of scanners and mobile scanning systems, there is a need to assess the achievable accuracies of TLS in various underground environmental conditions before assessing the feasibility of using Mobile Laser Scanning (MLS) for capturing geotechnical features such as JRC. Establishing a best practice for TLS techniques and an understanding of the achievable accuracies will help to minimise the impact of TLS on other mining activities, as well as to help to improve the efficiency and safety of surveyors and geotechnical engineers when working in an operating mine.

The following sections provide a background to laser scanning and JRC, the main topics of this dissertation.

2.1. Introduction to laser scanning

Laser scanning is a form of active remote sensing that acquires a 3D model of an area by transmitting a laser light towards an object and acquiring a distance by measuring the return rate. Scanners can collect a high-density and high-accuracy point cloud in a relatively short amount of time. Laser scanning can be used in a wide range of applications such as deformation monitoring, engineering disciplines, crime scene investigation, and heritage documentation, to name a few. It has quickly become an effective tool in many industries. The scanners available on the market today may offer a range of scan distances, Field-of-View (FOV) and achievable accuracies however they all work with common principals.

Two defining characteristics are a scanner's method for measuring the distance and its FOV. For measuring the distance (also known as range finding) laser scanners use active sensors, this means that they transmit their own light source to obtain a series of uniformly incremental distance measurements in both the horizontal and vertical planes. TLS scanners observe various horizontal and vertical angles within a scan by rotating on the horizontal axis as a whole unit, while the laser beam direction is changed with a deflection unit and digital encoders that can consist of multiple mirrors and servo motors. The deflection unit used determines the FOV and the way in which the angular observations are made. Figure 1 shows four common deflection systems used within laser scanners.

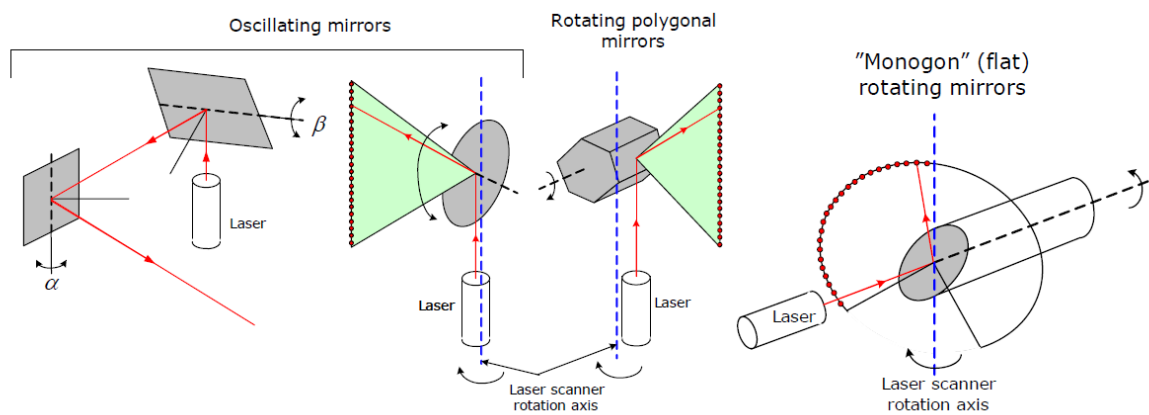


Figure 1: TLS laser beam deflection units (Reshetyuk 2009).

Oscillating mirror systems deflect the laser beam vertically and horizontally while the scanner as a whole unit remains stationary. This system has a limited FOV and is commonly used in camera scanners. With rotating mirror systems, the laser beam is deflected in the vertical plane while the scanner unit as a whole is rotated horizontally by servo motors so that successive vertical profiles can be scanned. This system is referred to as a hybrid scanner and is capable of 360° horizontal observations. A scanner using a monogon deflection system operates in a similar fashion to the hybrid scanner system, however due to the structure of the rotating mirror a greater vertical FOV is achievable. This system is referred to as a panoramic scanner (see Figure 2).

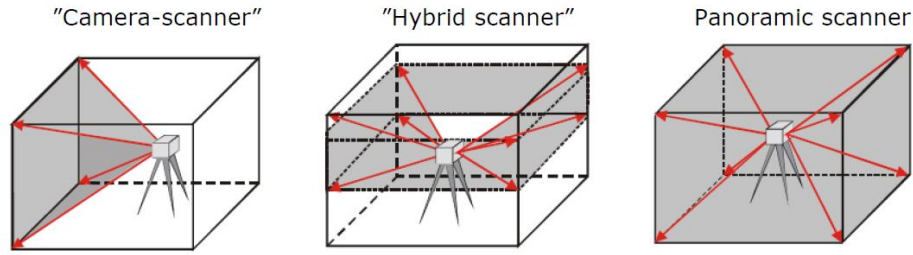


Figure 2: Scanner categories based on FOV (Reshetyuk 2009).

A scanner's FOV is the area scanned from a single scanning station. Figure 3 shows the FOV achievable for two scanners. The Faro Focus and Leica ScanStation2 both hold a 360° horizontal FOV but have different vertical FOV, this will influence the distance-to-object based on the height setup of the scanner when scanning at a close range.

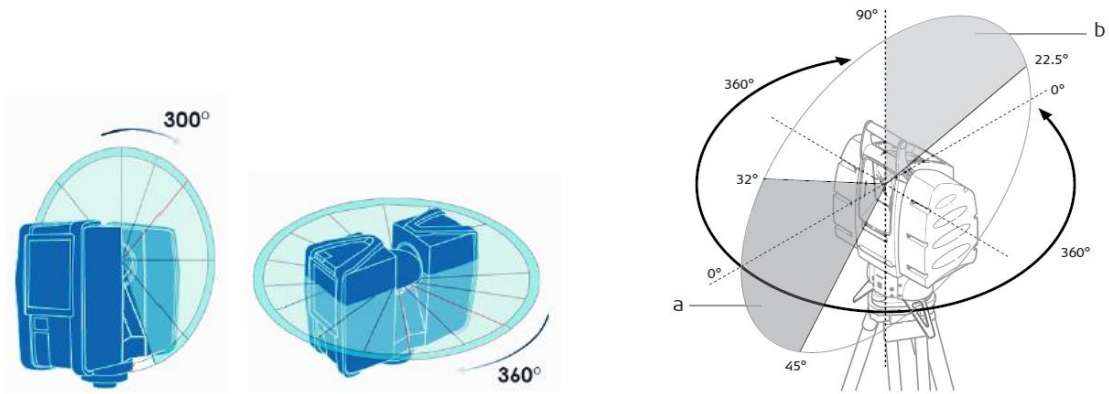


Figure 3: FOV, left Faro Focus (Faro 2013), right Leica ScanStation2 (Leica 2019).

Time-of-Flight (TOF) and Phase Shift (PS) are the two systems used to measure the distances for range finding the deflected laser beam. TOF scanners such as the Leica Scanstation2 send a short pulse of laser light that reflects off the object's surface and returns. This return time and the known speed of light are then used to calculate the distance to the object. A TOF scanner can measure between 2000 to 50000 points per second and scans the entire FOV one point at a time by changing the range finder's direction through the movement of the deflecting unit (Figure 4).

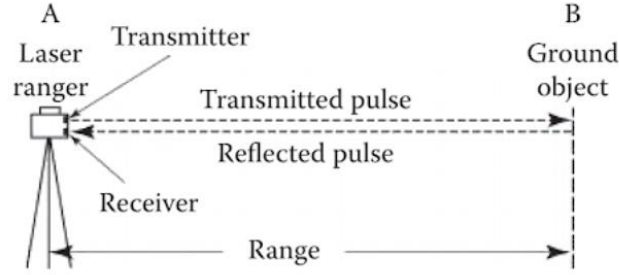


Figure 4: Principal of TOF (Shan & Toth 2009).

A PS scanner such as the Faro Focus uses a continuous modulated laser light. The distance is acquired by measuring the difference between the sent waveform and the return waveform as seen in Figure 5. For an amplitude-modulated laser light with a constant frequency, the measured phase shift can be used to calculate the time it takes for the light to travel to the object's surface and the reflected light to return. The acquired phase shift can then be used to calculate the distance to the object. PS scanners can collect up to one million points per second and are considered to produce a higher level of accuracy than TOF scanners although have a shorter distance-to-object range.

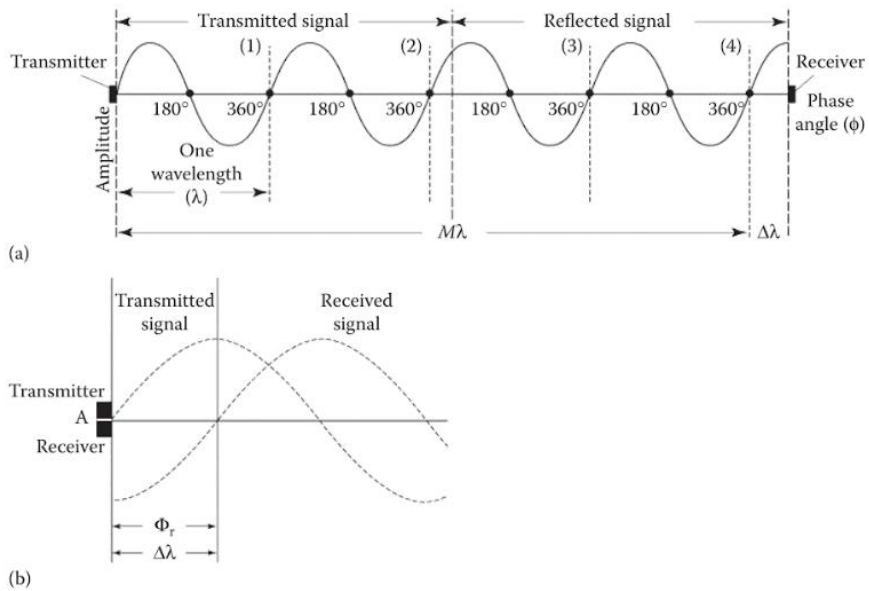


Figure 5: a) Phase comparison between sent and received wave form. b) Comparison of wave forms at the range finder to acquire $\Delta\lambda$ (Shan & Toth 2009).

This dissertation will be assessing the feasibility of using a PS scanner.

When referring to mobile platforms, this is generally a description of the equipment that houses or supports the laser scanner and provides mobility. In TLS the scanner is generally mounted on a set of tripod legs and is stationary. For MLS the platform can be ground-based and consist of a wheeled vehicle such as a work ute, a remote-controlled robot that can carry the weight of the scanner, a boat for riparian scans or anything you can mount the scanner on. The platforms can also be air-based, LiDAR is used in small aircraft to capture large areas and Unmanned-Aerial-Vehicles (UAV) are becoming a common tool in open cut mines for assessing the digs and stockpiles for volume calculations.

When using MLS however it is not just the mobile platform and scanner that is required, an Inertial Measurement Unit (IMU) is necessary to monitor the platform's angular rotation for its 3-dimensional orientation in the scan space and a Global Navigation Satellite System (GNSS) such as GPS for above ground monitoring of the unit's global position relative to a referenced point. In situations where GNSS is not suitable, such as underground or inside buildings, software such as Simultaneous Localisation And Mapping (SLAM) algorithms that construct a map of the environment while keeping track of the unit's location within the environment would be required.

2.2. Data processing as it applies to this dissertation

Once scan data is collected, it needs to be converted from raw data to processed data within a 3D point cloud processing software enabling the generation of usable point cloud and surface mesh files that can then be viewed in a 3D modeler software. The correct processing software to use may be restricted by the equipment used to capture the scans. Faro's Scene Process software is required when processing scan data collected with a Faro 3D scanner. Faro Scene Process 2019 was used for this dissertation.

Once the data is converted from raw to processed, it is then imported into a second software where the point clouds and surface mesh can be compared and assessed. There are many suitable 3D modeler software available that can be used for this stage; however, it should be noted that the processed data will need to be saved in the correct format depending on what 3D modeler software is used. Some companies like Leica may have additional software packages that can be used in conjunction with their processing software.

Data processing will be discussed in more detail in Section 4.2 *Data processing*.

2.3. Surface roughness analysis as it applies to this dissertation

JRC is the graded profile of the rock face used in a surface roughness analysis which is used to assess the shear strength of joint sets in a rock mass.

JRC can be manually assessed with a profilograph (profile comb) which consists of a series of pins held in a line that conforms to the surface texture of the rock face. The profilograph is then reviewed visually against a Barton and Choubey scale (BC scale) (Barton 2013), which can be a time-consuming process. The data acquired is used in rock mass analysis to assist in engineering design decisions and stability analysis of tunnels. Studies have been done in regard to assessing joint sets using data obtained through TLS, and the process was found to be successful, this will be discussed in more detail in Chapter 3 *Literature review*.

Chapter 3. Literature review

This literature review shows a general background into studies that have been conducted on the accuracy of TLS through to MLS when used for different purposes such as land studies, construction, archaeology, and structural deformation. TOF and PS scanners have been thoroughly assessed regarding their geometric accuracies in distances and object acquisition as well as the resulting data quality. MLS has also come under similar scrutiny where assessments have been conducted on the platform used such as a wheeled vehicle, UAV or manned aircraft. The most relevant case studies are discussed below.

This chapter will investigate and answer the following research sub questions:

What is already known about the use and function of TLS and MLS? Combined with information from Chapter 1 section 1.1 and 1.2.
What is the best scan setup geometry for TLS?

3.1. Terrestrial Laser Scanning (TLS)

It is known from the specifications of individual laser scanners that different laser scanners will achieve different results, and the scanner best suited for the task should be used wherever possible. Mechelke, Kersten & Lindstaedt (2007) conducted a study of four laser scanners that used the two methods of distance measuring, TOF and PS discussed in Section 1.1 *Introduction to laser scanning*. In their study they assessed the four models shown in Table 1.

Table 1: Scanner technical specifications (Mechelke, Kersten & Lindstaedt 2007).

Scanner/Criterion		Trimble GX	Leica ScanStation	FARO LS 880 HE	Z+F IMAGER 5006
Scan method		Time-of-flight		Phase difference	
Field of view [°]		360 x 60	360 x 270	360 x 320	360 x 310
Scan distance [m]		200	300	< 76	< 79
Scanning speed		≤ 5000pts/s	≤ 4000pts/s	120kHz	≤ 500000px/s
Angular re- solution [°]	Vertical	0,0017	0,0034	0,009	0,018
	Horizontal	0,0017	0,0034	0,00076	0,018
3D scan precision		12mm/100m	6mm/50m	n.a.	n.a.
Camera		integrated	integrated	add-on option	add-on option
Inclination sensor		compensator	compensator	yes	yes

A 3D test field was established using a known station location and known spherical target locations inside a building foyer. The volume of the field test area was $30 \times 20 \times 12 \text{ m}^3$ with 53 reference points, the minimum distance to the object being 1.5m and the maximum being 33.1m. When assessing the 3D distance accuracy of the four units, it was found that the Leica ScanStation using TOF yielded the best results. When assessed against the reference distance it was found that all units performed to an accuracy of $\pm 2 \text{ mm}$ when in a range of 20 to 40m between station and object; however, between 40 to 60m only the Leica and Z+F maintained the accuracy of $\pm 2 \text{ mm}$. Mechelke, Kersten & Lindstaedt (2007) noted that for longer distances in daylight the signal to noise ratio was affected.

When assessing the incident angle at a range of 10m for angles between 90° to 5° , it was found that the TOF scanners held a higher accuracy with a 3mm deviation between 5° to 10° . Mechelke, Kersten & Lindstaedt (2007) stated that at an incident angle of less than 45° shifts in the accuracy of the point cloud can be expected. Assessment of the colour of the object on the distance accuracy showed that the Leica and the Z+F held the best accuracies through a range of coloured targets. Inclination compensation tests show that the TOF scanners can be successfully compensated for; however, a trunnion axis error in the PS scanners will influence the results.

A more thorough study was conducted by Voegtli, Schwab & Landes (2008) on the effects of different materials and object colours on the measurements acquired using a Trimble GX TOF scanner. When assessing the geometric accuracy from scanning grey-scale targets it was found that the brightness of the object and the obtainable accuracies were dependant, the mean square error (MSE) increased over darker areas (Voegtli, Schwab & Landes 2008). This was confirmed by reviewing data from other research groups. When assessing colour targets, it was found that not only does the brightness of the target affect the accuracies but also the time of day the scan is conducted, scans conducted at night produced a smaller MSE result. The results of which can be seen in Figure 6.

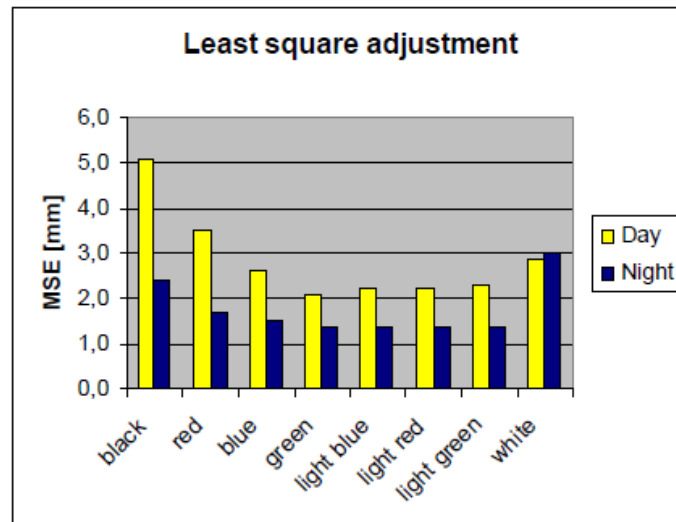


Figure 6: Range accuracy of day and night scans (Voegtle, Schwab & Landes 2008, p.1063).

When assessing different materials, it was found materials that transmit light and some metal surfaces produced large MSE results while different wood species and wetness only had marginal MSE variation. It was suggested that the same tests be conducted on PS scanners for a comparative assessment.

In a later study by Lemes and Zaimovic-Uzunovic (2009) it was found that when testing two specific light levels against the ambient light settings within a scanner, red targets produced the largest variation in points scanned at different ambient light levels. Ambient light levels had minimal effect on blue targets except in very bright conditions and no effect on grey targets. This study was conducted with a red wavelength laser, and results may vary for a green wavelength laser as noted by Lemes and Zaimovic-Uzunovic (2009).

3.2. Mobile Laser Scanning (MLS)

When conducting MLS, it is common for a TLS to be vehicle mounted with GNSS and IMU integration. Talaya et al. (2004) assessed the viability of combining TLS with aerial laser scanning techniques using GNSS and IMU to ascertain if it was a viable combination for a wheeled vehicle platform MLS. This system of integrated components required a uniform reference frame to be transferred from the orientation systems to the laser scanner which required a base structure for the systems to be mounted on that could be fixed to the vehicle.

To test the accuracies that could be acquired a network of known surveyed points were fitted with reflective targets, and the scan was conducted with the TLS being used as a pushbroom sensor. All the points measured were transferred to the mapping reference frame by using its known orientation and applying the required formula. The achievable accuracy for this

assessment was the Root Mean Square Error (RMSE) of 180cm in Easting, 350 cm in Northing and 130 cm in the vertical when compared to a 1:1000 map of the same area. In regard to using this system for mobile mapping Talaya et al. (2004) noted that further study in this area was required at the time.

When assessing erosion and deposition of ambulatory riverine topography Vaaja et al. (2011) used both a cart-mounted scanner and a boat-mounted scanner (Figure 7) to compare the MLS data acquired against TLS data as a reference for accurate analysis.



Figure 7: Boat mounted scanner and Cart mounted scanner (Vaaja et al. 2011).

MLS is more commonly conducted using a wheeled vehicle which results in an almost uniform point spacing in the 3D point cloud. When using a boat, the 3D point cloud is impacted by the shift in speed and orientation of the boat as it is affected by the river water movement, this results in variations in the point cloud density (Vaaja et al. 2011). A single sphere target was used to orientate each scan, the location of which was acquired by VRS-GPS and point bars were erected to compare point cloud results to. When establishing the reference point cloud from TLS, the precision was sub 10mm. When comparing the acquired boat and cart scanned data to the reference point cloud it was found that the RMSE ranged from 55 to 176mm when assessing the erected point bars from the boat and 40 to 53mm from the cart as seen in Table 2.

Table 2: Boat and cart DEM accuracies (Vaaja et al. 2011, p.593).

Target	Areas (m ²)	BoMMS 2008		BoMMS 2009		CartMMS 2009	
		RMSE	Bias	RMSE	Bias	RMSE	Bias
Point Bar 1	1,031	0.088	0.075	0.108	0.104	0.051	-0.018
Point Bar 2	1,045	0.176	0.174	0.122	0.120	0.040	0.024
Point Bar 3	1,772	0.055	-0.043	0.104	-0.072	0.053	0.006
Bank 1	1,072	0.254	-0.225	0.157	-0.057	–	–
Bank 2	1,041	0.203	-0.021	0.212	-0.065	–	–
Bank 3	485	0.284	-0.083	0.244	0.082	–	–
Overall	6,446	0.150	-0.003	0.150	0.019	0.042	0.019

It was found that accuracy could be increased with a steeper scanning angle when the scanner support structure was increased by 1m in height. The study confirmed the feasibility of using MLS for riverine topography changes to an accuracy of sub 50mm after processing.

In other studies, Lehtomaki et al. (2010) found that when collecting data for assessing pole like structures from a vehicle-mounted scanner, accuracy could be improved when traveling at a constant speed of 20 km/hr. Pu et al. (2011) found that when assessing road infrastructure and safety, providing enough GNSS satellites can be detected an accuracy of sub 30mm is achievable. Puente et al. (2011) conducted a study on the available MLS options in 2011 and found that the model of scanner used resulted in varying levels of accuracy and range as can be seen in Table 3, and found that while some scanners had greater ranges others had higher accuracy and the best scanner for the job was dependent on what the job was.

Table 3: MLS specifications (Puente et al. 2011).

MLS System	Road Scanner	IP-S2 Compact	MX8	StreetMapper 360 or Portable	VMX-250	Dynascan	Lynx Mobile Mapper
Scanner	Faro Photon 120	Sick LMS 291	VQ-250			MDL scanner	Lynx laser scanner
Maximum range	120m (p90%)	80m (p10%)	200m (p80%)			up to 500m	200m (p80%)
Range precision	1mm@25m, p90%	10 mm @ 20 m	5mm @150m, (1σ)				8mm, 1σ
Range accuracy	± 2mm@25m	± 35mm	10mm @150m, (1σ)			± 5cm	± 10mm, (1σ)
PRR	122- 976 kHz	40kHz	up to 600 kHz (2 x 300 kHz)			36 kHz	1000 kHz (2 x 500 kHz)
Scan speed	48Hz	75Hz	200 Hz (2x 100 Hz)			up to 30 Hz	200 Hz (2x 100 Hz)
Scanner FOV	H360° / V320°	180° ⁽¹⁾ / 90° ⁽²⁾	360° without gaps			360°	360° without gaps
Angular resolution	H0,00076° / V0,009°	1° ⁽¹⁾ / 0,5° ⁽²⁾	0,001°			0,01°	0,001°
Weight	14.5 kg	22.7kg	approx. 11kg			11kg	78 kg

3.3. Underground laser scanning

Underground scanning has been conducted in the past using standard static TLS and in some industries is used in common practice. Different accuracies have been achieved depending on the equipment used, the task being conducted, and the desired accuracies of the project. A reference system is still required for underground scanning to assist in georeferencing individual scans and for the stitching together of point clouds during processing. This can either be a geodetic coordinate location that is surveyed in or a localised scanner centred coordinate system that utilises target points and/or targets.

Yakar, Ulvi and Toprak (2015) stated that the tools and equipment used for scanning an underground shelter should be selected for their appropriate technical capabilities to produce the desired end result and that suitable lighting should be used. For their task a Faro Focus was used with pattern targets. It was found that the desired accuracy for the project was achieved for the external and internal scans to model the shelter as seen in Figure 8. However, the specific lighting level used and the desired level of accuracy in millimetres was not stated beyond the Faro specifications.



Figure 8: Toprak Kalinligi shelter model (Yakar, Ulvi & Toprak 2015, p.42).

Lerma et al. (2010) conducted a similar study for documenting complex archaeology in the Cova del Parallo underground cave system to obtain high accuracy 2D and 3D data. They required 15mm accuracy for the cave network and 2mm accuracy of the sample areas containing significant rock carvings. With the level of accuracy acquired and a suitable photogrammetry overlay, accurate 3D models were developed as seen in Figure 9 and 10.



Figure 9: 3D model of Cova del Parallo (Lerma et al. 2010, p503-4).



Figure 10: Point cloud of Cova del Parallo (Lerma et al. 2010, p503-4).

3.4. Mobile Laser Scanning in underground and indoor environment

Due to the fact that GNSS cannot be used underground, or in buildings, the accuracy of MLS inside structures in regard to a reference system needed to be assessed. As with underground TLS, the reference system can either be a geodetic coordinate location that has previously been surveyed in, or a localised reference system.

When assessing the use of localised data and SLAM algorithms on indoor MLS data, Kaijaluoto, Kukko and Hyypä (2015) found that the RMSE of 17mm horizontally and 36mm for vertical positions was achievable in post-processing when data was collected at a slow vehicle speed.

When assessing data collection in an underground mine, Zlot and Bosse (2014) conducted an assessment on the obtainable data accuracy when driving within the maximum mine site speed of 30km/hr. This was to reduce interruption to production and the time required for traditional

tripod-mounted scans. The vehicle-mounted scanner platform consisted of one spinning and two fixed scanners, as seen in Figure 11, integrated with an IMU and SLAM for data acquisition.



Figure 11: Scanner mount (Zlot & Bosse 2014, p.764).



Figure 12: Processed ramp decline view (Zlot & Bosse 2014, p.777).

To produce the processed 3D model, a section of which can be viewed in Figure 12 17km of mine tunnels were driven at the average mine site speed. To generate a consistent point cloud an estimated trajectory of the sensor is calculated utilising a time stamped sequence of poses. Combined with a trajectory estimate and timestamped laser range data a common coordinate frame was established, and the system was set up in a pushbroom configuration. The analysis conducted by Zlot and Bosse (2014) found that the forward direction bias was 2mm per metre and 1mm per metre in the vertical; however, the point cloud density was not specified. The result produced a 3D model of the mine that matched closely to the previously surveyed map.

While this study produced a suitable 3D model of the tunnel system, it did not assess to what level of accuracy geological features such as joint sets, fractures, cracks, and blast damage were captured.

For specifically assessing joint orientation, Gallant and Marshall (2016) assessed the use of the three-dimensional axis mapping (3DAM) algorithm in conjunction with a TOF scanner and IMU mounted on a robotic wheeled platform. They compared their field tests with traditional manual measurements of the joint orientation using a compass and inclinometer. Below in Figure 13 the MLS system Gallant and Marshall utilised can be seen. The Clearpath Husky A200 robot was designed to minimise the need for humans to enter dangerous environments (Gallant & Marshall 2016), mounted with an IMU and low-cost Microsoft Kinect v2 scanner the system was deemed to be comparatively low cost compared to TLS systems.



Figure 13: MLS system utilised by Gallant and Marshall (2016).

Testing in three locations the system was compared against the traditional manual measurement and TLS. Gallant and Marshall (2016) assessed and compared the joint orientation as well as the time taken to acquire the data. In all instances they found the 3DAM and MLS produced satisfactory results, not only producing the required joint orientation but also performing the task in less time than both manual measurements and TLS. Table 4 shows the results from one of the Myra-Bellevue test locations.

Table 4: Test results comparing manual measurements and MLS with 3DAM.

Results of the Myra-Bellevue experiments.

	Hand measurements	3DAM using a mobile robot
Number of poles	25	234
Joint orientations (dip / dip direction)		
Set 1	87/237	87/065
Set 2	89/292	89/286
Angular difference with respect to hand measurements (deg)		
Set 1	–	9.9
Set 2	–	6.0
Approximate effort (min)		
Setup / take down	0	10 ^a
Data collection	45	1
Data processing	10	10
Total	55	21

The study found that the advantages of using MLS include being less labour intensive, potentially more efficient and less prone to human error when being utilised for assessing joint orientation. After completing their assessment, Gallant and Marshall (2016) concluded that even though their prototype was utilitarian a commercial version was feasible.

3.5. TLS in tunnel development and monitoring

When assessing the use of TLS in drill and blast tunnels for geotechnical features Fekete, Diederichs and Lato (2010) found that while scanning at 300 rotations per second collecting approximately 2000 points per second was sufficient for producing a 3D model suitable for construction and contracting calculations it was not sufficient for identifying geotechnical features, this required a higher resolution scan.

Some of the issues noted while scanning during the construction phase of a tunnel include time allocations for scanning that did not impede the workflow but still produced the desired results and the fact that the tunnel environment was dusty with no established lighting. Fekete, Diederichs, and Lato (2010) note that laser scanners are effective in the dark as they are an active sensor and the undissipated airborne dust did not unduly affect the scan results.

Fekete, Diederichs, and Lato (2010) set up 7m from the face for a scan span of 10-15m diameter, the ideal distance-to-object being noted as a ratio of no less than 0.5: scan span diameter. Scans were undertaken using a Leica Geosystems HDS6000 PS scanner. The tests produced high speed and high-resolution scans at 500,000 points per second producing 6mm intervals between points and distance accuracy of <4mm. The limitations of using TLS include the effects of shadowing in the point cloud requiring multiple setups for adequate coverage to minimise occlusion and bias in the data due to the scan line and drill hole orientation causing misleading results in the point cloud.

However, the results of the scans after data processing were deemed to have many geotechnical applications. These applications included permanent documentation of the rock condition prior to being obscured by ground support and enhancing the ability to identify discontinuity features such as joint sets seen in Figure 14. This enabled the creation of more extensive rock mass models and post-processed geotechnical feature assessments.

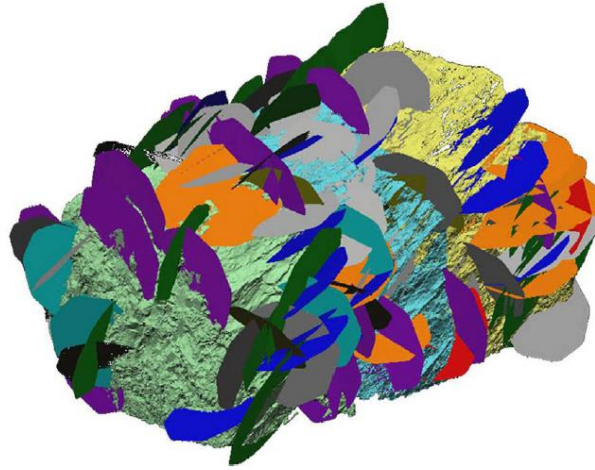


Figure 14: Identified joint sets, colours represent orientation. (Fekete, Diederichs & Lato 2010).

More recent studies into utilising TLS for assessing rock mass characteristics in underground mines have used software such as ‘dips’ (Monsalve et al. 2019) to assist in assessing and classifying the structure of the rock mass into joint sets during data processing. Referencing Fekete, Diederichs and Lato’s 2010 study into the feasibility of using TLS for assessing geotechnical features Monsalve et al. (2019) conducted a study in an underground limestone mine to assess the rock mass characteristics of a section undergoing a structurally controlled mode of failure. Monsalve et al. (2019) aim to use the acquired data to analyse the discontinuities statistically and to produce further discontinuity modelling and thus produce reliable models that allow engineers to establish a clearer understanding of the rock mass behaviour.

Using a Faro PS scanner, they established a network within the tunnels using nine setup stations and spherical targets for georeferencing the individual scans during processing. The resulting 3D virtual structure was produced with the required accuracy to identify the four joint sets as seen in Figure 15.

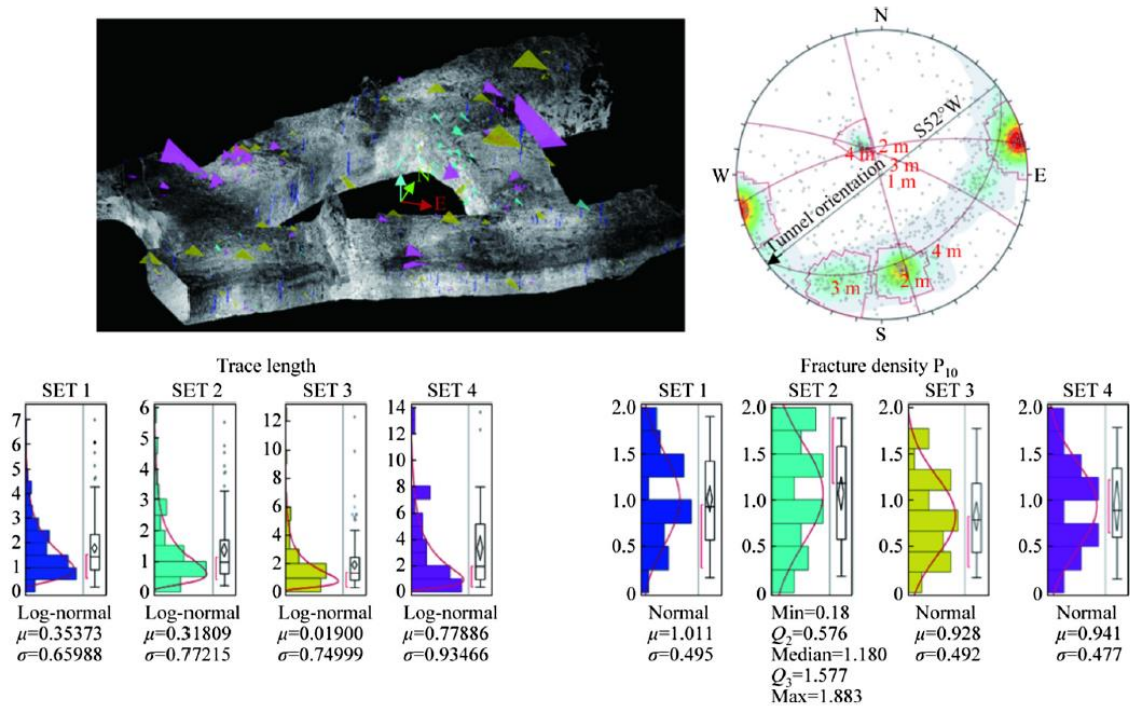


Figure 15: Summary of statistics and 3D virtual structure of target area (Monsalve et al. 2019).

Monsalve et al. (2019) note that there are currently no existing guidelines for conducting TLS in underground environments. However, by following Fekete, Diederichs and Lato's 2010 findings they achieved their desired results. Further noting that planning the scanning project is essential for reducing the time required underground, reducing potential error propagation in both the procedure and the point clouds as well as ensuring the information required is gathered without the need to perform the scans a second time.

3.6. Summary

This review has provided a brief overview of the progression in TLS and MLS with a view to being used in underground environments, helping to answer the research sub question:

What is already known about the use and function of TLS and MLS?
Combined with information from Chapter 1 section 1.1 and 1.2.

Through the review, it was found that when considering using MLS for geotechnical assessments consideration needs to be given to the scanner to be used, how it functions and if the required accuracies can be achieved with the scanner selected. At this stage, the more accurate results are not specific to TOF or PS style scanners but rather the overall scan unit itself. Using the correct

scanner for the task based on the scanner's provided specifications is the first step to achieving the best possible results.

When considering the target object and its colour, it was found that in a testing environment grey coloured targets produce more constant results, however blue and green targets do provide fair results with only minor variations between scans conducted at different lighting levels. In all studies it was found that scanning at night or in a dark environment has produced a better RMSE result and a higher level of points collected. However, so far, no studies have been conducted regarding the effects on scan results and point clouds from the amber flashing safety lights commonly used in underground environments.

When scanning, consideration needs to be given to the results required. A high-resolution scan will take longer but yield a denser point cloud. The incident angle between the scanner and target can affect the accuracy of the point cloud, an incident angle of 45 ° to 90 ° is recommended. It is also recommended that a ratio of (0.5 to 1): scan span diameter be used for target distance offset.

When using MLS, it was found that holding a constant steady vehicle speed improves the point cloud accuracy. Consideration needs to be given to the vehicle's distance from the object and the height of the scanner to ensure the target area is captured within the FOV. These parameters will vary depending on the scanner being used. The use of SLAM for location and mapping when scanning underground was effective within the studies reviewed.

The software being used varies between studies and is dependent on what is being assessed. 3DAM was found effective when assessing joint orientation, while 'dips' was also found to be effective in another study for analysing rock mass characteristics, including joint orientation.

The list of key points below helps to establish an answer for the research sub question:

What is the best scan setup geometry for TLS?

Key points to consider when conducting scans include:

- Distance-to-object ratio of (0.5 to 1): Scan span diameter (Fekete, Diederichs and Lato 2010).
- Incident angle no more than $\pm 45^\circ$ from the centre of object (Mechelke, Kersten & Lindstaedt 2007).
- Target object colour for testing ideally grey (Lemes and Zaimovic-Uzunovic 2009).

- Resolution of scan, scanner speed suitable for the required point cloud density of the task.
- Station setup separation of 1 to 2 times the tunnel radii (Fekete, Diederichs and Lato 2010).
- Consistent mobile platform speed (Lehtomaki et. al. 2010).

To summarise, when planning for a scanning project consideration must be given to the scanner being used, its capabilities and the software required to produce the desired results. When considering the scanning environment, further testing is required into the effects of amber flashing lights and airborne dust particles on the scan data acquired.

Chapter 4. Methodology

This chapter aims to convey the methodology used to answer the research question and sub-question:

How might an underground working environment affect laser scan data when assessing JRC?

What affects will changes in the environment have on the scan data?

The testing aimed to ascertain if a standard terrestrial laser scanner (Faro Focus^{3D}) could be used to capture the JRC of rock surfaces in various environmental conditions that simulate common underground occurrences in a functioning mine tunnel, with a view to assessing the feasibility of using a mobile platform in future studies.

The literature review found that various projects had attempted similar tests; however, the author found that some variables had not been considered. The effects of an amber flashing light on scans and the impact of airborne dust on the results were variables that had not been researched to date. It was also noted that there were no established best practice scan geometry setup guidelines when conducting TLS in a tunnel environment.

As stated in the Aim in Chapter 2, the lab testing assessed the following variables:

- Three scan station distance-to-object ranges
- Two Scan speeds to assess potential accuracies
- If there was a significant difference between unpainted and painted targets
- The effects of natural light and simulated darkness
- The effects of an amber flashing light on scan data
- The effects of airborne dust on scan data
- Considerations required for using a mobile platform.

4.1. TLS lab-based test

4.1.1. Test area setup

The scanning geometry for the lab-based TLS testing was developed through the literature review research, addressing the research sub question:

What is the best scan setup geometry for TLS?

Scan geometry setup key points:

1. Distance-to-object ratio of (0.5 to 1): Scan span diameter (Fekete, Diederichs & Lato 2010).
2. Incident angle of no more than $\pm 45^\circ$ from centre of object (Mechelke, Kersten & Lindstaedt 2007).
3. Target object colour for testing ideally grey (Lemes and Zaimovic-Uzunovic 2009).
4. Resolution of scan, scanner speed suitable for the required point cloud density of the task.
5. Station setup separation of 1 to 2 times the tunnel radii (Fekete, Diederichs & Lato 2010).
6. Consistent mobile platform speed (Lehtomaki et. al. 2010).

From the acquired information, the testing area was set up to ensure that key points 1 to 4 were considered. Table 5 shows the setup selection for each scan station for assessing any variation between the unpainted and painted targets.

Table 5: Key points considerations.

Dist-Obj Ratio.	Angle of incident. FOV window.	Target colour	Scan-Speed 1.	Scan-Speed 2.
5m Ratio (m) 1.75 < 10 ϕ	10° from centre. 5° 80° 100° -5°	1 st round unpainted 2 nd round painted	1/10 x6 Points 4096 pt/360 Speed 122 kpt/sec	1/2 x2 Points 20480 pt/360 Speed 488 kpt/sec
3m Ratio (m) 1.75 < 6 ϕ	20° from centre. 10° 70° 110° -10°	1 st round unpainted 2 nd round painted	1/10 x6 Points 4096 pt/360 Speed 122 kpt/sec	1/2 x2 Points 20480 pt/360 Speed 488 kpt/sec
1m Ratio (m) 1.75 < 2 ϕ	45° from centre. 12° 45° 135° -12°	1 st round unpainted 2 nd round painted	1/10 x6 Points 4096 pt/360 Speed 122 kpt/sec	1/2 x2 Points 20480 pt/360 Speed 488 kpt/sec

Close range distance-to-objects were selected to assess the achievable scan results based on potentially using a mobile platform in future studies. This was to simulate the distance a vehicle may travel off the tunnel wall as it drives through. The width of an underground mine tunnel varies depending on the equipment used, the author's industry contact advised that 5m to 10m are common mining and construction widths respectively. Therefore, distances of 1m, 3m, and 5m were deemed realistic distances a vehicle may travel off the wall.

The target objects were scanned in two rounds, one with the objects unpainted and the second with the objects painted grey as seen in Figure 16. This was to assess if the natural colour of the objects affected the results due to different reflectance values. Due to the small scan area, no additional artificial targets were included in the scan. The temperature in the test area ranged from 22°C to 26°C.



Figure 16: Target objects a) painted and b) unpainted.

The Faro Focus^{3D} has 38 possible scan resolution and quality combinations which dictate the scan speed and achievable accuracy. Scan speed 1 with a resolution of 1/10, quality of x6 and a scan speed of 122kpt/sec was selected to assess if the desired accuracy could be achieved in a quicker time than with a higher resolution scan. Scan speed 2 with a resolution of 1/2, quality of x2 and a scan speed of 488kpt/sec was selected to assess if a higher accuracy scan could be used effectively to identify different JRC. The Faro Focus^{3D} specification sheet can be viewed in Appendix B *Faro Focus^{3D} Performance Specifications*.

A suitable testing location was used to enable the researcher to scan in both light and dark conditions. The lighting was controlled by ensuring internal windows were covered and using the roller door to either let in or block out natural light as seen in Figure 17.



Figure 17: Test area a) natural daylight, b) closed to light.

Under advisement from the industry professionals the target objects were selected to represent four different JRCs based on the Barton and Choubey (BC) scale (Barton 2013) as seen in Figure 18.

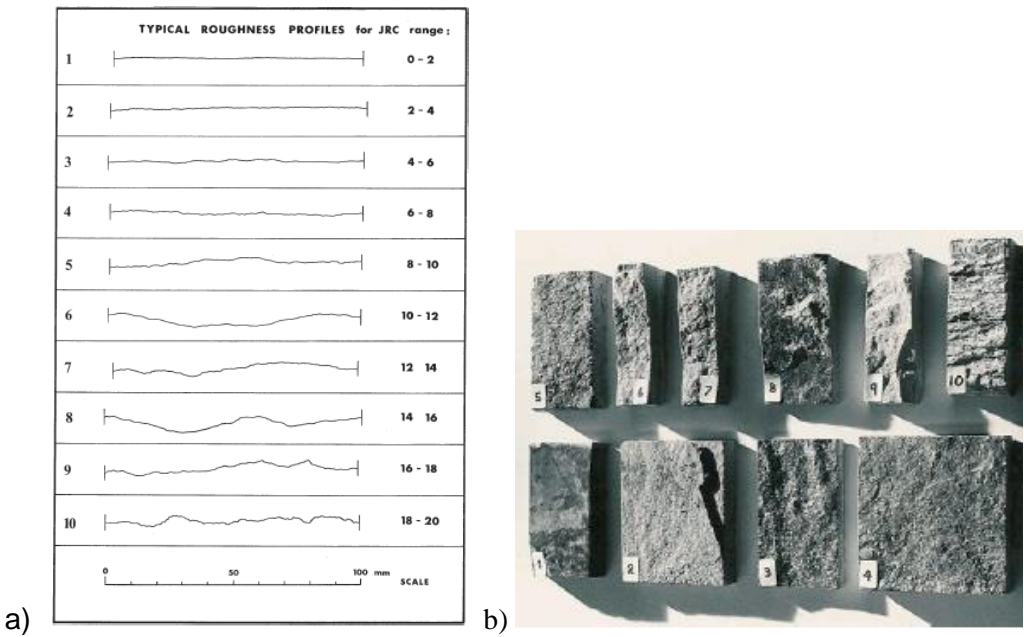


Figure 18: a) Barton and Choubey scale, b) Sample rock (Barton 2013).

The four target objects selected for scanning visible in Figure 19 showing the BC scales 14-16, 10-12, 6-8 and 2-4 selected as a scaled overlay on the target objects. A visual assessment and comparison between the BC scale and the potential target objects was done to assess the suitability of each target prior to testing.

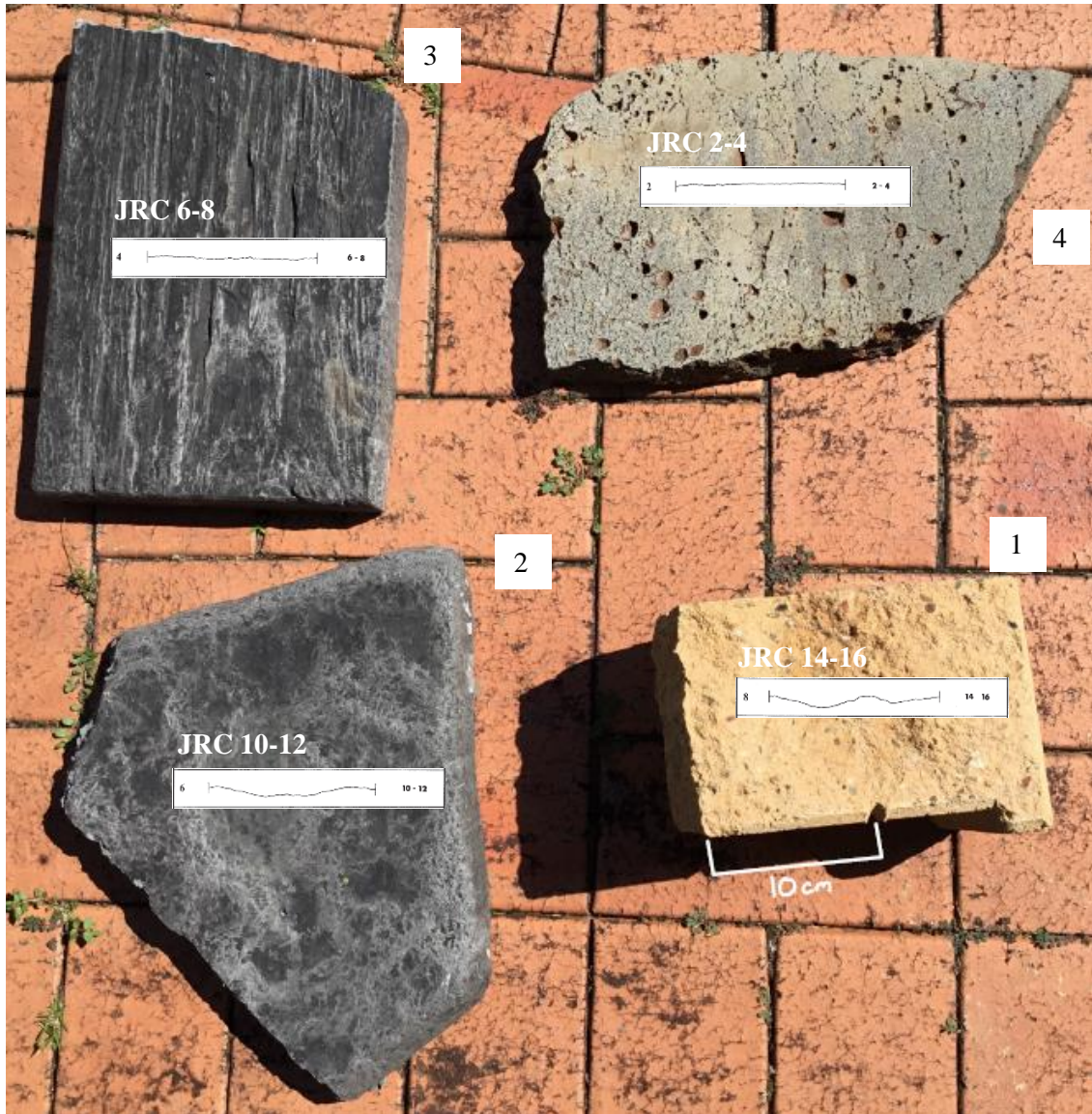


Figure 19: Target objects with Barton and Choubey scale.

Following the previously established scan setup geometry parameters, the test area was set to enable the three distance-to-object scan stations to capture the target objects within the defined parameters. The target objects were set at different angles to the bench face to better represent a natural surface angle, as advised by the industry professional. The diagram in Figure 20 shows the relevant distances of the objects within the test area. An amber flashing

light was located to the right of the scanner path and flour was used to simulated airborne dust in the atmosphere to complete the testing area scenarios.

While the test scenario was designed to test the pre-established variables of both light and dark conditions, the effects of an amber flashing light and the effects of airborne dust at two scan speeds there are limitations to this scenario. The accurate level of lighting was not measured, the effects of airborne dust were simulated and not actual rock dust particles, and only two of the available scanner speeds were tested using a Faro PS scanner.

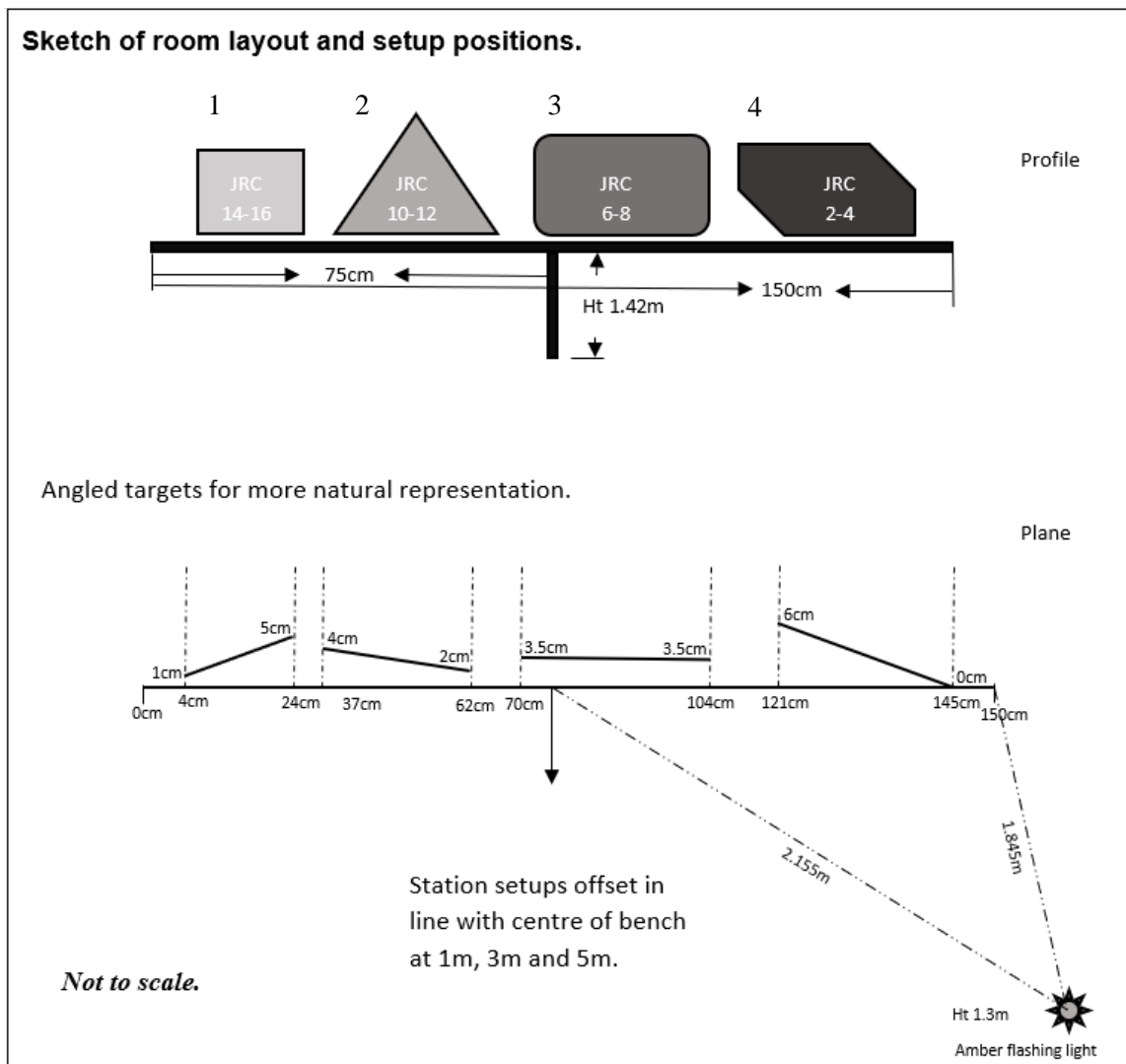


Figure 20: Sketch of target objects within the test area.

4.1.2. Data collection

The target objects were scanned multiple times capturing the different test variables. This required a system of repeated setups conducted in two rounds requiring a total of twelve scans

per setup (six per scanner speed) as seen in Table 6. The scanner once setup over a station scanned at both scan speeds covering all the test variables prior to being moved, requiring a total of 72 scans to cover the three stations. The time required for each scan varied depending on the quality and resolution of the scan. The scanner heated up through repeated use which resulted in the scanner slowing down, listed below are the average scan times only.

Scan speed 1:

- 5m = 3min 17sec
- 3m = 2min 0 sec
- 1m = 1min 30sec

Scan speed 2:

- 5m = 4min 00sec
- 3m = 2min 35sec
- 1m = 1min 48sec

Table 6: Data collection check list.

Round 1 – unpainted target objects:	Round 2 – painted target objects:
Scan speed 1 and 2	
<ul style="list-style-type: none"> • At 5m offset scan station <ul style="list-style-type: none"> ○ Natural light <ul style="list-style-type: none"> ▪ Dust ▪ Flashing amber light ○ Simulated darkness <ul style="list-style-type: none"> ▪ Dust ▪ Flashing amber light 	<ul style="list-style-type: none"> • At 5m offset scan station <ul style="list-style-type: none"> ○ Natural light <ul style="list-style-type: none"> ▪ Dust ▪ Flashing amber light ○ Simulated darkness <ul style="list-style-type: none"> ▪ Dust ▪ Flashing amber light
<ul style="list-style-type: none"> • At 3m offset scan station <ul style="list-style-type: none"> ○ Natural light <ul style="list-style-type: none"> ▪ Dust ▪ Flashing amber light ○ Simulated darkness <ul style="list-style-type: none"> ▪ Dust ▪ Flashing amber light 	<ul style="list-style-type: none"> • At 3m offset scan station <ul style="list-style-type: none"> ○ Natural light <ul style="list-style-type: none"> ▪ Dust ▪ Flashing amber light ○ Simulated darkness <ul style="list-style-type: none"> ▪ Dust ▪ Flashing amber light
<ul style="list-style-type: none"> • At 1m offset scan station <ul style="list-style-type: none"> ○ Natural light <ul style="list-style-type: none"> ▪ Dust ▪ Flashing amber light ○ Simulated darkness <ul style="list-style-type: none"> ▪ Dust ▪ Flashing amber light 	<ul style="list-style-type: none"> • At 1m offset scan station <ul style="list-style-type: none"> ○ Natural light <ul style="list-style-type: none"> ▪ Dust ▪ Flashing amber light ○ Simulated darkness <ul style="list-style-type: none"> ▪ Dust ▪ Flashing amber light

The scan number was logged against the checklist along with any notes regarding issues or changes to ensure that during processing the correct scans were being referenced to the changing variables.

4.2. Data processing

In order to compare the scan data collected, the raw scans required processing to generate point cloud and surface mesh files from individual scans. This processed data was then imported into a 3D modeler software where the resulting point clouds and surface mesh files could be assessed for variations resulting from the changes in environmental conditions.

The results help to answer the research sub question:

What affects will changes in the environment have on the scan data?

Three assessments were made:

1. A comparison of surface models between unpainted and painted target objects to assess if there was a significant enough difference to affect further assessment.
2. A cross section of the target object surface for a JRC comparison to the BC scale from each distance-to-object range and both scanner speeds.
3. A comparison of different environmental conditions on the surface models generated.

4.2.1. Raw data processing

For processing the raw scan data into usable file formats Faro Scene Process (Faro 2019) software (Scene) was used. When processing the raw scan data, a scan was imported into Scene to load the data allowing for pre-processing. No filters were applied during the pre-processing stage to enable a clear impression of the actual scan pickup including airborne dust particles, as this ensured no points were lost during processing. Figure 21 shows the Scene processing window where only the 'create scan point cloud' option was selected.

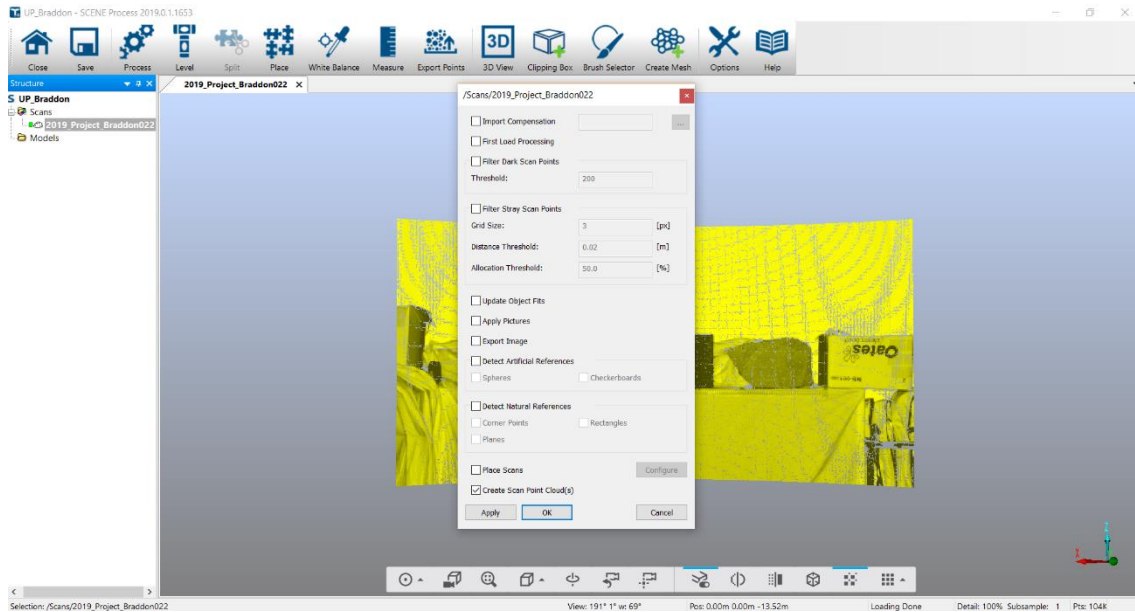


Figure 21: Pre-processing window options in Scene (Faro 2019).

Figure 22 is an example of a point cloud created during processing prior to being cleaned of the excess background points. Once cleaned of excess points a surface mesh could be created as seen in Figure 23 where both a triangular frame view (also called a TIN or wire mesh depending on the software used) and a surface mesh view can be seen.

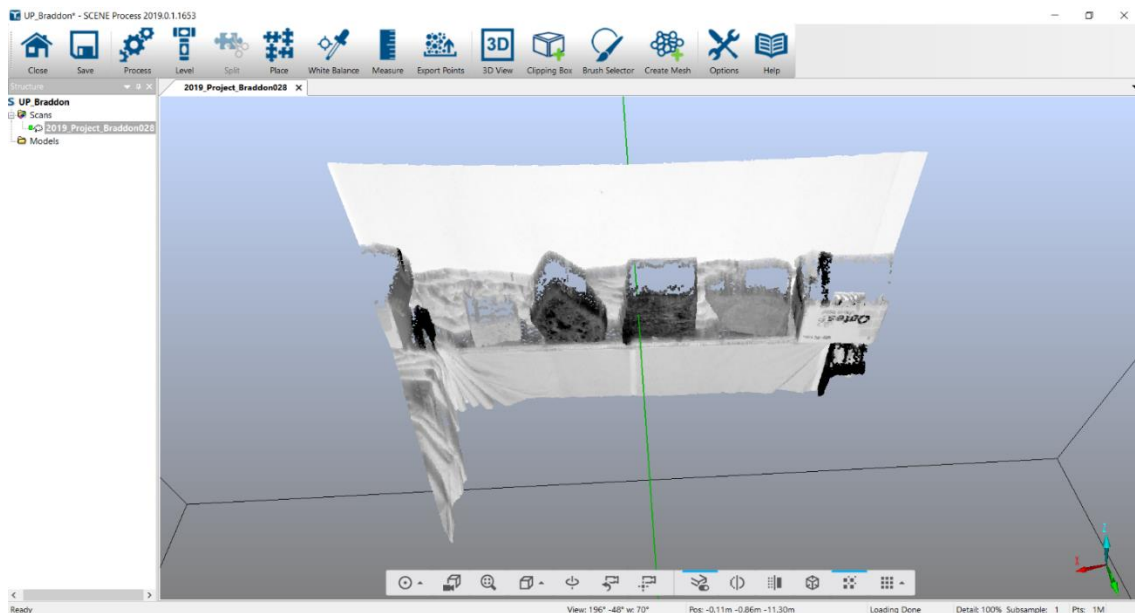


Figure 22: Point cloud created during processing.

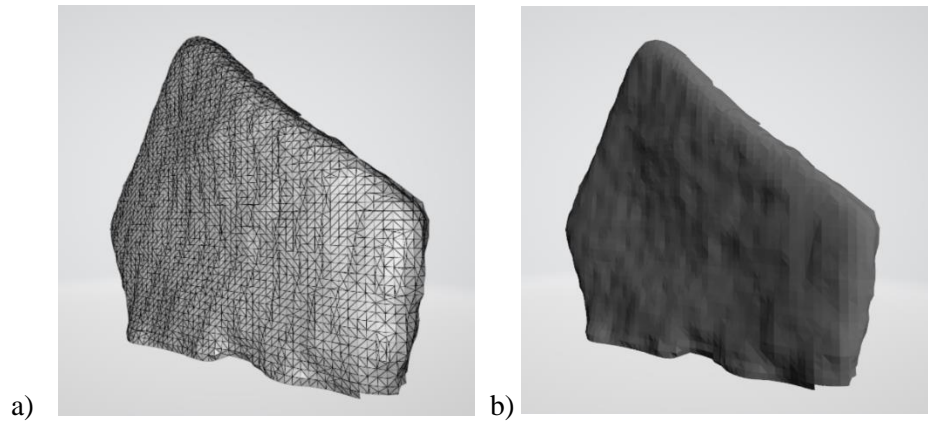


Figure 23: Surface mesh created a) with triangular frame visible, b) solid mesh view.

Once the point clouds and mesh surfaces were created the files were then exported in the following formats:

- | | |
|---|--|
| <ul style="list-style-type: none"> • Point cloud files • Unordered .E57 • Ordered .ptx | <ul style="list-style-type: none"> • Mesh surface files • All targets .stl |
|---|--|

An ‘.E57’ file is a compact, vendor-neutral format that is used to store data produced by 3D imaging software like Scene in both binary and ASCII. A ‘.PTX’ file is a binary file format that stores data directly in binary code the same as the Faro .FLS, however the .PTX format is compatible with more 3D modeler software packages. The mesh surface format ‘.STL’ is another neutral format similar to .E57, it is widely used to share models across different 3D modelling software packages and once imported can be converted to the required native format (Thomson 2019). These three file formats were chosen because of their flexibility and usability within different 3D modeler software packages.

When exporting the file formats from Scene, an Unordered format means that the scan points of the selected scan are exported, whereas an Ordered format means that the point cloud generated from the selected scan is exported (Faro 2019).

The processed file formats needed to be imported into a 3D modeler software to allow results to be compared. CloudCompare was used to compare 3D models for this dissertation.

4.2.2. Processed data comparison

CloudCompare is a free 3D modelling software that can perform many 3D modelling tasks, including cloud-to-cloud and cloud-to-mesh comparisons as well as surface slicing (CloudCompare 2019). These three specific tasks were required in order to assess the processed point clouds for the changes in environmental conditions and scan settings.

CloudCompare itself does not hold a set unit of measure; all results produced are in the value of the imported point cloud. Faro point clouds are measured in millimetres; therefore, all CloudCompare results are in the metric system for this dissertation.

Prior to any comparison between point clouds the excess background points were cleaned and the individual targets were extracted to ensure all copies of the targets were covering the same surface area. This enabled a cleaner alignment of individual targets and quicker processing time due to the time demand excessive points place on the software.

As seen in Figure 24 the individual targets were cleaned and extracted from the point cloud and saved for future use in comparison testing.

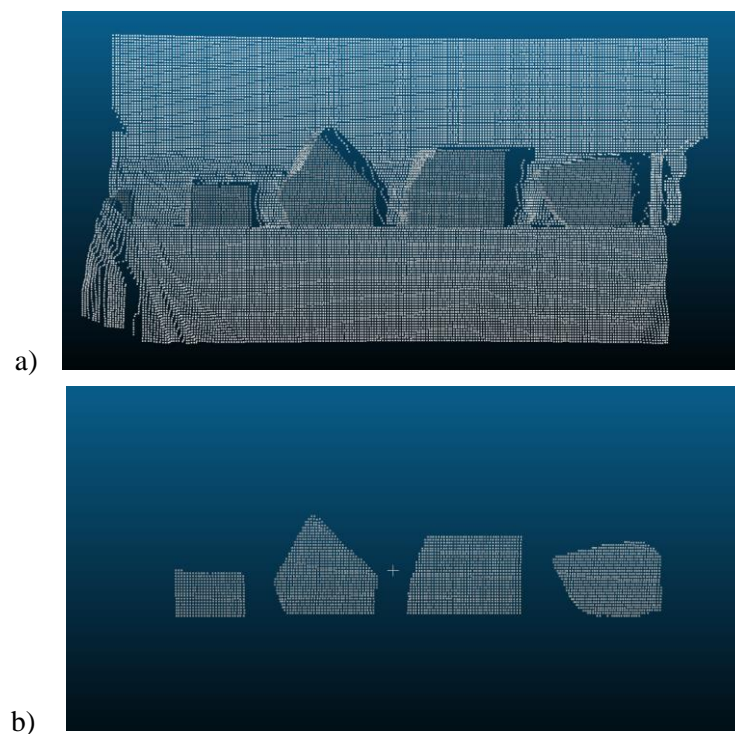


Figure 24: Point cloud a) pre-clean, b) post clean.

The density of the point clouds from the two scan speeds were assessed. The difference in density not only provides a difference in the quality of the surface once modelled but is also required for conducting cloud-to-cloud comparison which are discussed in Section 4.2.2.2 *A distance comparison of 3D models*. The results will vary depending on which point cloud is used as the *reference* model and which the *comparison* model (CloudCompare 2019). The variation in points collected between the unpainted and painted target listed is partially due to the cleaning of the point cloud. It is clear however, that Speed 2 collected a significantly larger amount of points, increasing the 3D model accuracy of the surface captured.

The density of point clouds for Target 1 with an average distance between points:

- | | |
|------------------------------------|------------------------------------|
| • Unpainted | • Painted |
| Speed 1 = 3496 pt, 8mm between pt | Speed 1 = 3401 pt, 8mm between pt |
| Speed 2 = 10465 pt, 1mm between pt | Speed 2 = 10559 pt, 1mm between pt |

4.2.2.1. 3D model alignment and registration

Before a cloud-to-cloud or cloud-to-mesh comparison can be made, the two models selected must be aligned. This is done by performing a rigid transformation to make one model move relative to the other (CloudCompare 2019). CloudCompare has two main ways of performing a rough registration and alignment:

- **Match bounding-box** is the easiest and simplest alignment tool in CloudCompare; it aligns the centres of the two bounding-boxes into the same position; however, it cannot rotate them to fully align the clouds. This final rotation and translation can be performed using the Rotate/Translate tool.
- **Picking equivalent point pairs** enables the selection of common points within the two point clouds to be selected and used for registration and alignment. This manual selection method can produce quite accurate alignments with no need to perform a second rotation and translation.

After the rough registration and alignment is complete, a fine registration can be performed using the Iterative Closest Point (ICP) algorithm available in CloudCompare. The three main parameters are:

- **The number of iterations/Root Mean Square (RMS) difference** to be run; this can be a set maximum number of iterations or a threshold value of the RMS difference.
- **Final overlap**, the portion of the register cloud to overlap the reference cloud enabling models with only a partial overlap to be aligned.
- **Adjustment scale** determines a potential difference in the scale of the models and adjusts it to the reference clouds scale.

Advanced parameters include:

- Random sampling limit
- Rotation
- Translation
- Enable farthest point removal
- Use displayed model/data scalar field as weights.

The alignment does not alter the point clouds themselves, just their relative position to each other.

For this dissertation, the ‘picking equivalent point pairs’ option was used for aligning the targets followed by a fine registration of 100% overlap with 6 iterations to match the closest points. This resulted in a clean overlap that enabled an assessment of the difference in distance between the two point clouds. Figure 25 shows the registration results for a target object during alignment with the transformation matrix and RMS that were calculated.

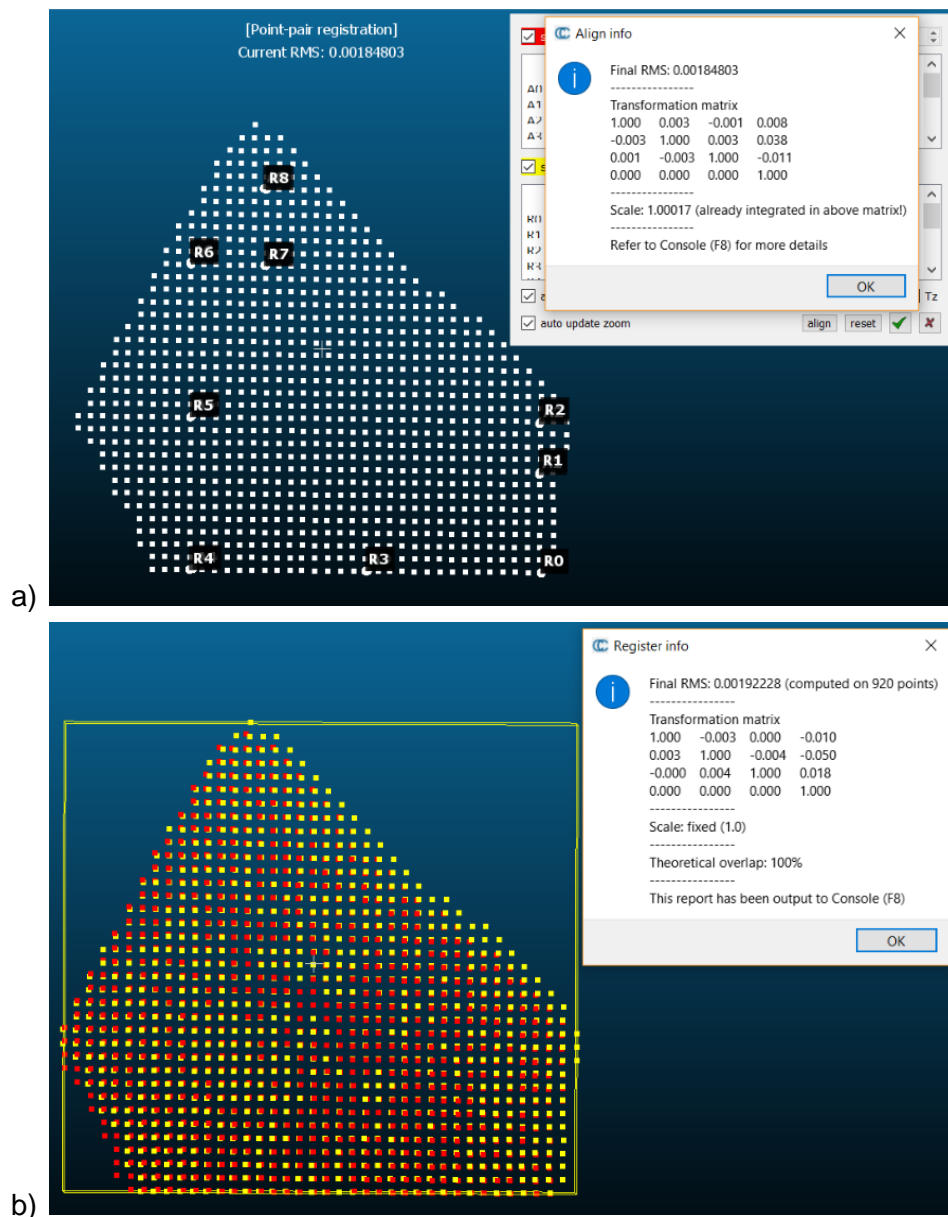


Figure 25: a) Rough alignment, b) Fine registration of a target object.

It was found that the best rough alignment results and subsequent fine alignment results were achieved from selecting four to five points at the corners of each target. Once the selected point clouds or mesh were aligned comparisons could be conducted.

4.2.2.2. A distance comparison of 3D models

Initially, a comparison between the unpainted and painted point clouds was conducted to assess if there were any notable difference between the two due to the natural colour of the target objects. This enabled a decision to be made on what set of point clouds to proceed with for further assessment.

When performing a cloud-to-cloud comparison the *reference* cloud should hold the widest extent and the highest density whenever possible. The distances will be computed relatively to the *reference* cloud points. The distance variations in the *comparison* cloud will be calculated relative to the *reference* cloud and the results show how the *comparison* cloud differs.

CloudCompare initially computes the approximate distances, this is done by selecting a mathematical model to use from the list below:

- **Least Squares Plane**, this plane is used directly to compute the distances and is more robust and good for compensating for noisy data.
- **2D1/2 Triangulation**, the projection of the original 3D points are used as vertices to generate a 2.5D mesh.
- **Quadratic Height Function**, the plane normal is used to choose the right dimension for 'Z' by running a 6-perimeter quadratic function, which is good for clean data with high curvature.
- If no preference option is selected the default setting is nearest neighbour as seen in Figure 26. However, this is the least accurate option.

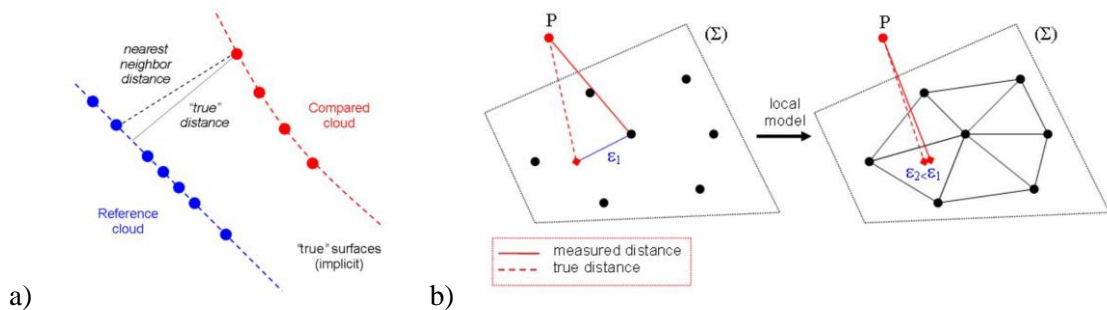


Figure 26: Two methods of measurement computation. a) Nearest Neighbour, b) 2D1/2 Triangulation. (CloudCompare 2019)

The resulting computation then generates a colour scale model representing the distance variations between the *reference* cloud and the *comparison* cloud. The results can be viewed as a histogram. Figure 27 shows the results of an assessment between an unpainted and painted target at the two scanner speeds which produce different point cloud densities. All four targets at the 1m and 5m distance-to-object ranges, at both scanner speeds were compared to assess for a difference between unpainted and painted targets. The 3m distance-to-object range was not required for this assessment.

The 2D1/2 Triangulation mathematical model was used for this assessment as the original 3D points are used as vertices.

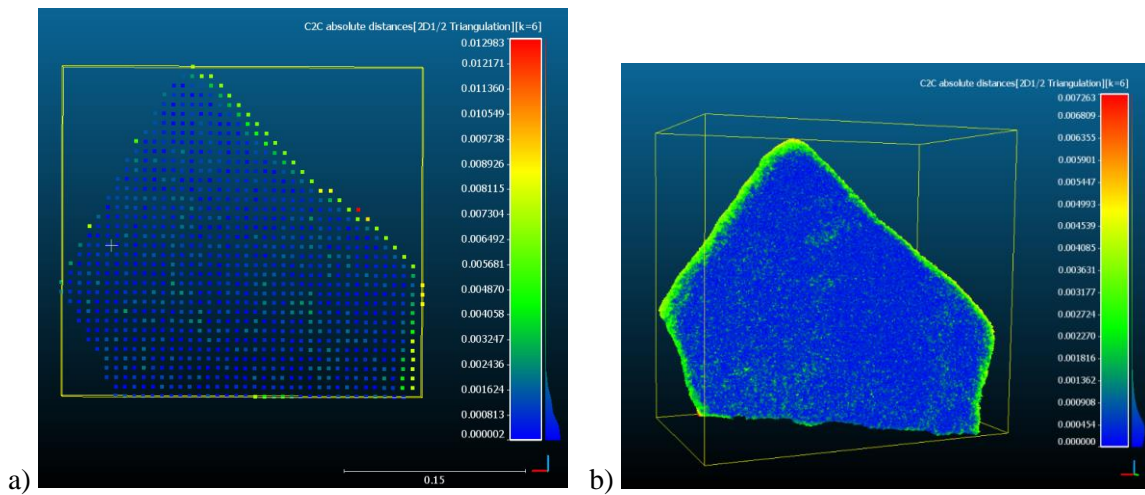


Figure 27: Point cloud alignment a) Scanner speed 1, b) Scanner speed 2.

The histogram scale to the right shows that at both speeds the targets can be matched to within 1 millimetre for the majority of points. This will be discussed in further detail within the next chapter however it can be noted that the differences in the two images is due in part to the number of points collected at each scanner speed and therefore the number of calculations that can be performed for the alignment.

The distance comparison assessment was used for both assessing the difference between unpainted and painted targets and in assessing the effects of the changes in the environment on the targets captured.

4.2.2.3. Cross section of the target object surface for comparison to the BC scale.

A surface mesh of the individual targets was created and used to compare a section of a target to the BC scale. This enabled a visual comparison between a sample of the target surface to the BC scale. The assessment was done to see if the slices generated from scan data produced a comparable result to the manual method of using a profile comb. The manual method using a profile comb involves pressing the comb against the rock face to gain an impression of the surface, then laying the comb down on the paper report to trace the captured impression. The traced impression is then compared in a side by side visual assessment to the BC scale. Figure 28 shows the Barton comb produced by Matest (2018) for this task and the BC scale.

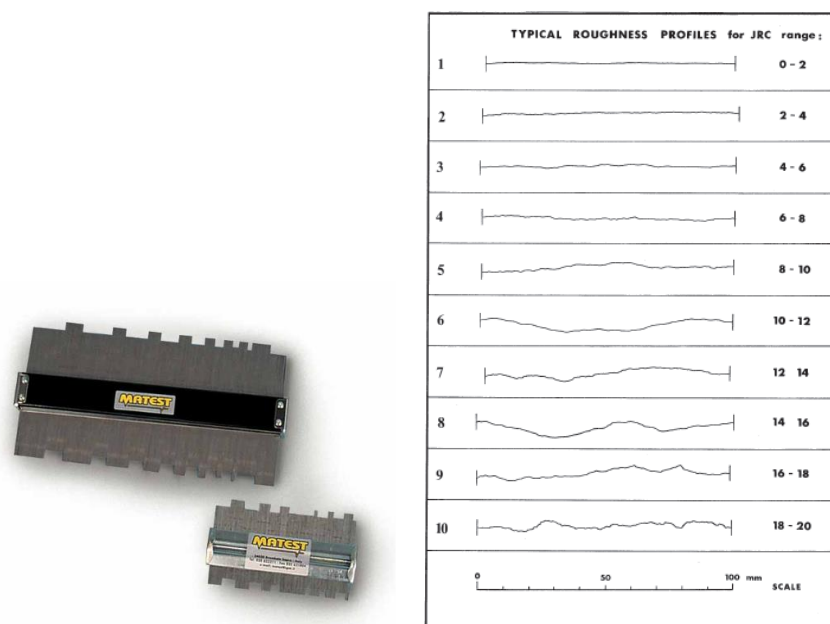


Figure 28: Matest Barton comb and Barton and Choubey scale.

When creating a mesh in CloudCompare (2019) there are four ways the surface mesh can be generated, the orientation of the point cloud and the desired results will influence which method is used.

CloudCompare mesh generation options:

- **Delaunay 2.5D (x,y)**, corresponding 2D points are triangulated and the mesh is applied to the 3D points. A length for the triangle edges must be specified to ensure no large or elongated triangles are generated. Used for point clouds orientated as a horizontal surface.

- **Delaunay 2.5D (best fit)**, the 3D point cloud is projected onto a best fit plane using least squares before the 2D points are triangulated and the mesh created as with Delaunay 2.5D (x,y).
- **Surface between two polylines**, the mesh can be created on the polylines best fit plane or by its current orientation in the workspace window.
- **Mesh scan grid**, creates a robust mesh per scan grid generated from Faro files. A minimum angle is selected to remove thin triangle structures.

As the raw scan data was captured and processed in Faro systems producing ordered point clouds the 'Mesh scan grid' option was selected for all surface mesh created for the data analysis.

Within CloudCompare there is a 'slice' function, this enables a 3D object to be segmented either by selecting a specific location on the 3D surface or by specifying the spacing distances between repeated slice segments. The orientation of the 3D surface in the workspace window affects the repeated slicing as the operation is conducted from the top of the workspace window down.

By selecting a specific location on the surface mesh of the individual target objects a comparison between a measured section of the surface captured and the BC scale was achieved. The CloudCompare slice box can be set to the desired length, depth and width of the slice as seen in Figure 29. The slice box initially covers the full target extent, the same location on each repeat target can be located by adjusting the x and z positions accordingly. Due to the orientation of the target in the workspace window the y value represents the targets depth, to gain the profile of the surface this value was not adjusted.

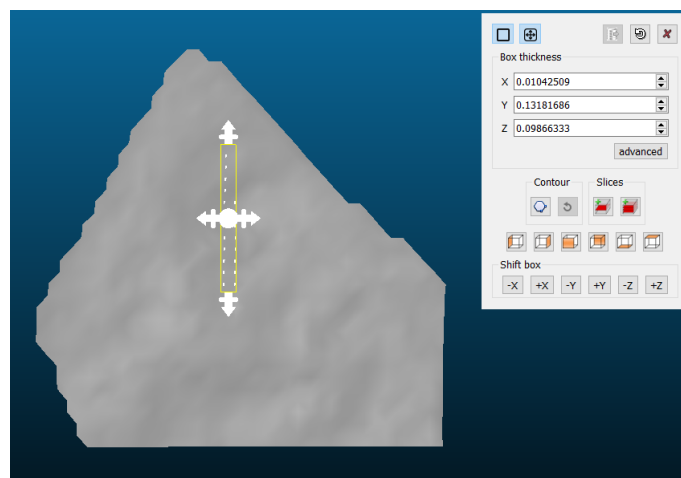


Figure 29: CloudCompare 'slice' function.

The slice was a section 100mm by 10mm to match the BC scale length, taken from the same location of the target for each scan variation. This enabled a rough comparison between the target and the BC scale as seen in Figure 30. This was performed for all four targets at both scanner speeds on all station offsets to assess if a suitable JRC estimate could be made. The slice was then thinned to 100mm by 2mm for a clearer comparison to the BC scale sample.

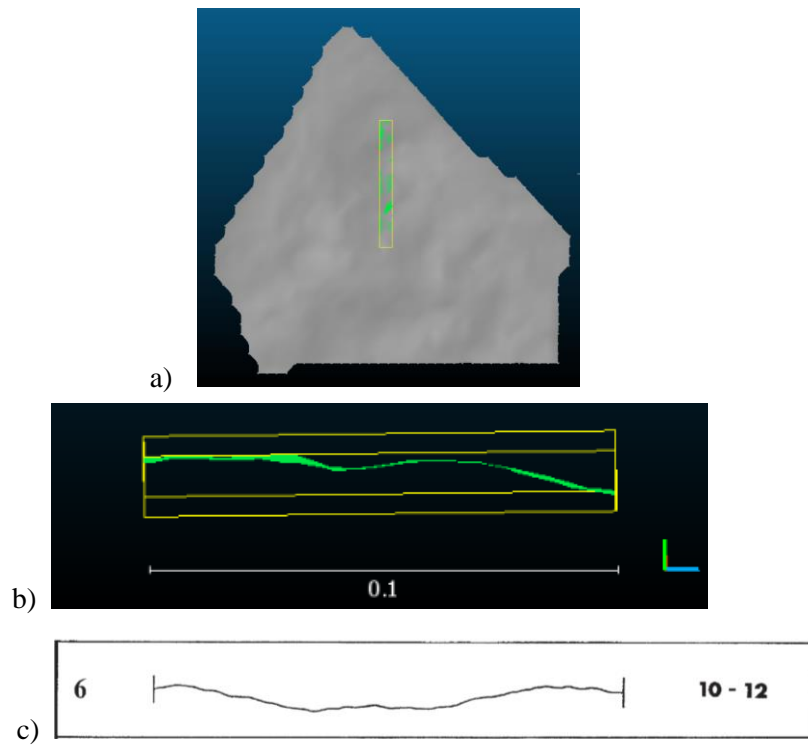


Figure 30: a) Target object 2 with slice box (yellow), b) Slice side profile in horizontal for comparison, c) BC scale sample 10-12.

4.2.2.4. Comparing the different environmental conditions on the 3D models.

To ensure all the scans were tracked and assessed as intended a naming convention was used. This was established during the raw processing stage and followed through into all subsequent stages. Table 7 provides a guide to the shorthand terms used within this section and in Section 5 *Analysis and Results*.

Table 7: Data file naming convention.

Shorthand	Full meaning
Sp1	Scanner speed 1: 1/10 x6, Points 4096 pt/360 Speed 122 kpt/sec
Sp2	Scanner speed 2: 1/2 x2, Points 20480 pt/360 Speed 488 kpt/sec
Lt	Light: Room light was on and roller door open to let in natural light.
D	Dust: Dust was dispersed between the scanner and target.
FL	Flashing Light: The amber flashing light was on.
Dr	Dark: The room light was off and roller door shut to block light.
P	Painted targets.
UP	Unpainted targets.
1m	Distance-to-object in metres.
P_Sp1_Dr_D_Comment	Painted target at scanner speed 1 in dark conditions with dust, and a comment if required.

To assess the effects of changes in the environment on the target scans the process was broken down into stages.

Stage 1: The sets of scans, such as the six scans associated with Sp 1 at 1m distance-to-object, were cleaned of excess points as seen in Figure 31. The initial scan for the set was cleaned to retain the curved edges of the targets, the five subsequent scans in the set were then cleaned exclude the curved edges. This was to ensure when the cloud-to-mesh comparison were conducted the reference surface mesh held the larger surface area as mention is Section 4.2.2.2 *A distance comparison of 3D models*. This reduced the risk of producing outliers from the point cloud that could affect the results of the assessments conducted.

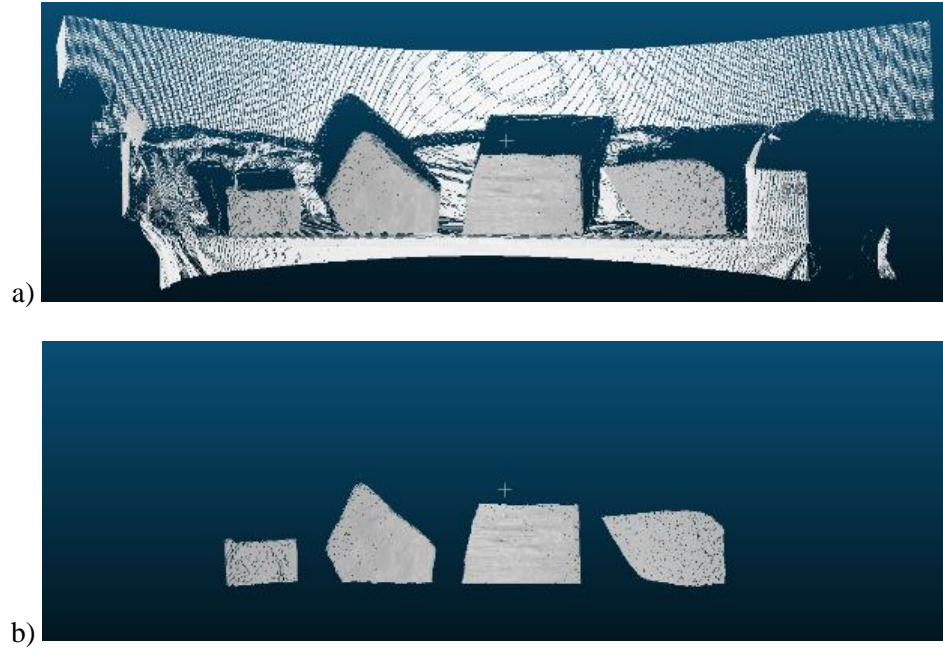


Figure 31: Scanner speed 1 at 1m in light a) uncleaned, b) cleaned.

Stage 2: The cleaned point clouds enabled a visual inspection for obvious differences as seen in Figure 32. It shows that the scan conducted in light (Lt) conditions and the scan conducted in light with airborne dust (Lt_D) conditions have a visual difference. This is from the scanner picking up the airborne dust in front of the target causing peaking in the point cloud.

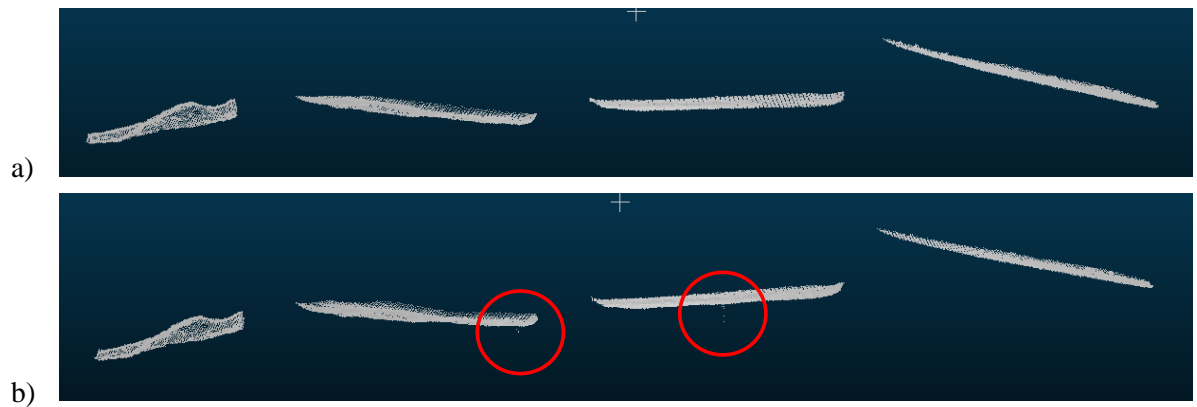


Figure 32: Visual inspection between scan a) Lt, b) Lt_D.

Stage 3: A surface mesh of the initial scan for the set was generated. This mesh was then used to conduct a cloud-to-mesh distance comparison to each of the following scans in the set, enabling an assessment on how closely the two 3D models being compared

matched. The point cloud of the following scan was aligned to the surface mesh using the same procedure mention in Section 4.2.2.1 *3D model alignment and registration*.

When performing a cloud-to-mesh distance comparison, CloudCompare first computes an approximate distance which is used initially to set the best octree level for the real distance computation. The octree is the recursive partition of a point cloud into cubes, the primary cube is divided into eight then those eight are divided into eight and so on as seen in Figure 33.

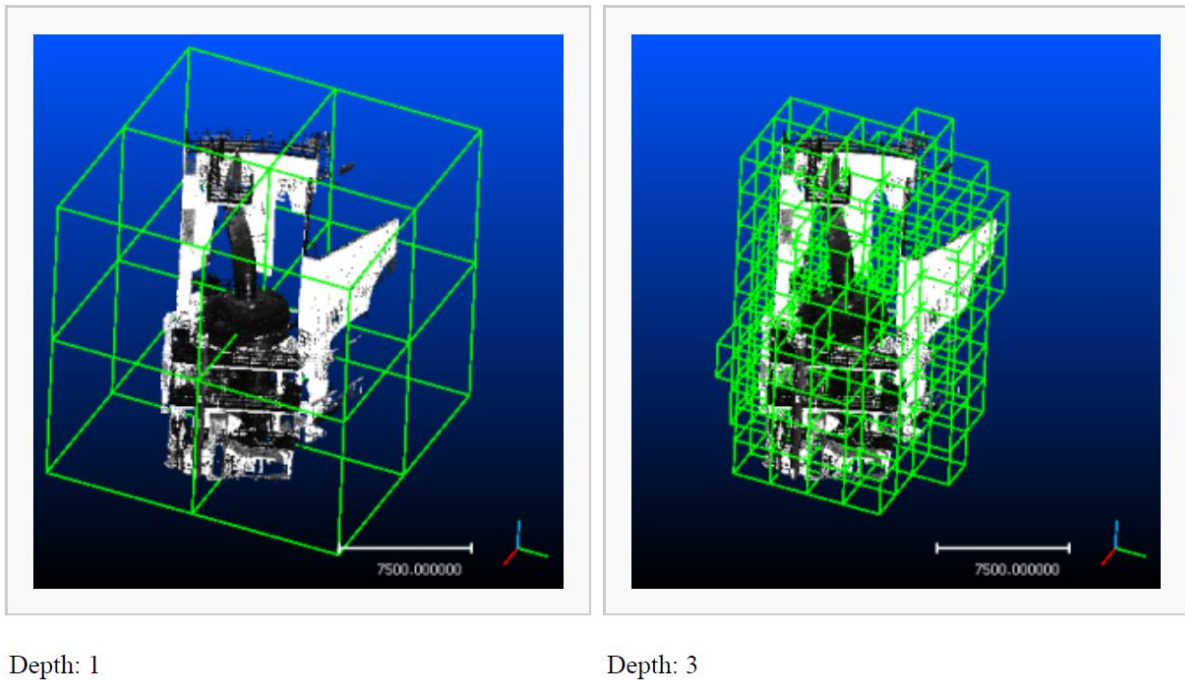


Figure 33: Recursive subdivision of octree cubes (CloudCompare 2019).

The octree in CloudCompare is a list of numerical values that locate the position of points with a code which is suited for spatial indexing (index value). The subdivision can be performed 10 times generating a 32 bit index value for the smallest sub-cubes, it is formed by concatenating the 3 bit location set for each sub-cube (Figure 34) (CloudCompare 2019).

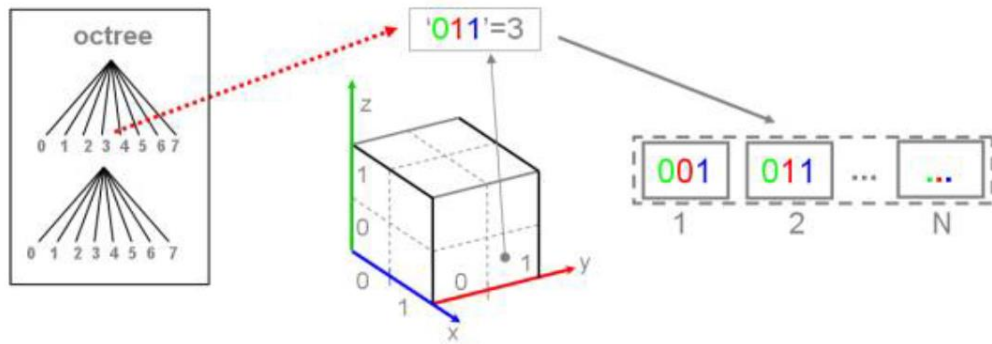


Figure 34: Octree numeric code principle (CloudCompare 2019).

The nearest neighbours calculation is run on the points within each sub-cube minimising the number of points that need to be assessed to those bound by the cube. This is performed for each individual cube to make up the whole assessment.

From the assessment, two results were gathered to gain an understanding of how reliable the measurements were and thus, how closely the two 3D models resembled each other after a change in environmental conditions:

- The resulting histogram for the distance comparison gave an understanding of how closely the point cloud being assessed matched the base surface mesh.
- The Gauss distribution (normal distribution) was calculated to gain the standard deviation of the points around the mean of 0mm to assess how closely the two models aligned, and to what extent there was deviation due to the change in environmental conditions.

The Gauss distribution was calculated at 0μ , 2σ , assessed against 16 nearest neighbours providing a confidence interval of 95%.

Figure 35 is an example of the results that were achieved. It shows that with airborne dust in the environment there is a range for -4.5mm to 3mm between the surface mesh and the compared point cloud. This is due to the peaking and shadowing caused by obstacles in the laser path. When assessing the point cloud in CloudCompare it could be seen where the airborne dust was captured and what target was affected. In this example it was Target 1 that produced the largest deviations (Figure 36).

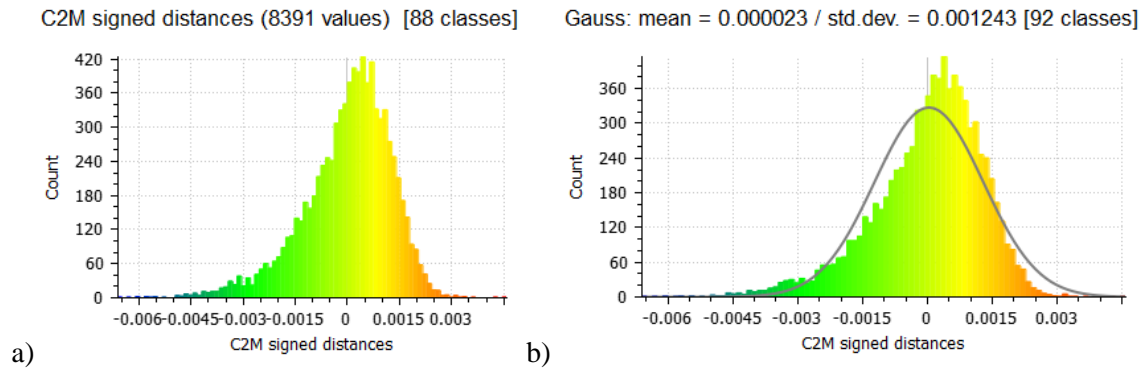


Figure 35: Sp1 3m flashing light a) C2M distance comparison, b) Gauss standard deviation.

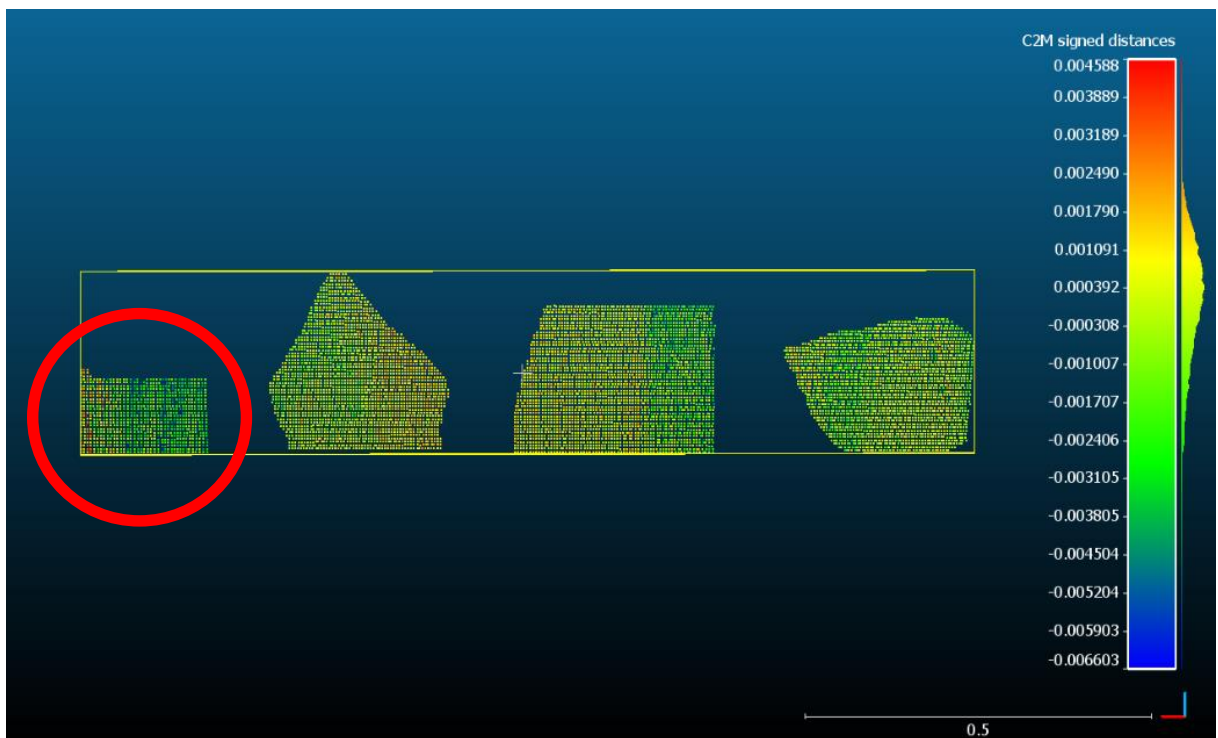


Figure 36: Target 1 (red circle) showing the effects of airborne dust.

This provided a model to assess the precision and accuracy of the cloud-to-mesh distance assessment. *Precision* is deemed as being how close the different observations are together, and *Accuracy* is how close the different observations are to the true value. In this assessment the true value is that of the surface mesh generated from the first scan of the set, therefore the *Precision* is how closely the point cloud of the subsequent scan matched the surface mesh providing the degree of consistency, while the *Accuracy* of the point cloud to the surface mesh provided the level of exact duplication between the two 3D models.

A table of the individual results was produced to assess common variables in the scans that produced deviations. This assessment enabled the author to gain an understanding of what environmental changes would affect the scan and if it was to a degree that would affect gaining a viable slice sample for a JRC assessment as described in Section 4.2.2.3

Cross section of the target object surface for comparison to the BC scale.

4.3. Feasibility assessment of using a mobile platform

With the acquired data from the TLS setups consideration into the feasibility of using a mobile platform to achieve the same results was given. This consisted of what additional tests would be required in a future study to ascertain if the same results from a TLS could be achieved. These tests may include the effects of a change in platform speed and scanner speed on the target, and the difference between various mapping algorithms.

4.4. Summary

The methodology conducted was aimed at providing information and data to answer the research question and sub-question:

How might an underground working environment affect laser scan data when assessing JRC?
What affects will changes in the environment have on the scan data?

The software processes used were systematic to ensure duplication was possible. Faro and CloudCompare both provide thorough guides on how to use their software for both simple and complex tasks.

During the raw data processing, the output results were saved in a format that was usable in a wide range of available modelling software packages. This was done to ensure that the data could be used in multiple software packages for redundancy as both the E57 format and PTX format are widely accepted.

A uniform naming convention was used for all files produced to ensure all data was traceable and correctly grouped.

The standards used during the modelling analysis were:

- For aligning two point clouds, the ‘picking equivalent points’ option was used followed by a fine registration of 100% overlap with 6 iterations to match the closest points.
- The best alignment results were achieved by selecting four to five points on each target located at the corners.
- Point cloud distance comparisons were conducted using the ‘2D1/2 Triangulation’ mathematical model as the original 3D points are used as vertices.
- Mesh generation was conducted using the ‘Mesh scan grid’ option, which is complementary to point clouds processed in Faro software.
- The slice function was used to extract a 10cm segment of the targets to compare with the BC scale JRC guide, replication the manual method.
- For comparing the changes in the environment, a surface mesh of the first scan in light conditions of the set was developed retaining the curved edges.
- Subsequent scans in the set were cleaned to not include the curved edges of the targets to ensure the surface mesh held the larger surface area minimising the effect of outlier points on the Gauss distribution results.
- Images and data of the resulting histograms were gathered, and standard deviation data was compiled for an analysis of the results from each assessment.

The processes chosen for this dissertation are just one of many available in the software used, similar results can be achieved in a number of ways. The author chose this procedure based on the desired end results and accuracies for the project, its simplicity, and repeatability.

Chapter 5. Analysis and Results

This chapter assesses the results of the data analysis answering the research questions:

How might an underground working environment affect laser scan data when assessing JRC?
What affects will changes in the environment have on the scan data?
Is it feasible to use a mobile platform for this task?

The analysis was conducted to assess if a manual sample of a JRC from the BC scale could be duplicated effectively using the Faro Focus^{3D} scanner, what effects changes in the environment would have on scan data, and if it was feasible to move forward into testing MLS using the Faro Focus^{3D} scanner to achieve the same results in a future project.

5.1. Unpainted target versus painted targets

As described in Chapter 4 Section 4.2.2.2 *A distance comparison of 3D models*, after the point clouds were cleaned of unrequired background points a distance comparison between two aligned point clouds was conducted to assess if any significant variation was visible between the unpainted and painted targets. The point cloud comparison between the unpainted and painted targets at both 5m range and 1m range showed that minimal variation in the point cloud surface could be seen, with the variation in the painted targets being a fraction of a millimetre (Figure 37).

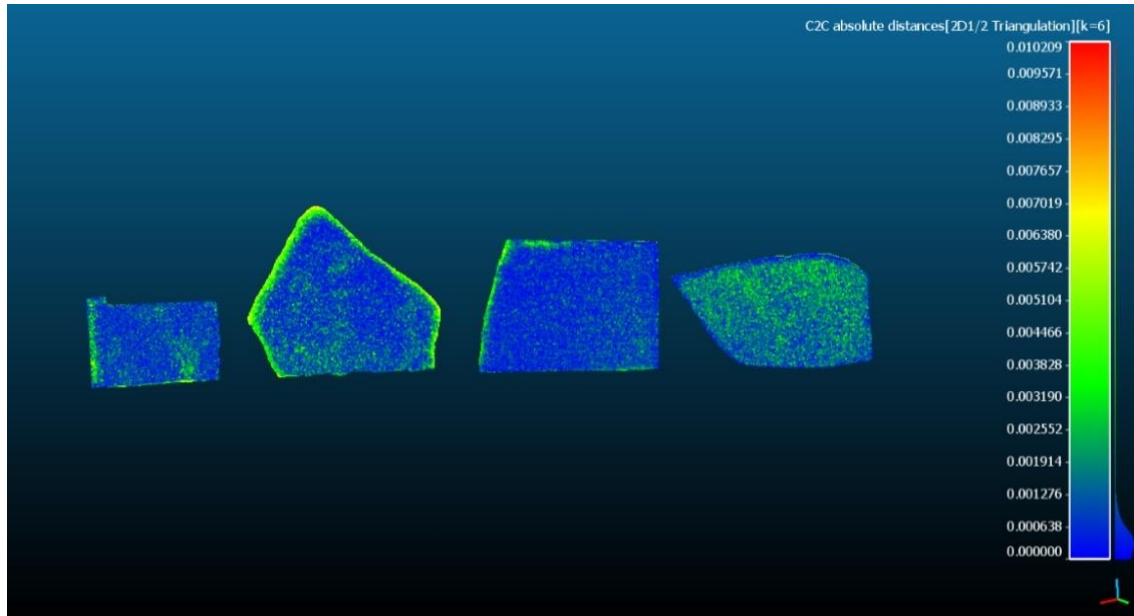


Figure 37: Difference between unpainted and painted targets at scanner speed 2.

Variations created between the two scanner speeds and the distance-to-object ranges are evident due to the density of the point clouds as seen in Table 8. This is most visible in the histogram graphs where the vertical bars are indicative of the number of points calculated. Minor variations can also be attributed to the process of cleaning the point clouds prior to alignment and the alignment itself, but this had no significant impact on this assessment.

A closer inspection of Target 1 (T1) in Table 8, showed the minor variations between the unpainted and painted targets had a consistent change relevant to the way the target was aligned, the first sample being aligned down the centre of the target only. Care was taken to ensure a uniform alignment after the initial sample as the accuracy of the alignment impacts the distance comparison results as discussed in Chapter 4 Section 4.2.2.1 *3D model alignment and registration*.

The histograms show clearly the variation in point cloud density based on the scanner speed and the distance-to-object range of the station; at a closer range more points will be collected regardless of the scanner speed. This is evident when looking at the difference between row: *T1 SPI_1m* and row: *SPI_5m* in Table 8. The histograms show that the majority of points had a variation of less than 0.6mm between the unpainted and painted targets. The variation could be the result of paint filling in finer surface textures.

Table 8: Target 1 Unpainted and painted comparison.

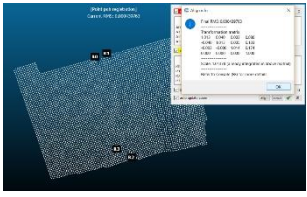
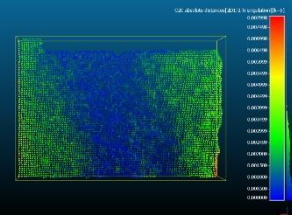
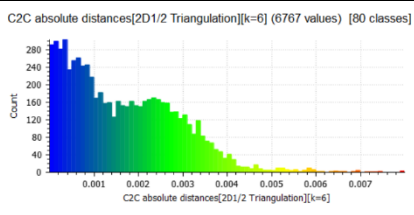


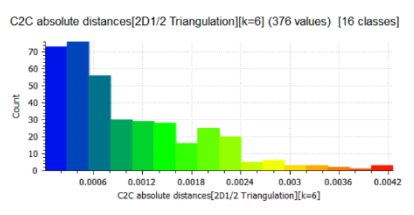
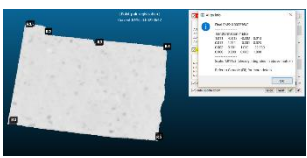
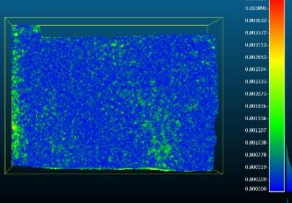
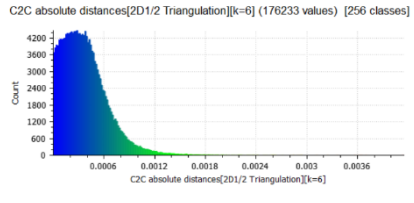
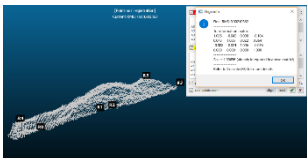
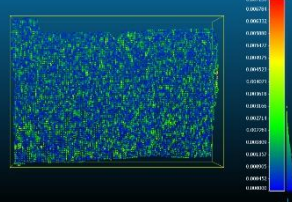
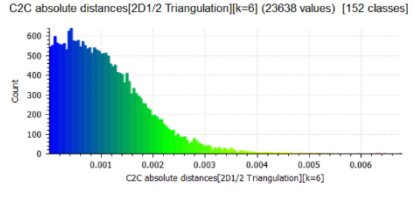
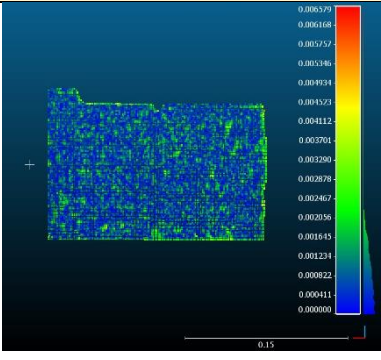
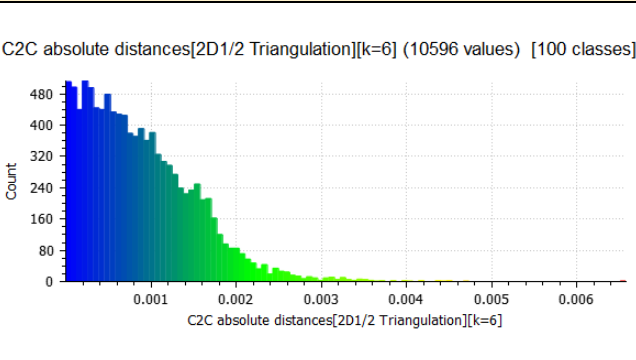
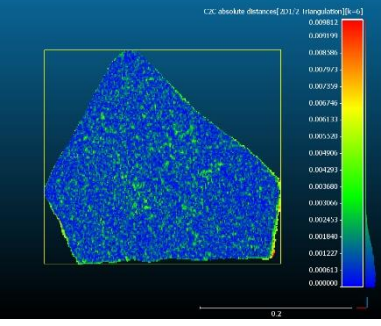
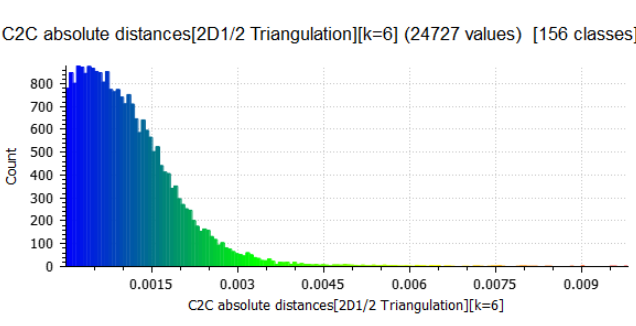
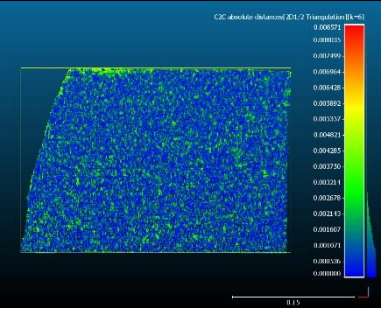
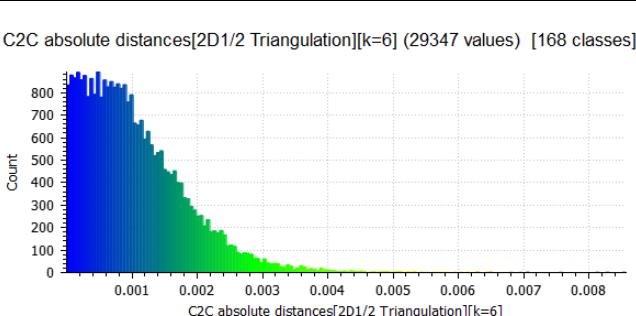
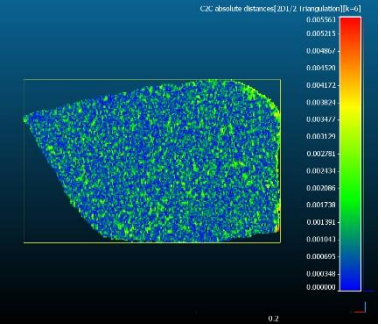
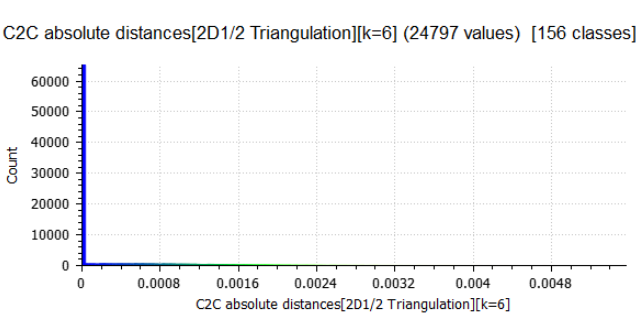
Target	Alignment	Distance comparison	Histogram
T1 SP1_1m			
SP1_5m			
SP2_1m			
SP2_5m			

Table 9 *Unpainted and painted comparison of Sp2 at 5m* shows the test results for all four targets at Sp2 with a distance-to-object of 5m. The results are consistent with the initial assessment of Target 1 in Table 8, the majority of points assessed were within 1mm or less. The variation for Target 4 (T4) in Table 9 is due to a difference in points cleaned along the right-hand side of the target prior to the test. In all future assessments the surface being assessed was trimmed smaller than the reference surface as mentioned in Section 4.2.2.2 *A distance comparison of 3D models*, to minimise the risk of outliers.

Table 9: Unpainted and painted comparison of Sp2 at 5m.

Target	Distance comparison	Histogram
SP2_5 m T1		C2C absolute distances[2D1/2 Triangulation][k=6] (10596 values) [100 classes] 
T2		C2C absolute distances[2D1/2 Triangulation][k=6] (24727 values) [156 classes] 
T3		C2C absolute distances[2D1/2 Triangulation][k=6] (29347 values) [168 classes] 
T4		C2C absolute distances[2D1/2 Triangulation][k=6] (24797 values) [156 classes] 

Due to the minimal variation between the two sets of scans the painted target scans were used for all further assessments within this dissertation, this was to reduce the potential effect of different rock surfaces holding different reflectivity values. Lemes and Zaimovic-Uzunovic (2009) demonstrated that the target colour can influence the data collected therefore the potential

variation between targets as a result of different reflectivity values was minimised to ensure they all held the same reflective value at this stage. It is the author's opinion that in a real-world application the natural rock surface would yield acceptable results for the assessments conducted in this dissertation, however it must be noted that different rock types hold different reflectivity values, and this should be taken into account in a real world scenario.

5.2. Density of point clouds

The density of the point clouds collected can be viewed in Table 10. This shows the average spacing between points from five sample locations on the individual targets providing an average density for each target at both scan speeds. As mentioned in Chapter 4 Section 4.2.2 *Data processing*, during data comparison tests the density of the point clouds not only provides a difference in the quality of the surface once modelled but is also required for cloud-to-cloud and cloud-to-mesh comparisons.

The density of the point cloud also provides a guide to the achievable accuracy that can be gained at different distance-to-object and scanner speeds. As the BC scale is a 10cm long profile sketch of the rock surface that shows changes in the surface texture of a millimetre or two, knowing the achievable point cloud density of different scan setups can help eliminate trial and error. The results in Table 10 show that Sp1 at a distance-to-object of 5m and 3m may not provide enough detail as the point spacing is $>5\text{mm}$, and Sp2 at 1m may provide too much detail as the point spacing is $<1\text{mm}$.

The Faro Focus^{3D} had a point cloud density estimate of 15.340mm at a range of 10m at SP 1 and 3.068mm at 10m for SP2 (Figure 38). This means at a range of 5m at SP2 the point cloud density should be approximately 1.5mm

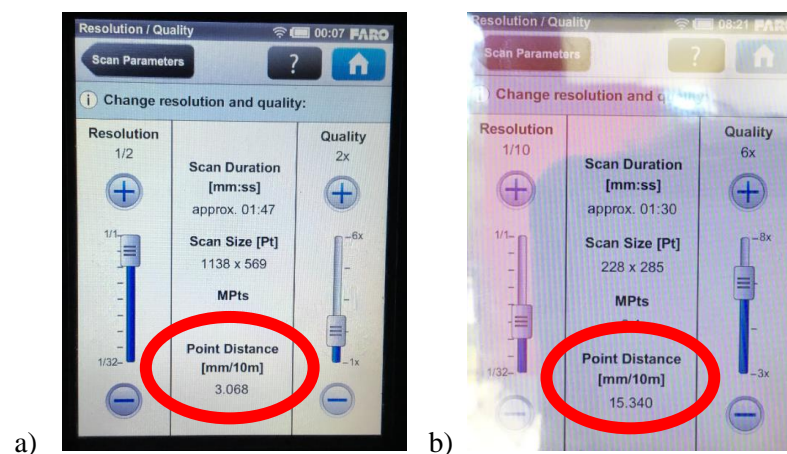


Figure 38: Faro Focus3D perimeter settings a) SP2, b) SP1.

Table 10: Point cloud density.

	SP1			SP2		
	5m	3m	1m	5m	3m	1m
T1	0.0079	0.0048	0.0018	0.0019	0.0019	0.0015
	0.0079	0.0053	0.0020	0.0016	0.0019	0.0009
	0.0072	0.0047	0.0024	0.0030	0.0021	0.0004
	0.0079	0.0050	0.0021	0.0019	0.0016	0.0004
	0.0090	0.0056	0.0027	0.0019	0.0015	0.0004
mm	0.0080	0.0051	0.0022	0.0021	0.0018	0.0007
T2	0.0079	0.0048	0.0018	0.0031	0.0010	0.0010
	0.0086	0.0049	0.0019	0.0024	0.0014	0.0003
	0.0081	0.0049	0.0024	0.0022	0.0014	0.0016
	0.0080	0.0048	0.0023	0.0030	0.0011	0.0006
	0.0077	0.0046	0.0016	0.0027	0.0009	0.0004
mm	0.0081	0.0048	0.0020	0.0027	0.0012	0.0008
T3	0.0078	0.0050	0.0016	0.0018	0.0013	0.0003
	0.0074	0.0046	0.0016	0.0032	0.0014	0.0003
	0.0080	0.0048	0.0019	0.0015	0.0016	0.0004
	0.0079	0.0050	0.0019	0.0022	0.0015	0.0005
	0.0079	0.0047	0.0017	0.0015	0.0021	0.0013
mm	0.0078	0.0048	0.0017	0.0020	0.0016	0.0006
T4	0.0080	0.0048	0.0023	0.0022	0.0013	0.0005
	0.0079	0.0051	0.0025	0.0017	0.0010	0.0009
	0.0079	0.0050	0.0023	0.0014	0.0009	0.0006
	0.0087	0.0050	0.0019	0.0025	0.0022	0.0008
	0.0081	0.0049	0.0020	0.0018	0.0020	0.0004
mm	0.0081	0.0050	0.0022	0.0019	0.0015	0.0006
Average mm	0.0080	0.0049	0.0020	0.0022	0.0015	0.0007

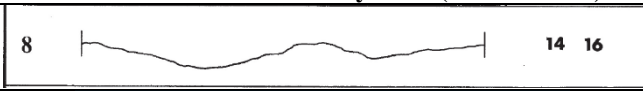

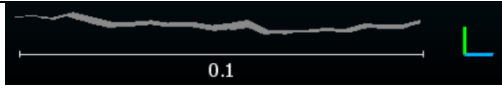
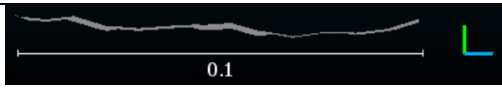
The data in Table 10 suggest that the best options for assessing the JRC against the BC scale would be Sp1 at 1m distance-to-object and Sp2 at both 5m & 3m distance-to-object as they produce point clouds with a density between 1.5mm and 2.2mm. This is representative of what can be achieved from a manual JRC assessment using a profile comb as mentioned in Chapter 4 Section 4.2.2.3. *Cross section of the target object surface for comparison to the BC scale.* It should be noted that the Faro Focus point cloud density estimates at a range of 10 were not accurate, being consistently smaller than the reality as SP2 at 5m range had a point cloud density of approximately 2mm not the Faro estimate of 1.5mm.

5.3. Cross section for JRC comparison to BC scale

As discussed in Chapter 4, Section 4.2.2.3. *Cross section of the target object surface comparison to the BC scale*, slices from the surface mesh generated from each target were taken and compared to the JRC sample from the BC scale. The slices taken were 100mm by 2mm to simulate a traced profile from a profile comb and positioned horizontally to compare against the BC scale. As the slices were a 3D model that was being compared to a 2D line, the 2mm width of the slice does appear wider in some areas, this was due to the 3-dimensional shape of the slice. Consideration was given to using a thinner width profile to better represent a drawn line; however, thinner slices produced gaps in the line and were not as easily visible in the software.



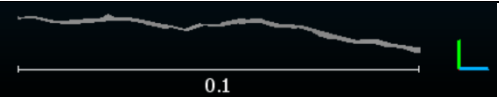

When comparing the slices taken from Target 1 at Sp1 for comparison with the BC scale, there was an identifiable difference between scans taken at the different distance-to-object ranges. The results in Table 11 show that at a distance-to-object of 1m a clear visual comparison can be made between the BC scale and the slice. However, when conducting a visual comparison on the slices from 3m and 5m a smoothing of the surface texture can be seen. This is in direct proportion to the point cloud density of the scans visible in the point density column.

Table 11: Sp1 T1 JRC 14-16 visual comparison.

T1	Slice comparison JRC 14-16 Barton and Choubey scale (Barton 2013)		Comment	Point density
BC scale				
1m			Comparable.	2.0mm
3m			Lack of detail.	4.9mm
5m			Lack of detail, smoothing of surface.	8.0mm



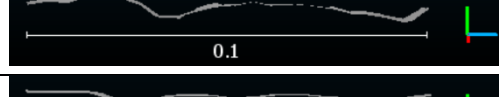
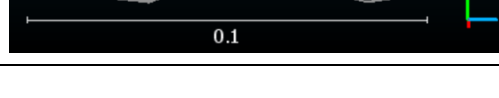
Slices taken from Target 2 produced the same results as from Target 1. While the overall target profile was visible as seen in Table 12 the surface texture was not comparable to the BC scale except at the 1m distance-to-object range. While some texture could be seen at the 3m range it was not sufficient for a clear comparison.

Table 12: Sp1 T2 JRC 10-12 visual comparison.

T2	Slice comparison JRC 10-12 Barton and Choubey scale (Barton 2013)		Comment	Point density
BC scale				
1m			Comparable.	2.0mm
3m			Lack of detail.	4.9mm
5m			Lack of detail, smoothing of surface.	8.0mm

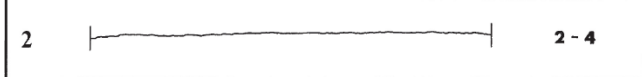

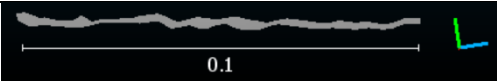

Slices taken from Target 3 showed the same trend as both Target 1 and 2. Due to the JRC 6-8 being more finely textured the smoothing of the slices at both the 3m and 5m range was more noticeable within Table 13.

Table 13: Sp1 T3 JRC 6-8 visual comparison.

T3	Slice comparison JRC 6-8 Barton and Choubey scale (Barton 2013)		Comment	Point density
BC scale				
1m			Comparable.	2.0mm
3m			Lack of detail.	4.9mm
5m			Lack of detail, smoothing of surface.	8.0mm

Slices taken from Target 4 produced the same results as the previous three targets. Table 14 showed the same lack of texture and smoothing of the surface as with the previous targets at the 3m and 5m range.


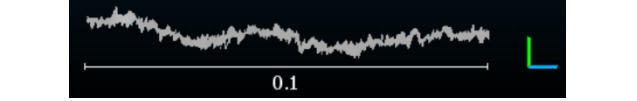
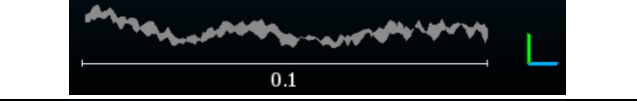
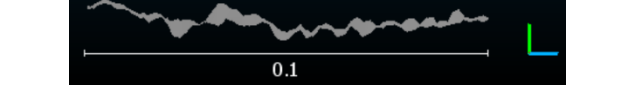
Table 14: Sp1 T4 JRC 2-4 visual comparison.

T4 JRC 2-4	Slice comparison JRC 2-4 Barton and Choubey scale (Barton 2013)	Comment	Point density
BC scale			
1m		Comparable.	2.0mm
3m		Lack of detail.	4.9mm
5m		Lack of detail, smoothing of surface.	8.0mm

The JRC comparison at Sp1 showed that the texture of the surface mesh developed for the targets is not always sufficient for a comparison test to the BC scale. The only viable slices at Sp1 were captured at the 1m distance-to-object range which produced a point cloud density of 2mm. Sp1 was resolution and quality setting 1/10 x6, Points 4096 pt/360, Speed 122 kpt/sec (Faro 2013).


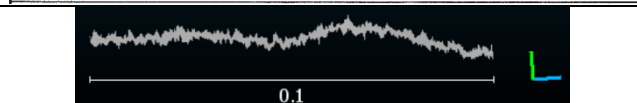
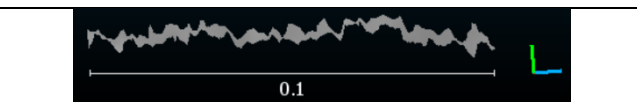
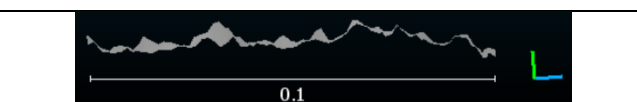
When assessing Target 1 slices at Sp2 for comparison with the JRC scale, as with the results from Sp1, there was an identifiable difference between the slices taken at different distance-to-object ranges. In Table 15, a visual comparison between the slice taken at a range of 1m showed an excess in the surface texture. This was a result from an increase in triangular pyramids generated during the surface mesh generation in CloudCompare, while a maximum side length for a pyramid can be set to reduce the creation of long slivers, a minimum length cannot be set (CloudCompare 2019). The excessive texturing made a direct comparison to the JRC scale unclear. The slice taken at range of 3m did appear to be highly textured; however, when comparing it to the JRC scale of 14-16 it does still provide a fair comparison. The clearest visual comparison was achieved at the 5m range, with a point cloud density of 2.2mm.

Table 15: Sp2 T1 JRC 14-16 visual comparison.

T1	Slice comparison JRC 14-16 Barton and Choubey scale (Barton 2013)		Comment	Point density
BC scale				
1m			Too much texture for comparison.	0.7mm
3m			Highly textured but comparable.	1.5mm
5m			Comparable.	2.2mm

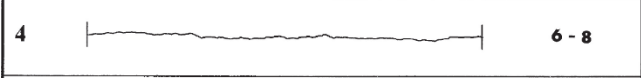
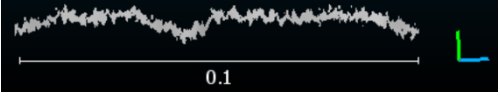


Slices taken from Target 2 produced results similar to those from Target 1. As seen in Table 16, the slice taken at a range of 1m was too textured for a clear visual assessment. The slice taken at 3m range was highly textured again but could still potentially be used for a visual comparison to the BC scale, however it is not ideal as the surface mesh slice does appear to be more textured than the actual target surface and only a familiarity with the actual target surface enabled the author to see the comparable nature of the slice. The slice taken at 5m range provided a clear comparison to the BC scale for Target 2.

Table 16: Sp2 T2 JRC 10-12 visual comparison.

T2	Slice comparison JRC 10-12 Barton and Choubey scale (Barton 2013)		Comment	Point density
BC scale				
1m			Too much texture for comparison.	0.7mm
3m			Highly textured but comparable.	1.5mm
5m			Comparable.	2.2mm


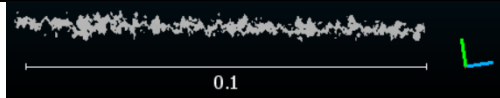
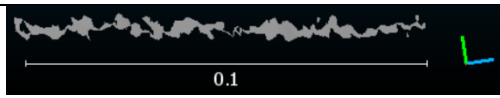
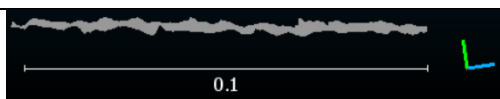
Slices taken from Target 3 showed the same trend as slices from Target 2. In Table 17, the slices taken at both 1m and 3m range were highly textured and did not produce a clear comparison to the BC scale. The slice taken at 5m range was the only slice that provided a clear visual comparison of the actual target surface to the BC scale.

Table 17: Sp2 T3 JRC 6-8 visual comparison.

T3	Slice comparison JRC 6-8 Barton and Choubey scale (Barton 2013)		Comment	Point density
BC scale				
1m			Too much texture for comparison.	0.7mm
3m			Highly textured but comparable.	1.5mm
5m			Comparable.	2.2mm

As with Target 3 slices taken from Target 4 only provide one clear visual comparison. In Table 18, it can be seen that the slices taken at both 1m and 3m ranges were highly textured and did not produce a clear comparison to the BC scale. The slice taken at 5m range was the only slice that provided a clear visual comparison of the actual target surface to the BC scale.

Table 18: Sp2 T4 JRC 2-4 visual comparison.

T4	Slice comparison JRC 2-4 Barton and Choubey scale (Barton 2013)		Comment	Point density
BC scale				
1m			Too much texture for comparison.	0.7mm
3m			Highly textured but comparable.	1.5mm
5m			Comparable.	2.2mm

The results showed that scans achieving a point density between 1.5mm and 2.2mm produced the best slice samples for comparison against the BC scale. Scans outside of this accuracy range produced surface textures that were not comparable to the BC scale. The resulting point clouds from Sp1 at distance-to-object of 3m or more did not generate enough texture due to the point density, causing smoothing of the surface model compared to the actual target surfaces. The increased point density from Sp2 at a distance-to-object of 3m or less produce excessive

texturing in the surface mesh. The increase in triangulated peaks resulted in a jagged surface that impacted the visual comparison to the BC scale and did not reflect the actual target surface.

The results from the visual slice comparison against the BC scale confirmed the estimation made in Section 5.2 *Density of point clouds*. The point cloud density could indicate the suitability of the surface mesh created for a JRC assessment against the BC scale; it is the author's opinion that a point cloud density of 2mm is ideal for the JRC visual comparison assessment. The results confirm Fekete, Diederichs, and Lato (2010) findings that satisfactory results could be achieved when using good TLS setup geometry for assessing JRC and joint sets in tunnel workings.

5.4. Environmental conditions variation analysis

When assessing the effects of changes in the environmental conditions on the point cloud data, a cloud to mesh (C2M) comparison that resulted in a deviation of 2mm or less was required. A surface mesh was generated as a reference model from the 'light conditions' point cloud from each of the six sets of scans as discussed in Section 4.2.2.2 *A distance comparison of 3D models* for the C2M comparisons.

When comparing the point clouds within a set to the reference model, the Gauss distribution (normal distribution) was calculated within CloudCompare (2019) with $\mu = 0$, $\sigma = 2$, calculated from an octree of 16 nearest neighbours as discussed in Section 4.2.2.4 *Comparing the different environmental conditions on the 3D models*. The standard deviation was plotted within the bar graph seen in Figure 39 to provide a visual comparison between the standard deviations of the 30 comparison tests conducted from the six sets of data.

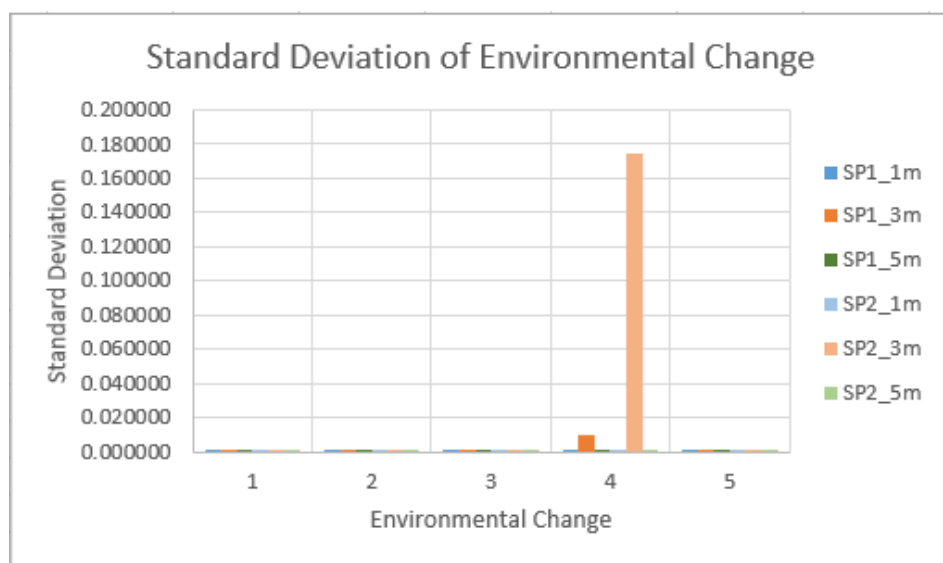


Figure 39: Standard Deviation of Environmental Changes.

The graph has the Standard Deviation on the Y axis and shows the difference in millimetres between the point clouds when compared to their relevant surface mesh within their set. The X axis (Environmental Change) is separated into five groups:

- 1 – Light conditions with airborne dust (Lt_D)
- 2 – Light conditions with amber flashing light (Lt_FL)
- 3 – Dark conditions (Dr)
- 4 – Dark conditions with airborne dust (Dr_D)
- 5 – Dark conditions with amber flashing light (Dr_FL)

The legend on the right indicates which colour bar belongs to which set of scans:

- SP1_1m – Scanner speed 1 at 1m distance-to-object
- SP1_3m – Scanner speed 1 at 3m distance-to-object
- SP1_5m – Scanner speed 1 at 5m distance-to-object
- SP2_1m – Scanner speed 2 at 1m distance-to-object
- SP2_3m – Scanner speed 2 at 3m distance-to-object
- SP2_5m – Scanner speed 2 at 5m distance-to-object

The following results are from the assessment discussed in Section 4.2.2.4 *Comparing the different environmental conditions on the 3D models*. Appendix C *C2M statistical analysis results* hold images of the CloudCompare assessments for all six sets of scans; key points have been selected and presented within this chapter.

5.4.1. Dark conditions

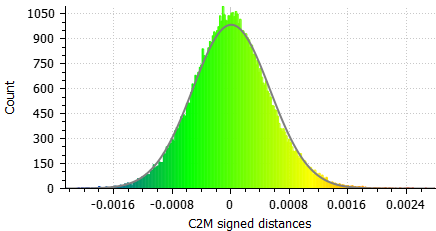
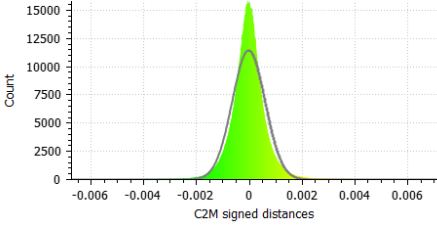
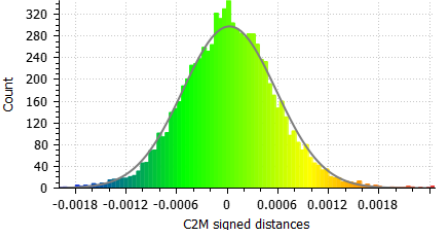
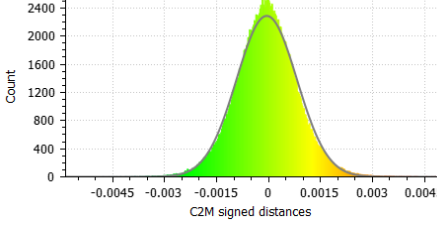
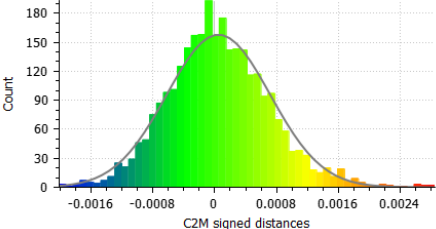
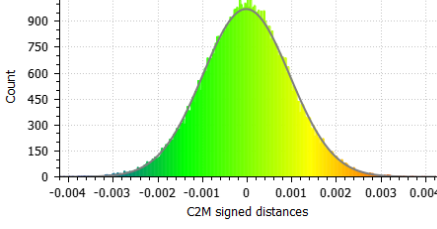
When comparing the effects of scanning in the dark with no airborne dust or flashing amber light it was found that there was minimal variation between the surface mesh and the point clouds. This is not surprising as laser scanners are active sensors in that they supply their own light source. In the case of the Faro Focus^{3D} the light source is an infrared light wave (Faro 2013).

Table 19 displays the results from all six sets of C2M distance comparison tests conducted. It can be seen that even with the variation in number of points collected from individual scans the majority of points deviate from the surface mesh between $\pm 3\text{mm}$ (row: *SP2_5m*) and

$\pm 1.6\text{mm}$ (row: *SP1_1m*) along the x axis. The y axis (Count) shows the sum of nearest neighbour calculations conducted, the point clouds at SP1 had less calculations than those at SP2 due to the point cloud densities.

The Gauss distribution was calculated at 2σ which represents the 95% confidence interval, the grey distribution line (bell curve) tells us that there is a 95% chance that the confidence interval calculated contains the true population mean. The shape of the grey bell curve reflects the deviation of the points, if the shape is more pointed at the peak then there are more calculated points that sit around the mean and if it is flatter in shape then there is a larger standard deviation range within the points calculated.

Table 19: Dark conditions Standard Deviation results.

SP1	Gauss distribution	SP2	Gauss distribution
SP1_1m	Gauss: mean = 0.000009 / std.dev. = 0.000524 [257 classes] 	SP2_1m	Gauss: mean = -0.000026 / std.dev. = 0.000623 [1286 classes] 
SP1_3m	Gauss: mean = 0.000029 / std.dev. = 0.000545 [92 classes] 	SP2_3m	Gauss: mean = -0.000054 / std.dev. = 0.000869 [466 classes] 
SP1_5m	Gauss: mean = 0.000056 / std.dev. = 0.000656 [54 classes] 	SP2_5m	Gauss: mean = -0.000022 / std.dev. = 0.000970 [281 classes] 

When comparing the histograms of the six point clouds captured in dark conditions it can be seen that the majority of the points sit neatly within the grey bell curve and hold low standard deviations (Std.Dev), this shows that the point clouds taken in dark conditions closely match the surface mesh developed from their relevant light condition scan.

When assessing the graphed results of the standard deviations seen in Figure 40 bound by the red box, the standard deviation is less than 1mm in all six sets. A trend can be seen that as the distance-to-object range increases so does the standard deviation. There may be a correlation between the point cloud density and the increase in the standard deviation however a more focused study on the effects of the distance-to-object on the standard deviation in dark conditions would be required to confirm this theory.

The results within this assessment show that scanning in dark conditions did not impact the desired results for conducting a JRC assessment.

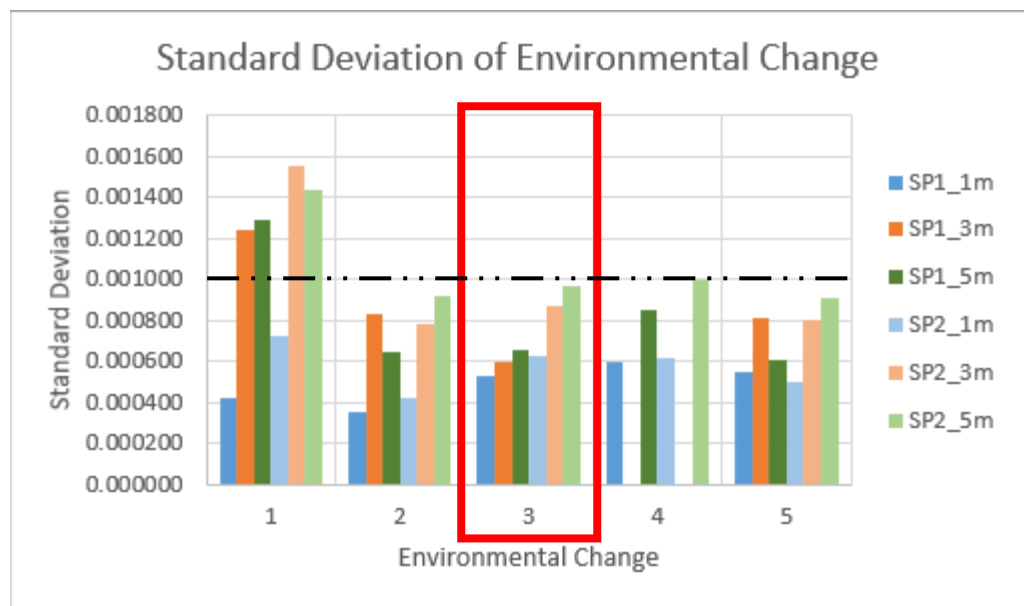


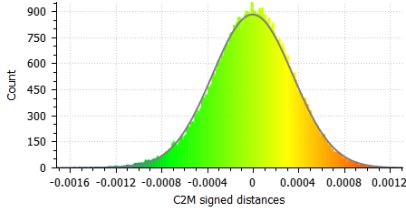
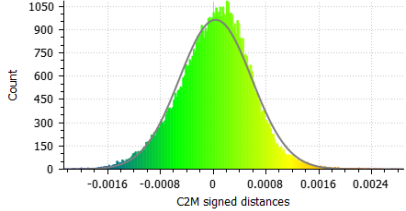
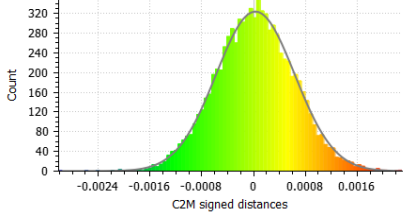
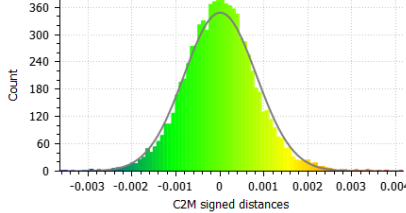
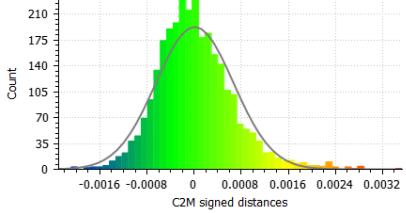
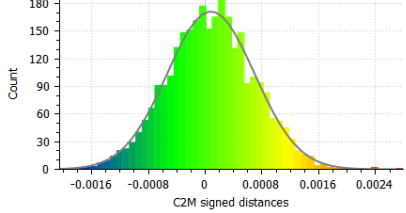
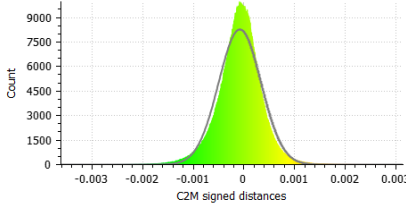
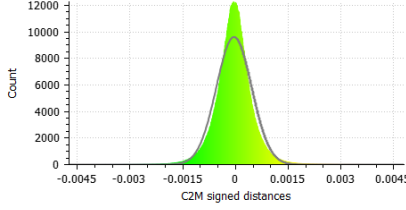
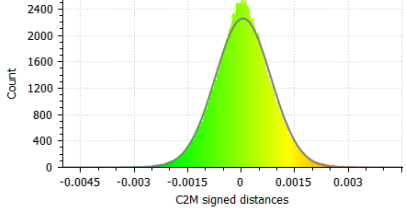
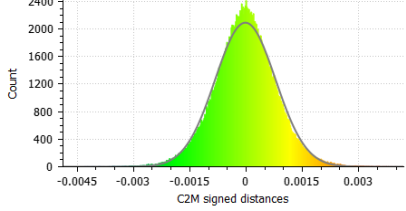
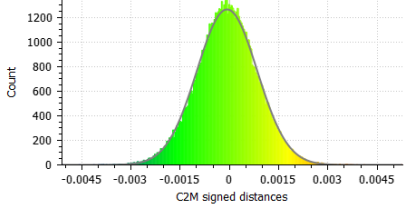
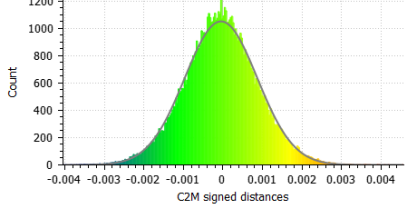
Figure 40: Dark conditions Std.Dev.

5.4.2. Flashing Light condition results

For this assessment a \$50 magnetic mounted flashing light with a standard bulb was purchased and placed to the side of the scan range as seen previously in Section 4.1.1 *Test area setup*, Figure 20.

Table 20 shows the Gauss distribution and histograms for the twelve point clouds collected in the flashing light conditions. The results from scans taken in the light conditions can be seen on the left and those taken in dark condition on the right.

Table 20: Flashing Light Standard Deviation results.

	Light Gauss distribution		Dark Gauss distribution
SP1_1m	<p>Gauss: mean = -0.000006 / std.dev. = 0.000350 [258 classes]</p> 	SP1_1m	<p>Gauss: mean = 0.000038 / std.dev. = 0.000546 [257 classes]</p> 
SP1_3m	<p>Gauss: mean = 0.000024 / std.dev. = 0.000600 [92 classes]</p> 	SP1_3m	<p>Gauss: mean = 0.000011 / std.dev. = 0.000811 [92 classes]</p> 
SP1_5m	<p>Gauss: mean = 0.000022 / std.dev. = 0.000646 [54 classes]</p> 	SP1_5m	<p>Gauss: mean = 0.000085 / std.dev. = 0.000603 [54 classes]</p> 
SP2_1m	<p>Gauss: mean = -0.000081 / std.dev. = 0.000418 [1284 classes]</p> 	SP2_1m	<p>Gauss: mean = -0.000041 / std.dev. = 0.000502 [1271 classes]</p> 
SP2_3m	<p>Gauss: mean = 0.000053 / std.dev. = 0.000777 [462 classes]</p> 	SP2_3m	<p>Gauss: mean = -0.000019 / std.dev. = 0.000801 [464 classes]</p> 
SP2_5m	<p>Gauss: mean = -0.000071 / std.dev. = 0.000914 [280 classes]</p> 	SP2_5m	<p>Gauss: mean = -0.000048 / std.dev. = 0.000912 [281 classes]</p> 

When comparing the histograms against their grey bell curve line as seen in Table 20 *Flashing Light Standard Deviation results*, there was a range of approximately $\pm 1\text{mm}$ (rows: *SP1_1m* and *SP2_1m*) to $\pm 2.5\text{mm}$ (row: *SP2_3m* and *SP2_5m*) along the x axis.

While the majority of the histograms were uniformly aligned with their grey bell curve it can be seen in row: *SP1_1m*, column: *Dark Gauss distribution* and row: *SP1_5m*, column: *Light Gauss distribution*, the histogram representing the points calculated do not appear as uniformly aligned with the grey bell curve. This meant that less of the points calculated held a 95% chance of representing the true population mean, which indicates the point clouds were a less accurate match to their referenced surface mesh.

This could be a result of the flashing light affecting the scanner's ability to accurately measure the divots and dents of the target surface as in both instances when assessing the surface comparison histogram; the targets affected held more surface texture.

In the scan at *SP1_1m* (Figure 41) Target 4 was affected with the divots showing in the subset blue. As all due care was taken when aligning the point cloud to the mesh and the other three targets were unaffected to such a degree, it was concluded that the deviation might have occurred due to the flashing amber light.

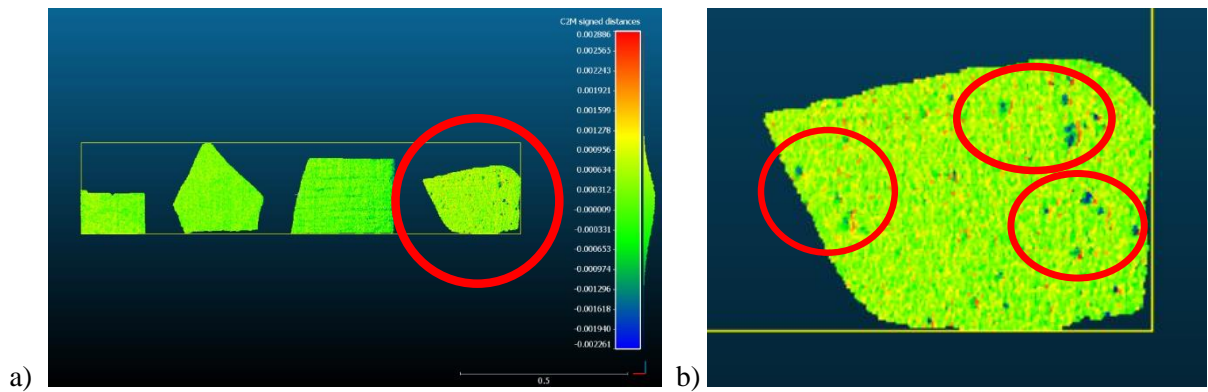


Figure 41: *SP1_1m* surface comparison histogram.

In the scan at *SP1_5m* (Figure 42) Target 1 was affected with the dents and curves of the surface showing both prominent red and subset blue sections. As with the previous sample, all due care was taken during alignment of the point cloud to the surface mesh, and the other three targets were unaffected.

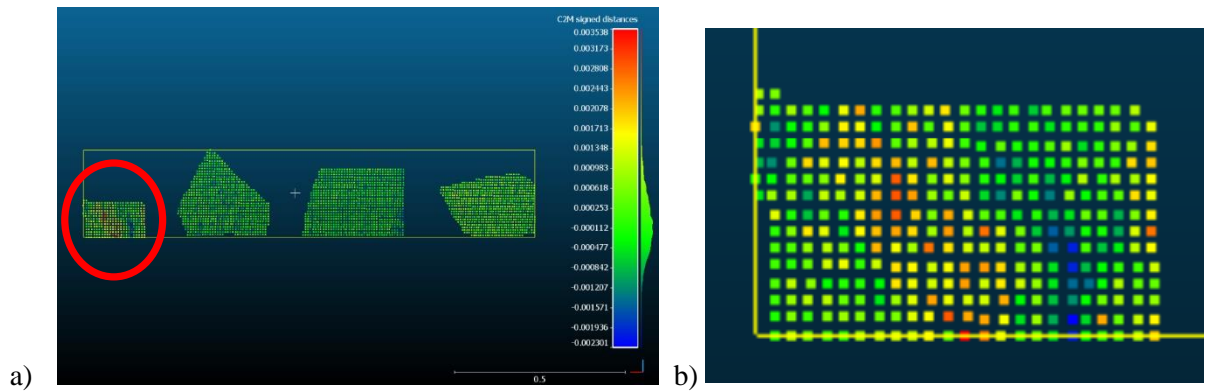


Figure 42: SP1_5m surface comparison histogram.

When assessing the standard deviation in Figure 43, the bar graphs bound in red (2 Light conditions (Lt), 5 Dark conditions (Dr)) show that both SP1_1m in dark conditions and SP1_5m in light conditions held low overall standard deviations regardless of the variations found in their individual targets, further supporting that the remaining three targets were unaffected.

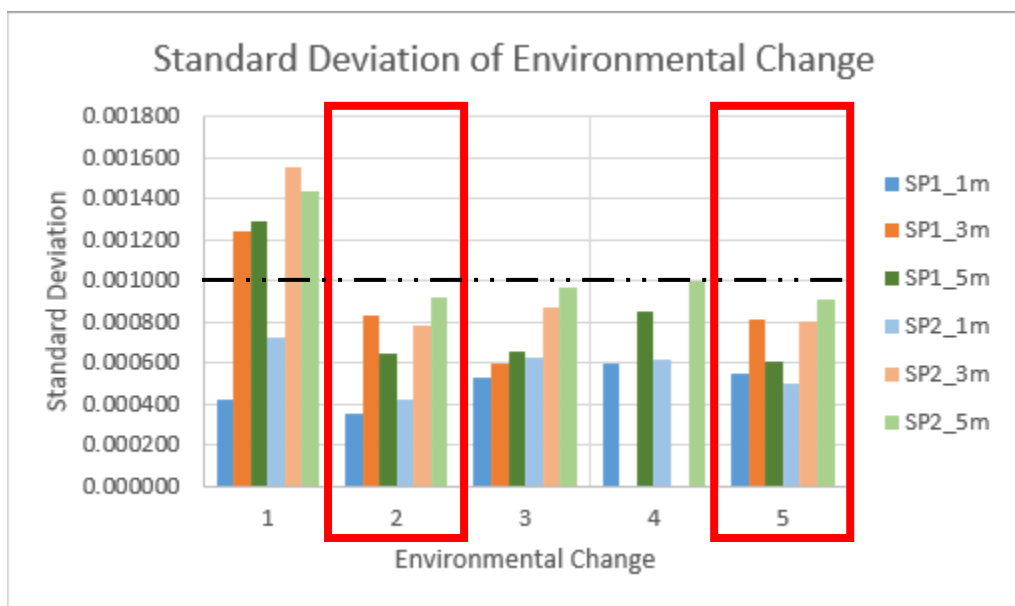


Figure 43: Flashing light conditions Std.Dev.

Regardless of whether the flashing light was tested in light or dark conditions, the standard deviation for each individual set of scans was similar, with a standard deviation of less than 1mm. This supported the evidence that in this study, the flashing light had no significant effect on the scan data when assessing JRC of the targets.

However, while the flashing amber light used for this assessment did not significantly affect the Faro Focus^{3D} scanner results for this assessment, the author believes that an assessment on

the effects of different coloured flashing lights at different luminosity strengths on a variety of scanners would need to be conducted to gain a thorough understanding of how different coloured flashing lights could affect different light wave frequencies of laser scanner.

5.4.3. Airborne Dust condition results

When assessing the results from scans conducted with airborne dust in the environment, the resulting histograms and Gauss distribution results were significantly impacted. The dust was distributed into the air by hand resulting in an unmeasured, non-uniform dust distribution.

The largest deviation was over 1.5m from a scan conducted in a dark, dusty conditions. Figure 44 shows the extent of the effect dust had on the resulting point cloud. Target 4 has both peaking and shadowing from the dust obscuring the light wave from reaching the target surface.

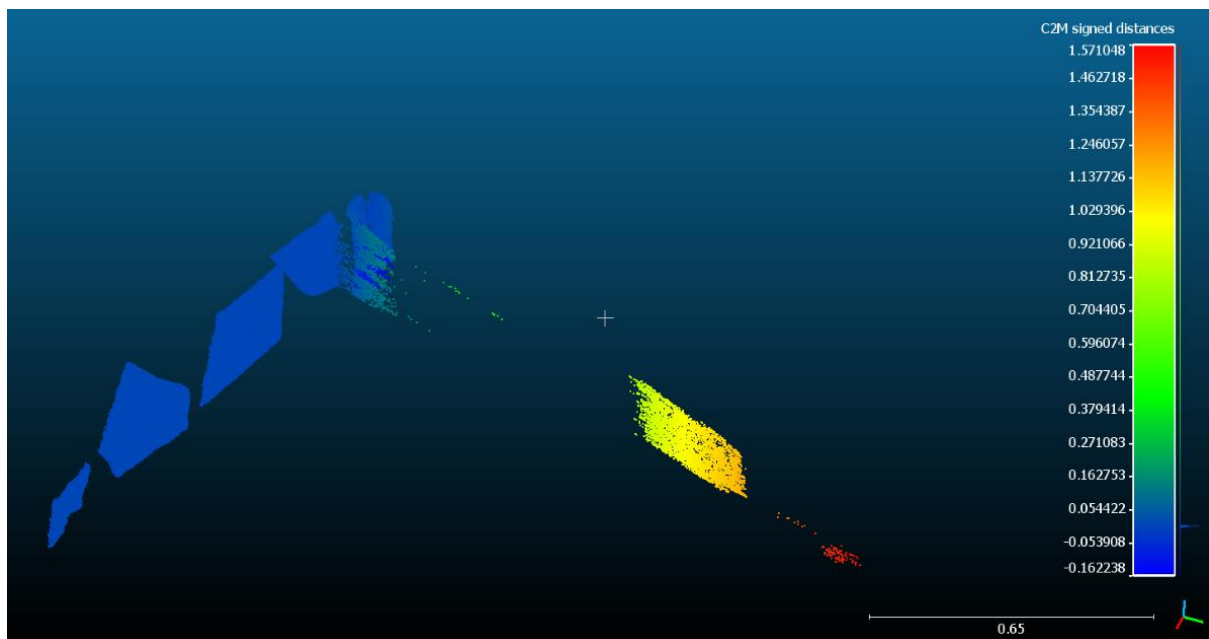


Figure 44: SP2_Dr_D_5m distance histogram.

Peaking is the result of the dust location being measured prior to the target's surface and shadowing is the result of dust obscuring the target surface creating a void in the point cloud of the target.

Figure 45 shows the effect of the dust captured by the scanner. With the white point cloud aligned with a grey surface mesh, it can be seen that on Target 4 there is peaking as a result of the dust closer to the target being captured and shadowing as a result of the dust in front of the target being captured.

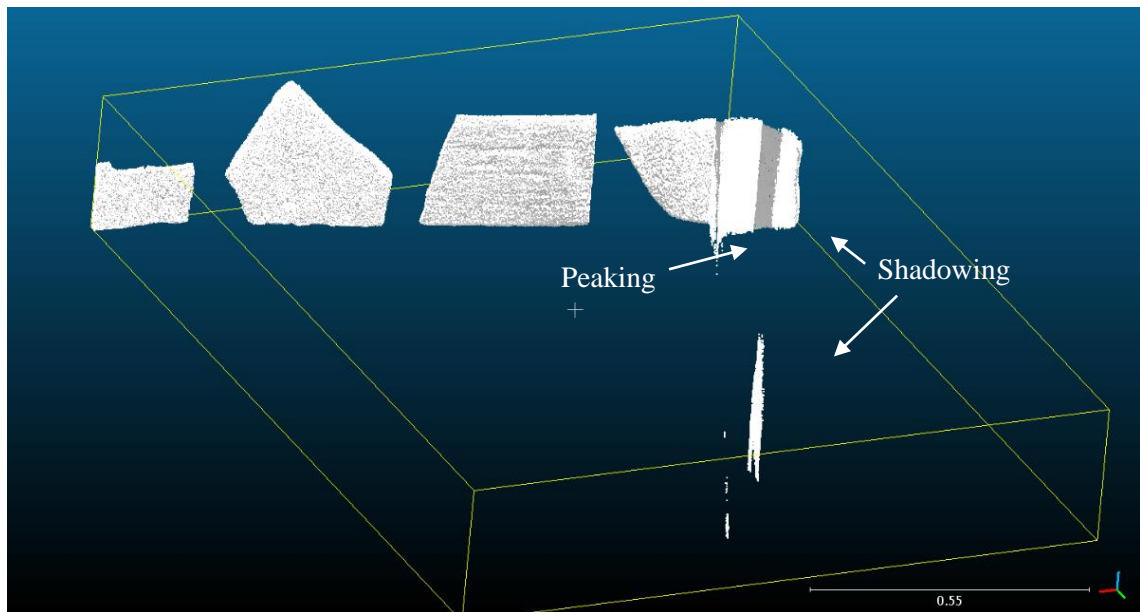


Figure 45: SP2_Dr_D_3m Point cloud overlay,

When closely analysing the C2M histogram it was found that Target 3, as well as Target 4, was affected by dust. Figure 46 gives a clear view of the impact dust can have on a point cloud. It shows that peaking on Target 3 had also occurred, this was over 50mm from the target surface and if it had been in a point cloud on its own would have been clearly visible; however, it was not clearly noticeable compared to the effect on Target 4 until a closer inspection was conducted.

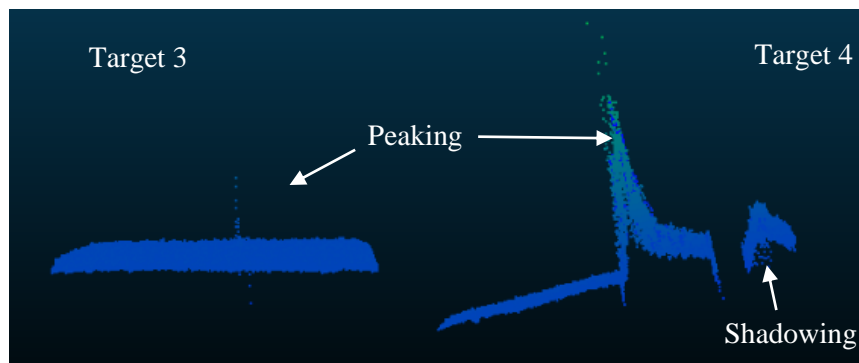


Figure 46: SP2_Dr_D_3m Targets 3 and 4.

When comparing the standard deviation results in the bar graphs bound in red (Figure 47, 1 Light Dusty conditions (Lt_D) and 4 Dark Dusty conditions (Dr_D)), it was clear that excessive peaking was unique to this scan however another scan conducted in the dark, dusty conditions also had significant peaking.

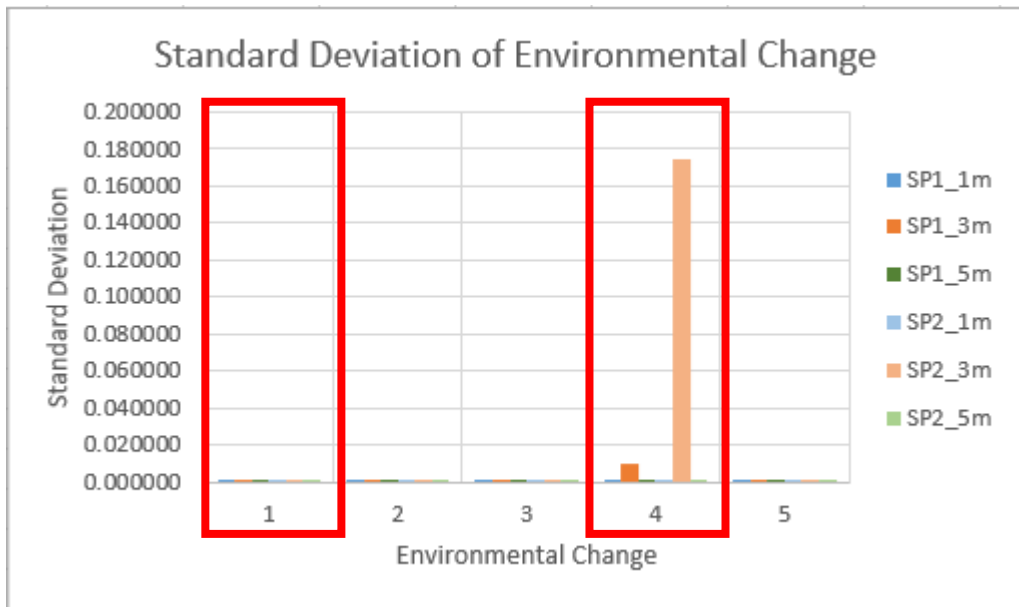


Figure 47: Dust conditions Std.Dev, all results.

The scan conducted in dark dusty conditions at SP1_3m resulted in a peaking of approximately 100mm from the surface of Target 3, visible in Figure 48. In this instance the dust only affects the right-hand edge of Target 3 with the majority of the surface and remaining targets unaffected.

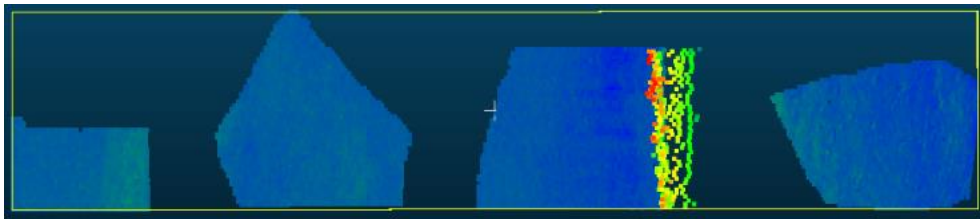


Figure 48: SP1_Dr_D_3m histogram.

When viewing the standard deviation results in the bar graph (Figure 49), the affect of airborne dust on the scan results showed that the majority of the standard deviations for the six sets of point cloud comparisons were less than 2mm. This was easily visible once the second outlier result was removed in Figure 50.

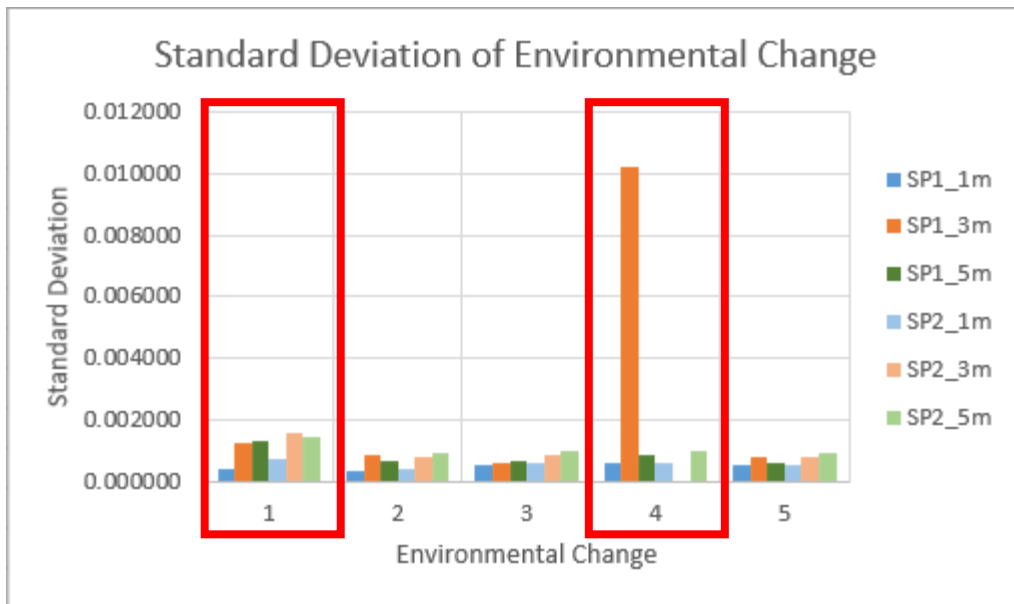


Figure 49: Dust conditions Std.Dev, largest outlier removed.

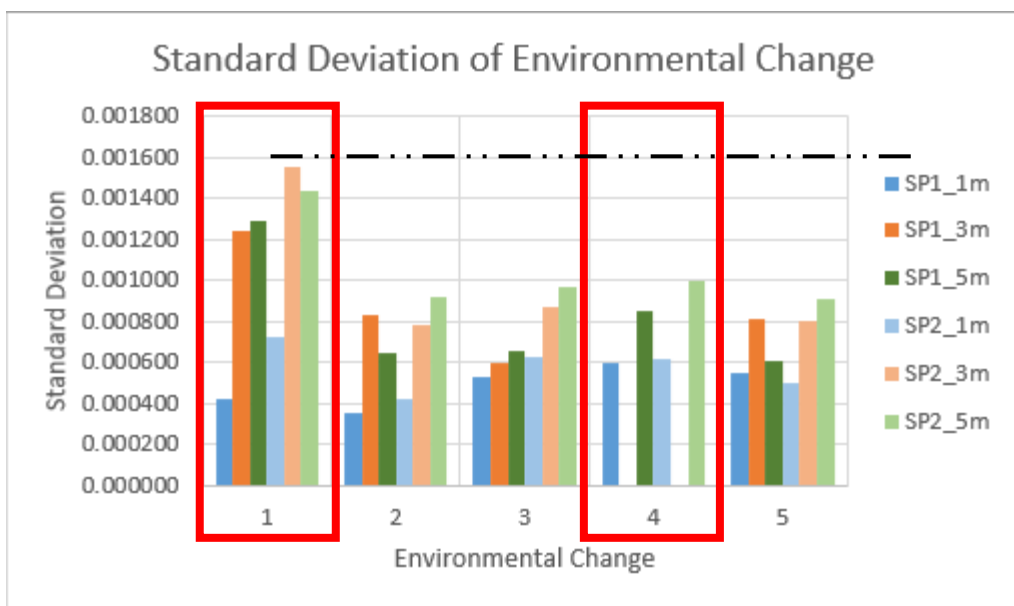


Figure 50: Dust conditions Std.Dev, second outlier removed.

With both outliers removed the results showed that the standard deviation for point clouds collected in a dusty environment was less than 1.6mm; however, the effects of dust on point clouds were more clearly evident in the Gauss distribution and histogram table.

Table 21 shows the effect scans conducted in dusty conditions had on the Gauss distribution. Within this table the resulting grey bell curve lines vary in shape. The most notable were the

two that result from the point clouds most affected by the dust seen previously in Figure 44 and Figure 48:

- Row: SP2_3m, column: Dark Gauss distribution, has an almost indistinguishable flat bell curve due to the exceptionally large positive standard deviation range of over 1.5m.
- Row: SP1_3m, column: Dark Gauss distribution, also holds a flat but slightly more prominent bell curve due to the positive standard deviation range of approximately 100mm.

Row: Sp2_1m in Table 21 for both light and dark conditions show a pointed grey bell curve line with a large standard deviation range, this shows that while the majority of points calculated sit around the mean there is a small amount that deviate away. Figure 51 shows that dust has caused peaking on Targets 2 and 3 in the dark conditions and on all four targets in the light conditions which accounts for the large standard deviation range.

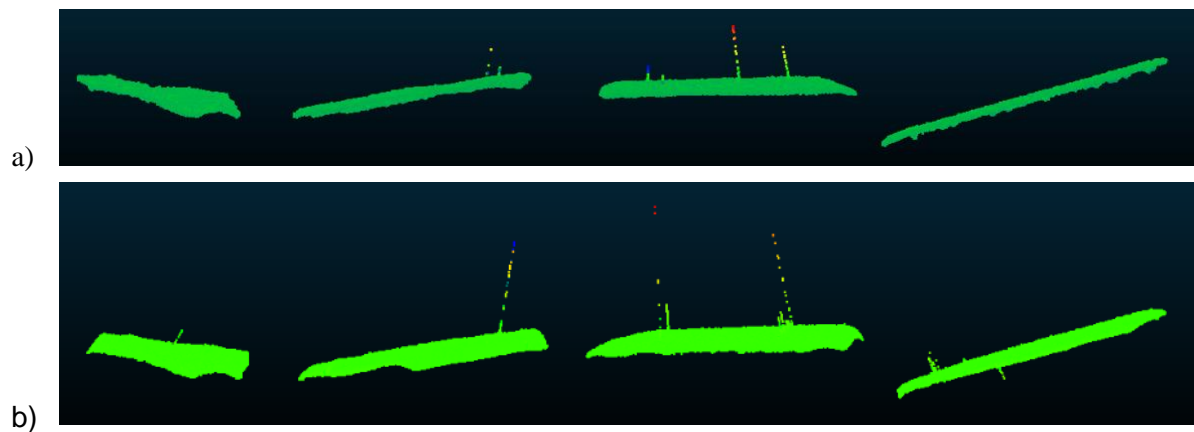
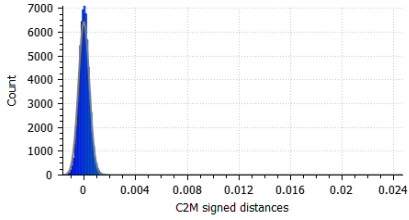
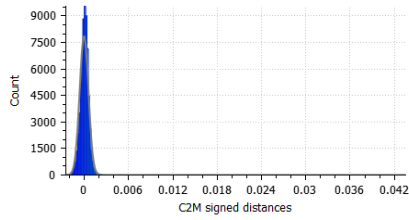
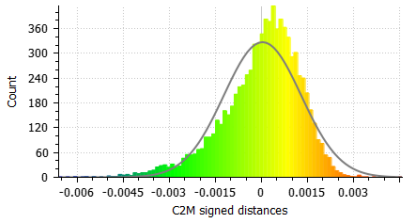
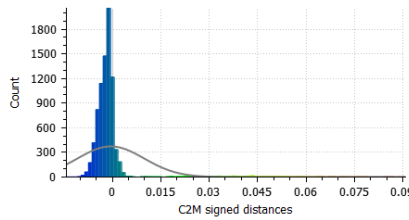
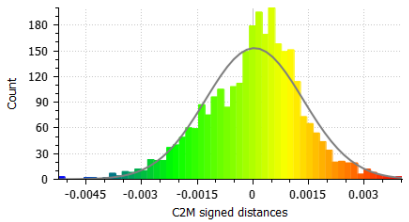
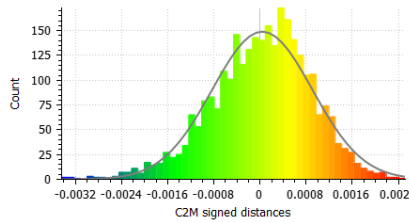
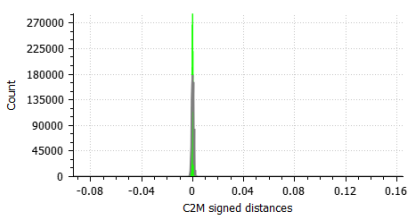
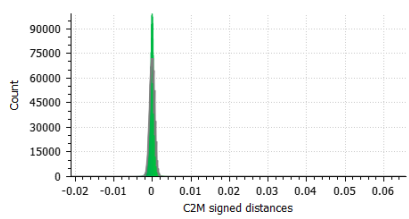
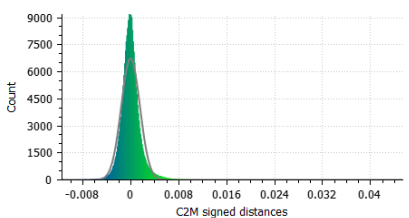
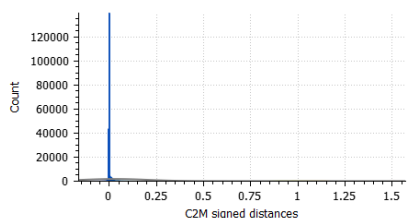
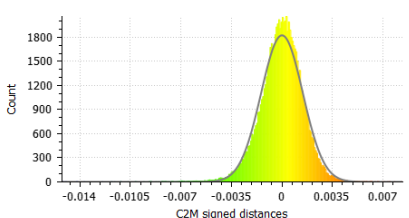
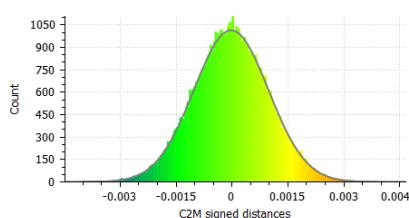


Figure 51: a) SP2_Dr_D_1m, b) SP2_Lt_D_1m.

Table 21: Dusty conditions Standard Deviation results.

	Light Gauss distribution		Dark Gauss distribution
SP1_1m	<p>Gauss: mean = 0.000029 / std.dev. = 0.000418 [258 classes]</p> 	SP1_1m	<p>Gauss: mean = 0.000039 / std.dev. = 0.000592 [257 classes]</p> 
SP1_3m	<p>Gauss: mean = 0.000023 / std.dev. = 0.001243 [92 classes]</p> 	SP1_3m	<p>Gauss: mean = -0.000040 / std.dev. = 0.010188 [92 classes]</p> 
SP1_5m	<p>Gauss: mean = 0.000026 / std.dev. = 0.001292 [54 classes]</p> 	SP1_5m	<p>Gauss: mean = 0.000030 / std.dev. = 0.000853 [54 classes]</p> 
SP2_1m	<p>Gauss: mean = -0.000044 / std.dev. = 0.000727 [1267 classes]</p> 	SP2_1m	<p>Gauss: mean = -0.000053 / std.dev. = 0.000619 [1290 classes]</p> 
SP2_3m	<p>Gauss: mean = -0.000017 / std.dev. = 0.001556 [462 classes]</p> 	SP2_3m	<p>Gauss: mean = 0.031791 / std.dev. = 0.175053 [463 classes]</p> 
SP2_5m	<p>Gauss: mean = -0.000008 / std.dev. = 0.001439 [280 classes]</p> 	SP2_5m	<p>Gauss: mean = -0.000022 / std.dev. = 0.000997 [279 classes]</p> 

In contrast to the point cloud comparisons that show obvious and visible peaking in the point cloud and obvious deviations in their bell curves, some of the point clouds were more subtly affected.

Row: SP1_5m in Table 21 shows in both light and dark conditions that the majority of the points sit within the 95% confidence interval of the mean, their resulting grey bell curve lines holding a normal shape when assessing the variation between the mean and the standard deviation. However, when assessing the histogram of the C2M there is a visible colour variation, this variation is of 3 to 4 mm and when it covers a larger area of the target (Figure 52) the point cloud surface may not provide an accurate representation of the actual target surface for a JRC assessment. This would require a judgment call on whether or not a suitable surface mesh slice could be taken or if the deviation was too large.

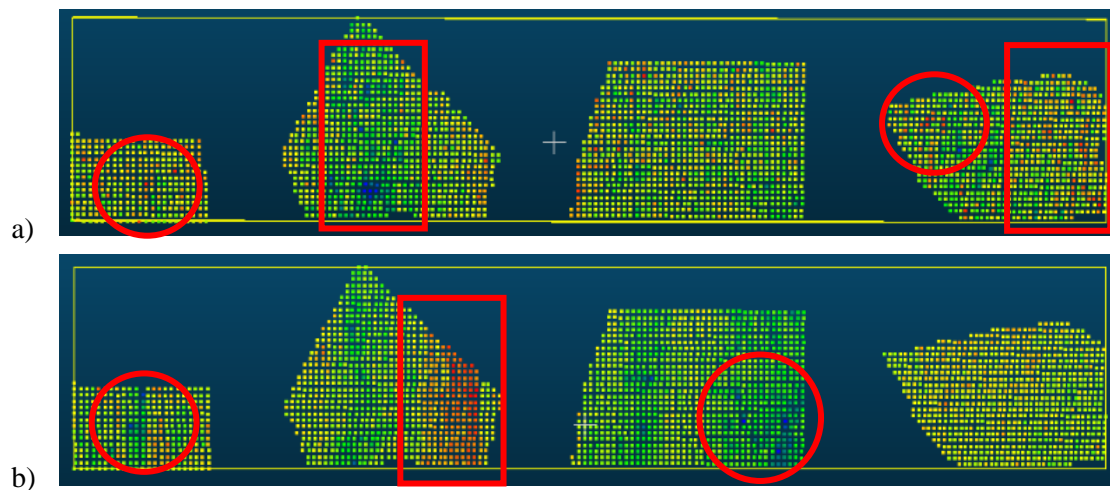


Figure 52: a) SP1_Dr_D_1m b) SP1_Lt_D_1m.

When looking at row: SP2_5m in Table 21 it is evident that these two scans were not affected by airborne dust, this was confirmed when assessing their respective C2M histograms as they showed no signs of either prominent red or subset blue sections.

Ten of the twelve C2M comparisons conducted when assessing the effects of airborne dust on scan data were impacted in some way.

If a suitable slice of the surface mesh from an unaffected area of the target could be taken it did not affect the JRC assessment. This was not always possible, in some cases targets clearly deviated from the mean to a point that would affect the integrity of the surface mesh generated in representing the actual target surface to within 2mm as specified in Section 5.3

Cross section for JRC comparison to BC scale.

It should be noted that the dust used in this assessment was not uniformly measured or distributed as dust, in reality, is rarely uniformly measured or distributed. An environment affected by airborne dust particles will affect the results of any scan conducted, and this should be taken into consideration when planning a scanning task as dust could affect the point clouds and surface mesh generated during processing. This can be managed by cleaning the point clouds of the obvious dust peaks, but this would result in a flat section in any surface mesh generated for the target and may not represent the actual surface to within the desired 2mm accuracy.

5.5. Future assessments for integration into an MLS format.

When considering using a mobile platform for conducting a scan to collect data for a JRC assessment that requires an accuracy of 2mm, significant research would need to be conducted, including:

- Integrating the scanner onto a mobile platform, including an Internal Measurement Unit (IMU) to calculate the platform's orientation.
- Registration of the starting location to accurately map the platform's position.
- Research into the current achievable accuracy of SLAM algorithms in computing the scanned points location relevant to the mobile platform's movement and position.

Kaijaluoto, Kukko, and Hyypä (2015) found that an accuracy of 17mm horizontally and 36mm vertically was achievable within their study. The author believes that at this stage to achieve the desired results within this dissertation it is not feasible to use a mobile platform.

5.6. Summary

Within this chapter the data collected was assessed for changes within the point clouds due to changes in the environmental conditions and analysed for their affect. The effects were assessed for their impact on the JRC comparison test. This helped to answer the research question and sub-question:

How might an underground working environment affect laser scan data when assessing JRC?
What affects will changes in the environment have on the scan data?
Is it feasible to use a mobile platform for this task?

When comparing the unpainted and painted targets, there was approximately 0.6mm different between the two. The variation could be the result of paint filling in finer surface textures however the painted targets were used to minimise the potential effect of the target surfaces holding different reflective values that could impact on the scan data results.

When assessing the JRC of the surface mesh slices from the target scans to duplicate the manual JRC assessment using a profile comb, it was found that a suitable visual comparison to the BC scale could be made if the surface mesh was generated from a point cloud with a density between 1.5mm and 2.2mm. It is the author's opinion that a point cloud density of 2mm is ideal for conducting the visual assessment between the surface slice taken and the BC scale.

When analysing the effects of changes in the environment on the point clouds, it was found that:

- Dark conditions
 - A trend could be seen that as the distance-to-object range increases so did the deviation. There may be a correlation between the distance-to-object range and the increase in the standard deviation however a more focused study on the effects of the distance-to-object on the standard deviation in dark conditions would be required to confirm this theory.
 - A standard deviation of less than 1mm from the reference surface mesh was achieved.
 - Scanning in dark conditions did not impact the desired results for conducting a JRC assessment.
- Amber flashing light condition
 - While the amber flashing light did not have a significant or impacting effect in this study, it should not be assumed that all flashing lights will not affect laser scanning.
 - A standard deviation of less than 1mm was achieved.
 - Within this assessment, it showed that a \$50 flashing amber light with a standard bulb does not significantly affect an infrared laser scanner. However, different scanners use different light frequencies; these different light frequencies may be affected by different coloured flashing lights at different luminosity strengths such as LED bulbs that are significantly brighter than a standard bulb.

- Airborne dust conditions
 - The standard deviations within the six sets of data varied depending on the amount and distribution of dust captured in the scan.
 - Dust affected the reliability of generating an accurate point cloud, and therefore surface mesh, for representing the true target surface to within 2mm of the reference surface mesh in most cases.
 - While some targets were unaffected and a JRC assessment could be done on them, others were obviously distorted and not a true representation of the target surface.
 - Dust can have a negative impact of scan data collected if the accuracy of 2mm is required as with the JRC assessment.

Further environmental conditions could be assessed for their impact of laser scan data such as water seepage on the rock surface, moisture in the air found in shafts, and tunnel temperature.

When considering using a mobile platform for conducting a scan to collect data for a JRC assessment that requires an accuracy of 2mm, significant research would need to be conducted into the mobile platform setup as well as the required SLAM algorithms (or equivalent) to achieve the required accuracy for mapping a tunnel. At this stage within this dissertation it is not feasibility to use a mobile platform for the same assessments.

Chapter 6. Discussion

Within this chapter, the research question established in Chapter 2 *Research question, Aim and Objective* will be reviewed, and relevant answers, as well as potential further studies will, be discussed.

How might an underground working environment affect laser scan data when assessing JRC?
Sub questions:
What is already known about the use and function of TLS and MLS?
What is the best scan setup geometry for TLS?
What affects will changes in the environment have on the scan data?
Is it feasible to use a mobile platform for this task?

The aim of this study was to assess a PS scanner for its ability to acquire point cloud data that could be used to assess the JRC of rock when in an underground working environment. To simulate a underground working environment, six variables were assessed:

- Three scan station distances offset from the target objects being scanned
- Two Scan speeds to assess potential accuracies
- If there is a significant difference between unpainted and painted targets
- The effects of natural light and simulated darkness
- The effects of an amber flashing light on scan data
- The effects of airborne dust in the atmosphere

When looking into the use of TLS within the mining industry for assessing tunnel structures and geotechnical attributes of rock structure, the use of TLS is well established. When considering using a mobile platform to conduct the same task, several considerations must be made. Within this dissertation a study was done on the use of TLS for assessing the JRC of rock surfaces. In the past, the JRC assessment was conducted manually with a profile comb as discussed in Section 1.3 *Surface roughness analysis as it applies to this dissertation*. Within this study, the JRC assessment was conducted using TLS data to assess the effects of a close distance-to-object range to simulate the potential distances a vehicle may travel from the target surface when used as a mobile platform as well as changes in the environment to answer the research question.

6.1. Review

The overarching research question ‘How might an underground working environment affect laser scan data when assessing JRC?’ is answered by looking at the sub questions:

What is already known about the use and function of TLS and MLS?

When using TLS accurate and detailed scan data can be collected, and software exists for calculating joint sets from TLS. Fekete, Diederichs & Lato (2010) produced scan data with joint sets plotted and colour coded on a 3D model. Monsalve et al. (2019) utilise ‘dips’ software to classify the rock mass into joint sets during data processing. Previous studies have shown that when using TLS comprehensive 3D models of tunnel structures can be generated to provide accurate models of the rock mass including discontinuities in the rock mass such as joint sets. Although thorough studies had been conducted in the use of TLS very little information regarding the effects of the environment of the tunnels on scans was documented which lead to this dissertation testing changes in the environment.

However, when looking into the use of MLS for the same task current studies show that while a scan of the tunnel can be made it is not of an accuracy to enable an assessment of the rock mass to be conducted. Kaijaluoto, Kukko, and Hyypä (2015) found that the RMSE of 17mm horizontally and 36mm vertically was achievable which is not within the 2 millimetre accuracy range required for a JRC assessment. It was apparent to the author that further study into Simultaneous Localisation And Mapping (SLAM) and three-dimensional axis mapping (3DAM) algorithms would be required for a greater understanding of how the calculations are conducted and if the accuracy could be improved.

What is the best scan setup geometry for TLS?

The test area was set up to assess the three distance-to-object ranges to simulate the distance a vehicle may drive off of the tunnel wall when used as a mobile platform. Two scanner speeds were assessed to gain an understanding of the effect scanner speed had on the point cloud data. Scans were conducted, processed, and assessed to ascertain what affect the different distances and speeds had on the JRC assessment. This was done to gain an understanding of how the manual method that uses a profile comb could be transferred into a digital method using scan data.

It was found that a distance-to-object range and scanner speed combination that produced a point cloud of a 2mm density would generate a surface mesh that accurately represented the target objects and could be used for an effective JRC assessment.

This means that during a scan setup consideration would need to be given to the accuracy required and what distance-to-object and scanner speed combination would produce that accuracy. Within this dissertation, only two scanner speeds of the potential 38 speed combinations within the Faro Focus^{3D} (2013) were assessed.

When establishing the best scan setup geometry for TLS tasks there is never going to be a one size fits all scenario however, there are five key points that would assist in planning for a scanning task.

Key points to consider when conducting scans include:

- Distance-to-object ratio of (0.5 to 1): Scan span diameter (Fekete, Diederichs and Lato 2010).
- Incident angle no more than $\pm 45^\circ$ from centre of object (Mechelke, Kersten & Lindstaedt 2007).
- Target object colour for testing ideally grey (Lemes and Zaimovic-Uzunovic 2009).
- Resolution of scan, scanner speed suitable for the required point cloud density of the task, this can be found in the scanner's manual.
- Overlap of point clouds between scan stations, station separation between 1 to 2 of the tunnel radii (Fekete, Diederichs and Lato 2010) for a full 360° scan.

When using a mobile platform, a consistent platform speed should be used. An assessment conducted on the effects of the combined scanner and platform speed on the point cloud data would need to be conducted.

What effects will change in the environment have on the scan data?

After researching what was already known about TLS and its use in underground tunnels, the lack of what effects changes in the tunnel environment had on scan data was noted.

This dissertation was focused on the JRC assessment when compared to the BC scale; this gave the author the foundation to assess the effects of changes in the environment. Initially, the assessment on the effects of the three distance-to-object ranges at the two scanner speeds was conducted to evaluate at what point cloud density a suitable JRC assessment could be done. The author established that a 2mm point cloud density was required.

When assessing the standard deviation, the cloud to mesh (C2M) distance calculation provided the maximum standard deviation of the point cloud being assessed. A standard deviation of 2mm or less was found between most C2M comparisons with the majority holding a standard deviation of 1mm or less.

Analysing the changes in the environment on the point clouds for their standard deviations showed that for:

- Dark conditions

Scanning in dark conditions did not impact the desired results for conducting a JRC assessment. A standard deviation of less than 1mm from the reference surface mesh was achieved. However, a trend could be seen that as the distance-to-object range increases so did the standard deviation. The author postulates that there may be a correlation between the distance-to-object range and the increase in the standard deviation. A more focused study of the effects between the distance-to-object and the standard deviation in dark conditions would be required to confirm this theory.

- Amber flashing light condition

The amber flashing light used had no significant impact on the point cloud data. A standard deviation of less than 1mm was achieved. While the amber flashing light did not have a significant effect in this study, it should not be assumed that all flashing lights will not affect laser scanning projects. Within this assessment, it showed that a \$50 flashing amber light with a standard bulb does not significantly affect an infrared laser scanner. However, different scanners use different light frequencies, and these different light frequencies may be affected by different coloured flashing lights at different luminosity strengths such as LED bulbs that are significantly brighter than a standard bulb.

- Airborne dust conditions

The dust had a significant impact on the reliability of generating an accurate point cloud representing the true target surface to within 2mm of the reference surface mesh in most cases. The standard deviations within the six sets of data varied depending on the amount and distribution of dust captured in the scan. While some targets were unaffected and a JRC assessment could be done, others were obviously distorted and not a true representation of the target surface. The dust had a negative impact on scan data collected where an accuracy of 2mm was required.

The author is aware that only three environmental variations were assessed. Within an underground working tunnel, there are also changes in the tunnel temperature, the amount of water seepage on the rock surface, airflow gusts within the tunnel network and water droplets in the atmosphere of shafts, which could also affect the point cloud data collected. It is the author's opinion that these variables could be assessed for their impact in future studies.

Can the acquired information be used in an MLS format?

When looking into collecting point cloud data from a mobile platform, it is not as simple as placing the scanner onto a roof mount and driving off. While a JRC assessment can be conducted from TLS data it is due to the fact a high point cloud density can be achieved. As mentioned before, current studies have achieved an accuracy range of 17mm to 36mm from an MLS platform. This is not within the 2mm accuracy range required for a JRC assessment.

When considering using a mobile platform for conducting a scan to collect data for a JRC assessment further research and testing is required. This includes but is not limited to:

- Integrating the scanner onto a mobile platform including an Internal Measurement Unit (IMU) to calculate the platforms orientation.
- Registration of its starting location to accurately map the platform's position.
- Research into the current achievable accuracy of SLAM and 3DAM (or similar) algorithms in computing the scanned points location relevant to the mobile platform's movement and position.
- The maximum platform speed achievable to gather the required point cloud density.
- The effects of the scanner position and height on the mobile platform blocking the FOV from capturing the base of the wall at close range.

At the time of writing this dissertation the author did not have enough information to say if using a mobile platform could achieve the same results as a TLS and was of the opinion that further studies would be required to assess all the variables.

Chapter 7. Conclusion

In conclusion, the objective of this study was to assess the effects of various conditions found in a underground working environment, primarily the effects of lighting conditions, flashing amber safety lights and dust particles in the atmosphere, as well as to determine the most effective combination of scanner setup geometry to produce point cloud data of an accuracy that could be used for a JRC assessment. The acquired findings were then used to assess the feasibility of using MLS to identify geotechnical discontinuities in underground environments.

It was found that TLS could be used at a close distance-to-object range to gather point cloud data, and a point cloud density of approximately 2mm was required to conduct the JRC assessment. The density of the point cloud was affected by both the scanner speed and its distance from the target object. Changes in the environmental conditions had varying effects, scanning in the dark had no impact on the point cloud data, the flashing amber light used for this assessment did not significantly impact the point cloud data but further testing is required to assess the effects of flashing safety lights on a range of scanners, and airborne dust had a significant impact on the point cloud data resulting in some scans that could not be used for a JRC assessment.

When considering the feasibility of using a mobile platform, at this stage the required accuracy for a JRC assessment is not achievable. MLS itself has many variables that need to be assessed.

This dissertation helps to establish an understanding of the impact of the environmental conditions within a tunnel structure on scan data, as well as establishing a guide to the best station setup geometry for TLS.

7.1. Key findings

1. A Faro Focus^{3D} is suitable for close range scans of 5m or less.
2. Best station setup geometry consists of:
 - a. Distance-to-object ratio (0.5 to 1): Scan span diameter
 - b. Angle of incident $\pm 45^\circ$ from centre of object
 - c. Target object colour for testing ideally grey
 - d. Resolution of scan, scanner speed suitable for the required point cloud density of the task, this can be found in the scanner's manual.
 - e. Station separation for overlap of point clouds between 1 to 2 times the tunnel radii for a full 360° scan.
3. No significant difference between unpainted and painted targets was found.

4. A JRC assessment can be conducted from scan data with a point cloud density of 2mm.
5. Distance-to-object and scanner speed combinations will affect the point cloud density.
6. A dark environment had no impact on scan data collected.
7. A flashing amber light with a standard bulb did not have a significant impact on the scan data.
8. Airborne dust in the environment had a significant impact on the scan data.
9. When considering using MLS for the same task further study is required.

7.2. Further studies

The areas within this dissertation that require further studies include:

1. A more focused study on the effects of the distance-to-object on the standard deviation in dark conditions.
2. The effects of different coloured flashing lights and their different luminosity strengths commonly used in mining and construction on a variety of laser scanners with different laser light frequencies.
3. The effects of changes in environmental conditions including temperature, water seepage on rock surfaces, airborne water droplets in shafts.
4. A study into mobile platform setups and the use of SLAM or equivalent software and its achievable accuracies when mapping a tunnel structure.

Reference List

- Barton N 2013, 'Shear strength criteria for rock, rock joints, rockfill and rock masses: Problems and some solutions', *Journal of Rock Mechanics and Geotechnical Engineering*, vol. 5, pp 249-261.
- CloudCompare 2019, CloudCompare open-source point cloud editing software v2.9.1, GPL software, CloudCompare.org, viewed 7 April 2019, <<http://www.cloudcompare.org/release/notes/20171026/>>.
- Faro 2013, *Faro Laser Scanner Focus^{3D} Manual*, FARO Technologies Inc, viewed 1 February 2019, <https://knowledge.faro.com/Hardware/3D_Scanners/Focus>.
- Faro 2019, *Scene Process 2019.0*, FARO Technologies Inc, viewed 1 April 2019, <https://knowledge.faro.com/Hardware/3D_Scanners/Focus>.
- Fekete, S, Diederichs, M & Lato, M 2010, 'Geotechnical and operational applications for 3-dimensional laser scanning in drill and blast tunnels', *Tunnelling and Underground Space Technology*, vol. 25, no. 5, pp 614-628, doi: 10.1016/j.tust.2010.04.008.
- Gallant, M & Marshall, J 2016, 'Automated rapid mapping of joint orientation with mobile LiDAR', *International Journal of Rock Mechanics Mining Science*, vol. 90, pp1-14.
- Kaijaluoto, R, Kukko, A & Hyypä, J 2015, 'Precise Indoor Localization for Mobile Laser Scanning', *The International Archives of the Photogrammetry, Remote Sensing and Spatial Sciences*, vol. XL-4/W5, Tokyo Japan.
- Lehtomäki, M, Jaakkola, A, Hyypä, J, Kukku, A & Kaartinen, H 2010, 'Detection of Vertical Pole-Like Objects in a Road Environment Using Vehicle-Based Laser Scanning Data', *Remote Sensing*, vol. 2, no. 3, pp 641-664, doi: 10.3390/rs2030641.
- Leica 2019, *Leica ScannStation2 Manual*, Leica Geosystems AG, viewed 1 March 2019, <<https://leica-geosystems.com>>
- Lemes, S & Zaimovic-Uzunovic, N 2009, 'Study of Ambient Light Influence on Laser 3D Scanning', 7th International Conference on Industrial Tools and Material Processing Technologies Conference, 4-7 October, Ljubljana, Slovenia, pp. 327-330.
- Lerma, JL, Navarro, S, Cabrelles, M and Villaverde, V 2010, 'Terrestrial laser scanning and close-range photogrammetry for 3D archaeological documentation: the upper Palaeolithic Cave of Parpallo as a case study', *Journal of Archaeological Science*, vol. 37, pp 499-507.

Matest 2018, Material testing equipment manufacturer, Via delle Industrie 25 – 24048 Treviolo (BG) Italy, viewed 1 July 2019, <<http://www.matest.com/en/product/a122-barton-combs-profilometers>>.

Mechelke, K, Kersten, TP & Lindstaedt, M 2007, ‘Comparative Investigation into the Accuracy Behaviour of the New Generation of Terrestrial Laser Scanning Systems’, Optical 3-D Measurement Techniques VIII, HafenCity University, Hamburg, Germany, vol. 1, pp 319-327.

Monsalve, J, Bagget, J, Bishop, R & Ripepi, N 2019, ‘Application of laser scanning for rock mass characterization and discrete fracture network generation in an underground limestone mine’, International Journal of Mining Science and Technology, vol. 29, issue. 1, pp. 131-137.

Pu, S, Rutzing, M, Vosselman, G & Elberink, SO 2011, ‘Recognizing basic structures for mobile laser scanning data for road inventory studies’, ISPRS Journal of Photogrammetry and Remote Sensing, vol. 66, pp S28-S30.

Puente, I, Gonzalez-Jorge, Arias, P & Armesto, J 2011, ‘Land-based Laser Scanning Systems: A review’, The International Archives of the Photogrammetry, Remote Sensing and Spatial Sciences, vol. XXXVIII-5/W12, pp 163-168, doi: 10.5194/isprsarchives-XXXVIII-5-W12-163-2011

Reshetyuk Y 2009, ‘Self-calibration and direct georeferencing in terrestrial laser scanning’, Doctoral thesis, Royal Institute of Technology (KTH), Stockholm.

Shan, J & Toth, CK 2009, Topographic Laser Ranging and Scanning: Principals and Processing, second edition, Taylor & Francis Group, 6000 Broken Sound Pkwy Suite 300, Boca Raton, Florida.

Talaya, J, Alamus, R, Bosch, E, Serra, A, Kornus, W & Baron, A 2004, ‘Integration of a terrestrial laser scanner with GPS/IMU orientation sensors’, International Society of Photogrammetry and Remote Sensing, viewed 2 August 2018, <<http://www.isprs.org/proceedings/xxxv/congress/comm5/papers/190.pdf>>.

Thomson, C 2019, What are the most common 3D point cloud file formats & solving interoperability issues, Vercator, 11-13 Macklin St London WC2B5NH, viewed 14 May 2019, <<https://info.vercator.com/blog/what-are-the-most-common-3d-point-cloud-file-formats-and-how-to-solve-interoperability-issues>>.

Vaaja, M, Hyypä, J, Kukko, A, Kaartinen, H, Hyypä, H & Alho, P 2011, ‘Mapping topographic changes and elevation accuracies using Mobile Laser Scanning’, Remote Sensing, vol 3, no.3, pp 587-600, doi: 10.3390/rs3030587.

Voegtli, T, Schwab, I & Landes, T 2008, 'Influences of Different Materials on the Measurements of a Terrestrial Laser Scanner (TLS)'. The International Archives of the Photogrammetry, Remote Sensing and Spatial Sciences, vol. XXXVII Part B, Beijing

Yakar, M, Ulvi, A & Toprak, AS 2015, 'The Problems and Solution Offers, Faced During The 3D Modelling Process of Sekiliyurt Underground Shelters with Terrestrial Laser Scanning Methods', International Journal of Environment and Geoinformatics, vol. 2, no. 2, pp 39-45.

Zlot, R & Bosse, M 2014, 'Efficient large-scale three-dimensional mobile mapping for underground mines', Journal of Field Robotics, vol. 31, no.5, pp 758-779, doi: 10.1002/rob.21504.

Appendix A - Project specification

ENG4111/4112 Research Project

Project Specifications v2

For: Megan Braddon.

Title: How might an underground working environment effect terrestrial laser scan data when assessing Joint Roughness Coefficient, and is it feasible to use a mobile platform?

Major: Surveying.

Supervisor: Primary: Dr. Zahra Gharineiat, Secondary: Dr. Ali Mizaghorbanali.

Enrolment: ENG4111 semester 1 2019, ENG4112 semester 2 2019.

Project Aim: To assess through lab-based testing the effects of environmental changes in a simulated underground environment on laser scan data obtained for the purpose of assessing the joint roughness coefficient of rock surfaces.

Programme: Version 2, 12th August 2019.

1. Research the current understanding for the use of Terrestrial Laser Scanning (TLS) and Mobile Laser Scanning in assessing geotechnical features in underground environments through a thorough literature review.
2. Data collection. Lab testing on TLS in a simulated underground environment, focusing on:
 - 2.1. Scanning at two scan speeds at three distance-to-object ranges.
 - 2.2. Scanning in light and dark conditions.
 - 2.3. The effects of an amber flashing light on scan results.
 - 2.4. The effects of airborne dust on scan results.

- 2.5. Accuracy at capturing four JRC grades to simulate the manual JRC assessment.
3. Analyse and assess the scan data in identifying JRC to simulate the manual JRC assessment.
 4. Analyse the effects of environmental changes on the scan data.
 5. Compile the acquired analysis and scan results for report.
 6. Assess the feasibility of using a mobile platform in future studies to achieve the same results.

Agreed by

Megan Braddon



12/08/2019

Student signature

Date

Dr. Zahra Gharineiat



14/08/2019

Supervisors signature

Date

Appendix B - Faro Focus3D Performance Specifications

FARO Focus^{3D}
www.faro.com/focus

FARO

Performance Specifications



Ranging Unit

Unambiguity interval: 153.49m (503.58ft)

Range Focus^{3D} 120i: 0.6m - 120m indoor or outdoor with low ambient light and normal incidence to a 90% reflective surface

Range Focus^{3D} 20i: 0.6m - 20m at normal incidence on >10% matte reflective surface*

Measurement speed: 122,000 / 244,000 / 488,000 / 976,000 points/sec

Ranging error¹: ±2mm

Ranging noise ²	@10m	@10m - noise compressed ⁴	@25m	@25m - noise compressed ⁴
@ 90% refl.	0.6mm	0.3mm	0.95mm	0.5mm
@ 10% refl.	1.2mm	0.6mm	2.20mm	1.1mm

Color Unit

Resolution: Up to 70 megapixel color

Dynamic color feature: Automatic adaption of brightness

Deflection unit

Vertical field of view (vertical/horizontal): 305° / 360°

Step size (vertical/horizontal): 0.009° (40,960 3D pixels on 360°) / 0.009° (40,960 3D pixels on 360°)

Max. vertical scan speed: 5,820rpm or 97Hz

Laser (Optical transmitter)

Laser power (cw Ø): 20mW (Laser class 3R)

Wavelength: 905nm

Beam divergence: Typical 0.19mrad (0.011°)

Beam diameter at exit: 3.0mm, circular

Data handling and control

Data storage: 3D, SDHC™, SDXC™; 32GB card included

Scanner control: Via touch-screen display

New WiFi(WLAN) access: Remote control, Scan Visualization and download are possible on mobile devices with iRish®

Multi-Sensor

Dual axis compensator: Levels each scan with an accuracy of 0.015° and a range of ±5°

Height sensor: Detects the height relative to a fixed point via an electronic barometer and adds it to the scan

Compass: Electronic compass gives the scan an orientation. A calibration feature is included.

1) Depends on ambient light, which can act as a source of noise. Bright ambient light (e.g. sunlight) may shorten the actual range of the scanner to lesser distances. In low ambient light, the range can be more than 120m for normal incidence on high-reflective surfaces. 2) Ranging error is defined as the systematic measurement error at around 10m and 25m, one sigma. 3) Ranging noise is defined as a standard deviation of values about the best-fit plane for measurement speed of 122,000 points/sec. 4) A noise-compression algorithm may be activated to average points in sets of 4 or 16, thereby compressing raw data noise by a factor of 2 or 4. Subject to change without prior notice.

Patented: US 7,430,068 B2; 7,733,544; 7,847,922 B2

*Focus^{3D} 20i not available for distributor resale



Hardware Specifications

Power supply voltage: 19V (external supply), 14.4V (internal battery)

Power consumption: 40W and 80W respectively (while battery charges)

Battery life: Up to 5 hours

Ambient temperature: 5° - 40°C

Humidity: Non-condensing

Cable connector: Located in scanner mount

Weight: 5.0kg

Size: 240x200x100mm³

Maintenance calibration: Annual

Parallax-free: Yes



For more information call 800.736.0234
or visit www.faro.com/focus

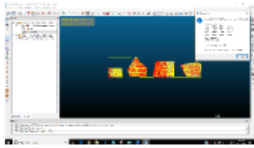
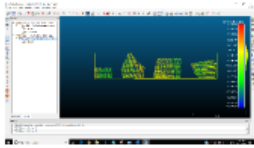
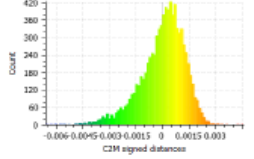
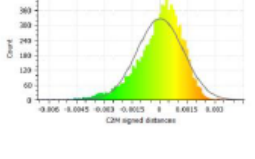
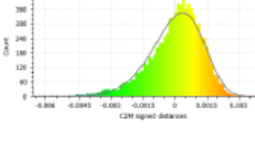
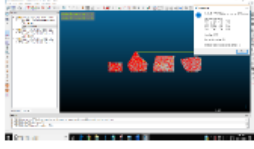
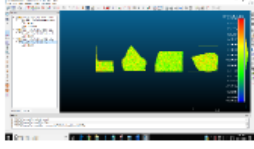
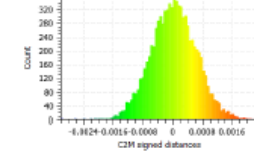
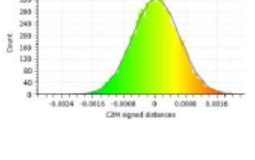
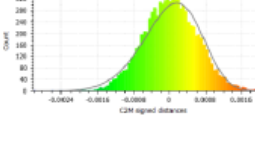
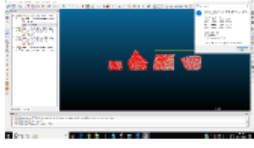
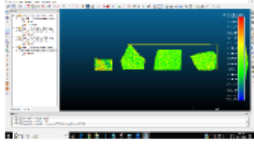
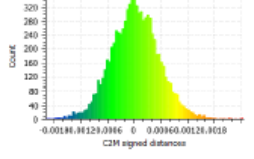
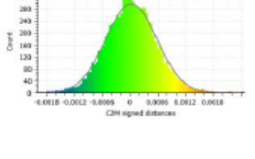
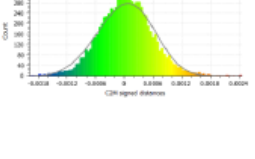
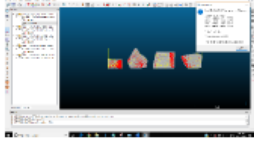
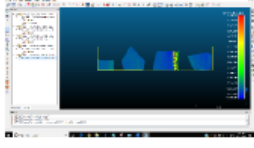
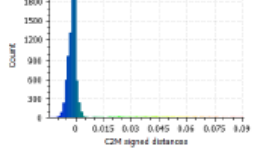
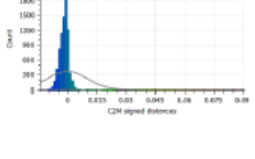
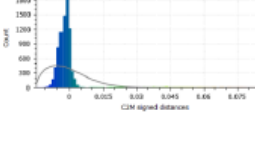
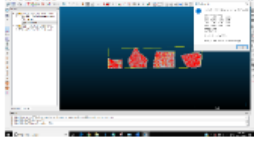
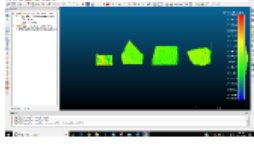
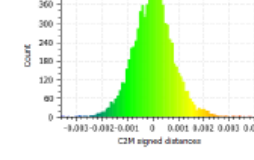
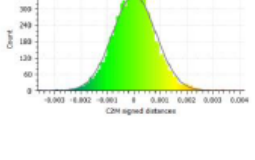
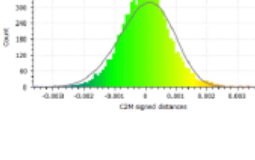
Appendix C – Scanning task risk assessment

Scanning Task Risk Assessment			
Phase	Hazard	Controls	Risk level
All of phase 3.	Poor lighting levels resulting in trips or falls.	Establish a clear access path to all required access points. Notify other personnel of change in lighting level. Exclude non-essential personnel from the area.	B3: Medium
	Lifting strains and skin pinches from equipment handling.	Ensure good lifting technique during setup and pack down. Set up as per manufacturers instruction.	A2: Low
3C	Strobe lighting affecting vision resulting in trips or falls. Effects on epileptics.	As per Poor lighting.	B3: Medium
3D	Dust inhalation. Dust in equipment.	Use non harmful dust, use dust mask. Ensure all equipment's is covered if not in use or sealed correctly if it is.	A2: Low
All of phase 3.	Laser to eye contact.	Follow the procedure when using scanners. Use appropriate eye wear for the task. Barricade work area and install signage when scanners are in use. Exclude non-essential personnel from the area.	C5: Low
		Ensure supervisor or suitable standby is aware of testing being conducted. Maintain a form of clear communication.	

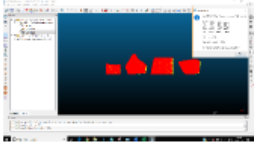
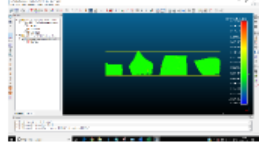
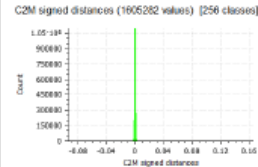
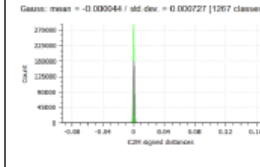
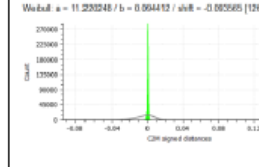
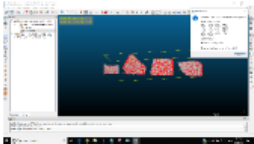
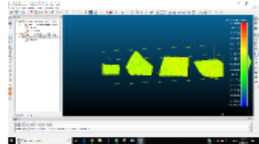
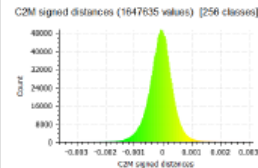
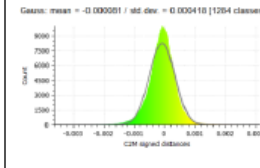
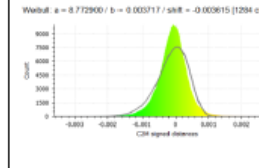
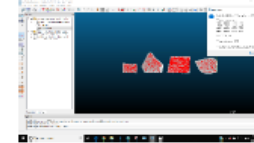
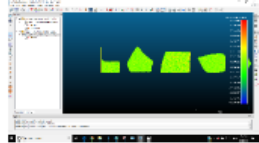
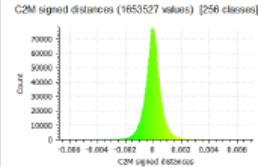
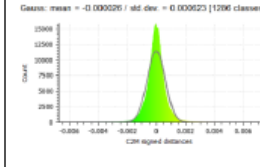
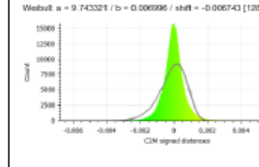
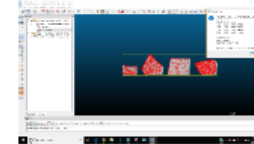
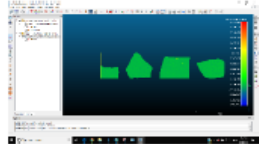
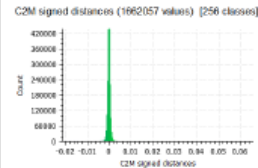
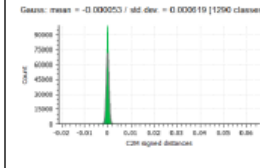
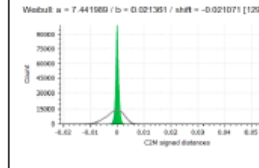
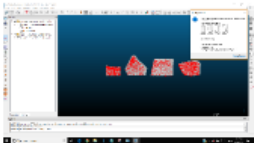
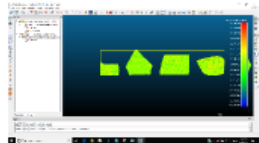
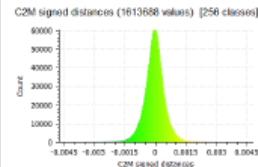
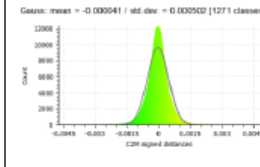
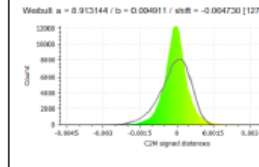
Likelihood		Consequence level				
		A Insignificant	B Minor	C Moderate	D Major	E Critical
1 Almost Certain		Medium	Medium	High	Extreme	Extreme
2 Likely		Low	Medium	High	High	Extreme
3 Possible		Low	Medium	High	High	High
4 Unlikely		Low	Low	Medium	Medium	High
5 Rare		Low	Low	Low	Low	Medium
Consequence		Description		Likelihood		Description
A	No treatment/action required			1	Will only occur in exceptional circumstances.	
B	Minor injury requiring first aid. No damage to equipment			2	Not likely to occur in the foreseeable future.	
C	Injury requiring medical treatment. Non distributive minor damage to equipment.			3	May occur within the project timeline.	
D	Serious injury requiring specialist treatment. Repairable damage to equipment.			4	Likely to occur within the project time line.	
E	Loss of life, permanent disability. Major damage to equipment requiring replacement.			5	Almost certain to occur in the project timeline.	
Risk level		Description			Action	
Low		If an incident were to occur there would be little likelihood of injury or damage.			Continue with existing controls and procedures.	
Medium		If an incident were to occur there would be some chance of injury requiring first aid of minor damage to equipment.			Consider additional controls or procedures to mitigate reoccurrence.	
High		If an incident were to occur there may be injury requiring medical attention or damage to equipment requiring repair.			Controls and procedures will need to be implemented prior to commencing the task.	
Extreme		If an incident were to occur death or disability may result or irreparable damage to equipment may occur.			Consider alternative means to conduct the task. Significant controls may be required to ensure safety.	



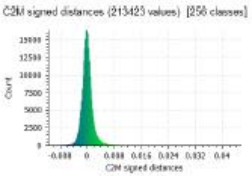
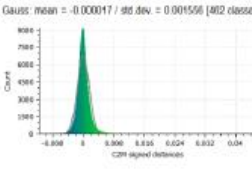
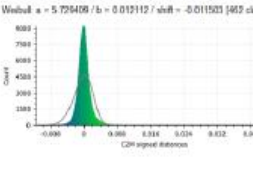


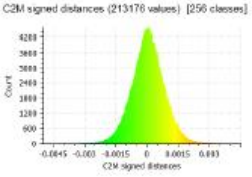
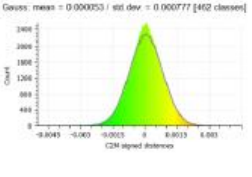
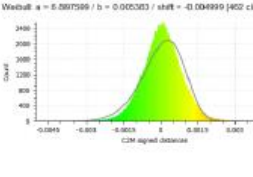


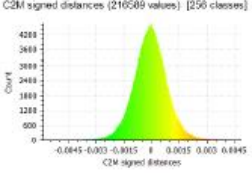
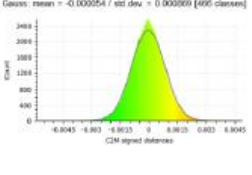
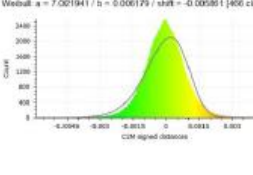
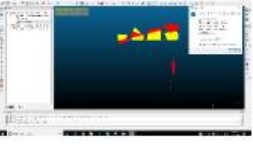

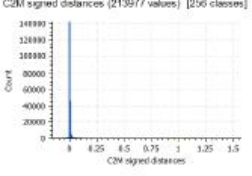
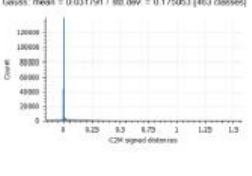
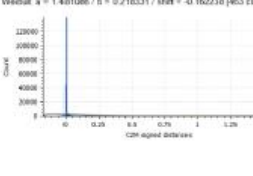


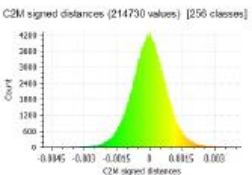
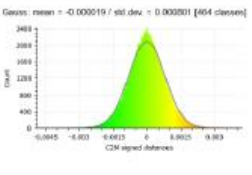
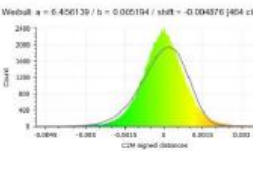
Appendix D - C2M statistical analysis table



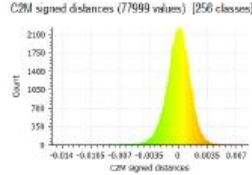
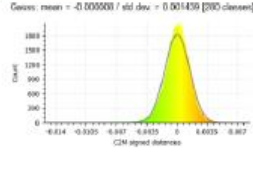
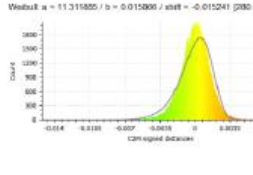


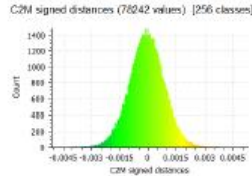
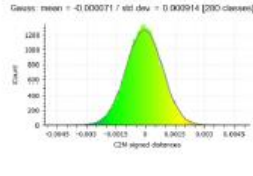
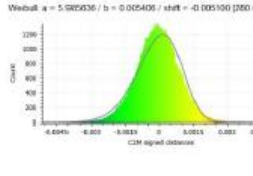


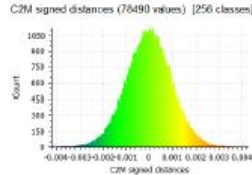
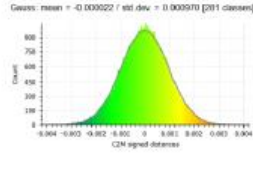
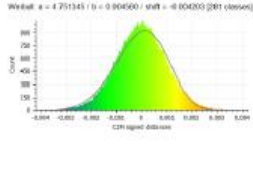


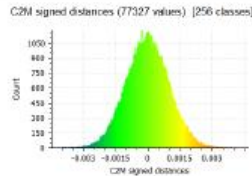
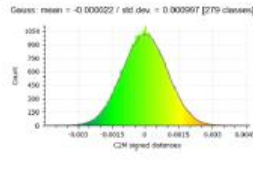
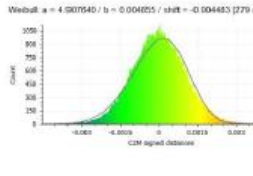
Set	Fine Align	Histogram	Histogram	Gauss	Weibull
SP1 1m Lt_D					
Lt_FL					
Dr					
Dr_D					
Dr_FL					

Set	Fine Align	Histogram	Histogram	Gauss	Weibull
SP1 3m Lt_D			C2M signed distances (R391 values) [88 classes] 	Gauss: mean = 0.000023 / std dev = 0.001243 [92 classes] 	Weibull: a = 6.488841 / b = 0.007108 / shift = -0.000065 [92 classes] 
Lt_FL			C2M signed distances (R434 values) [88 classes] 	Gauss: mean = 0.000029 / std dev = 0.000600 [92 classes] 	Weibull: a = 5.506721 / b = 0.003280 / shift = -0.000012 [92 classes] 
Dr			C2M signed distances (R414 values) [88 classes] 	Gauss: mean = 0.000029 / std dev = 0.000545 [92 classes] 	Weibull: a = 3.996999 / b = 0.002223 / shift = -0.001992 [92 classes] 
Dr_D			C2M signed distances (R346 values) [88 classes] 	Gauss: mean = -0.000040 / std dev = 0.010188 [92 classes] 	Weibull: a = 1.806770 / b = 0.010007 / shift = -0.014229 [92 classes] 
Dr_FL			C2M signed distances (R347 values) [88 classes] 	Gauss: mean = 0.000011 / std dev = 0.000611 [92 classes] 	Weibull: a = 4.782968 / b = 0.003905 / shift = -0.000636 [92 classes] 

Set	Fine Align	Histogram	Histogram	Gauss	Weibull
SP1 5m Lt_D			C2M signed distances (2891 values) [52 classes] 	Gauss: mean = 0.000026 / std dev = 0.001262 [54 classes] 	Weibull: a = 4.568833 / b = 0.005746 / shift = -0.000239 [54 classes]
Lt_FL			C2M signed distances (2891 values) [52 classes] 	Gauss: mean = 0.000022 / std dev = 0.000640 [54 classes] 	Weibull: a = 3.4551327 / b = 0.002591 / shift = -0.000290 [54 classes]
Dr			C2M signed distances (2887 values) [52 classes] 	Gauss: mean = 0.000050 / std dev = 0.000656 [54 classes] 	Weibull: a = 3.335013 / b = 0.002291 / shift = -0.000008 [54 classes]
Dr_D			C2M signed distances (2890 values) [52 classes] 	Gauss: mean = 0.000030 / std dev = 0.000653 [54 classes] 	Weibull: a = 4.4526811 / b = 0.003780 / shift = -0.003441 [54 classes]
Dr_FL			C2M signed distances (2890 values) [52 classes] 	Gauss: mean = 0.000085 / std dev = 0.000603 [54 classes] 	Weibull: a = 3.4877119 / b = 0.002356 / shift = -0.000501 [54 classes]

Set	Fine Align	Histogram	Histogram	Gauss	Weibull
SP2 1m Lt_D			C2M signed distances (1665262 values) [256 classes] 	Gauss: mean = -0.000044 / std dev = 0.00027 [1267 classes] 	Weibull: a = 11.229245 / b = 0.994412 / shift = -0.005985 [1267 classes] 
Lt_FL			C2M signed distances (1647635 values) [256 classes] 	Gauss: mean = -0.000091 / std dev = 0.000410 [1294 classes] 	Weibull: a = 9.722900 / b = 0.003717 / shift = -0.000615 [1294 classes] 
Dr			C2M signed distances (1653527 values) [256 classes] 	Gauss: mean = -0.000020 / std dev = 0.000323 [1296 classes] 	Weibull: a = 9.743321 / b = 0.000996 / shift = -0.000743 [1296 classes] 
Dr_D			C2M signed distances (1662057 values) [256 classes] 	Gauss: mean = -0.000020 / std dev = 0.000319 [1296 classes] 	Weibull: a = 7.441989 / b = 0.021361 / shift = -0.021071 [1296 classes] 
Dr_FL			C2M signed distances (1613666 values) [256 classes] 	Gauss: mean = -0.000041 / std dev = 0.000502 [1271 classes] 	Weibull: a = 5.913144 / b = 0.004011 / shift = -0.004730 [1271 classes] 

Set	Fine Align	Histogram	Histogram	Gauss	Weibull
SP2 3m Lt_D			C2M signed distances (213423 values) [256 classes] 	Gauss: mean = -0.00017 / std dev = 0.001556 [402 classes] 	Weibull: a = 5.729498 / b = 0.019117 / shift = -0.011503 [402 classes] 
Lt_FL			C2M signed distances (213176 values) [256 classes] 	Gauss: mean = 0.000053 / std dev = 0.000777 [402 classes] 	Weibull: a = 5.087599 / b = 0.005303 / shift = -0.004999 [402 classes] 
Dr			C2M signed distances (216589 values) [256 classes] 	Gauss: mean = -0.000054 / std dev = 0.000889 [402 classes] 	Weibull: a = 7.082194 / b = 0.006179 / shift = -0.009391 [402 classes] 
Dr_D	 Manual alignment required.		C2M signed distances (213977 values) [256 classes] 	Gauss: mean = 0.031791 / std dev = 0.175053 [402 classes] 	Weibull: a = 1.481086 / b = 0.218331 / shift = -0.162310 [402 classes] 
Dr_FL			C2M signed distances (214730 values) [256 classes] 	Gauss: mean = -0.000019 / std dev = 0.000801 [402 classes] 	Weibull: a = 6.456139 / b = 0.005194 / shift = -0.004876 [402 classes] 

Set	Fine Align	Histogram	Histogram	Gauss	Weibull
SP2 5m Lt_D					
Lt_FL					
Dr					
Dr_D					
Dr_FL	